NANOENGINEERED BIOMATERIALS FOR CELL AND THERAPEUTIC DELIVERY

A Dissertation

by

CHARLES W. PEAK

Submitted to the Office of Graduate and Professional Studies of
Texas A&M University
in partial fulfillment of the requirements for the degree of

DOCTOR OF PHILOSOPHY

Chair of Committee,	Akhilesh K. Gaharwar
Committee Members,	Michael J. McShane
	Jaime C. Grunlan
	Roland R. Kaunas
Head of Department,	Michael J. McShane

May 2018

Major Subject: Biomedical Engineering

ABSTRACT

Direct-write extrusion bioprinting, a form of additive manufacturing, is an useful technique to recapitulate anatomical complexity for tissue engineering applications. However, bioprinting has hit a bottleneck in progress due to the lack of available bioinks with high printability, mechanical strength, and biocompatibility. Here, we report a family of hydrogel-based bioinks for extrusion bioprinting from poly (ethylene glycol) (PEG) and two-dimensional (2D) nanoparticles. PEG, a non-fouling easily modifiable polymer, combined with biocompatible Laponite XLG nanoparticles (2D nanosilicates) to obtain shear-thinning hydrogel bioinks. Electrostatic interactions between nanoparticles and hydrogen-bonding between polymer and nanoparticles govern the flow behavior and printability of bioink. The evaluation of hydrogel bioink using flow sweeps, peak holds, and dynamic oscillatory rheology, suggest that minimum shear-thinning index of ~0.3, solution viscosities >1000 Pa·s, and 80% recovery within 30s are necessary for printing high fidelity constructs. Mechanically stiff 3D printed structures are obtained by covalently crosslinking polymeric chains using ultraviolet (UV) light. Modifications to the PEG system through inclusion of dithiothreitol linkage or combining with gelatin methacrylate are used to control matrix degradation, cell adhesion properties, and therapeutic release. We envision that PEG bioinks can be used to print complex, large-scale, cell-laden tissue constructs with high structural fidelity and mechanical stiffness for applications in custom bioprinted scaffolds and tissue engineered implants.

ACKNOWLEDGEMENTS

Foremost in my Ph.D. experience I would like to thank my family. Since the beginning my family has always valued education and through everything they have steadfastly supported me in my endeavors. With all that I have experienced at Texas A&M, thank you for always being there to support me. Even greater than my family, God has held me so deeply. Without His steadfast love and support I would not be here. His mighty acts and words working through others throughout this journey have been necessary.

With those dearest and most important personal acknowledgements said, I would like to thank my dissertation advisor Dr. Akhilesh Gaharwar. We have both grown immensely during this time together. I look forward to your continued career, aspirations, and growth. Additionally, I would like to thank my committee members (all present and past) Dr. Michael McShane, Dr. Jamie Grunlan, Dr. Roland Kaunas, and Dr. Elizabeth Cosgriff-Hernandez. Thank you for elevating my research, my thoughts, and my methodologies. The technical knowledge I gained in a relatively short amount of time is invaluable.

To my labmates, especially Lauren Cross and Jake Carrow, thank you. Thank you for support, for listening, for helping out, and for so much more. I am indebted to your help and knowledge with cell culture without which I would have taken longer to accomplish as much as I have. Thank you.

To Achu Byju and Lindsay Woodard: thank you for helping me set-up and get through the first year of Biomedical Engineering Graduate Student Association.

Two of my biggest mentors, supporters, and sounding boards have been Dr. Allison Sieving and Dr. Marcia Pool. Even though we all now work separate places, your perspectives have helped me through the process. For always believing in me and helping me through some tough times, thank you.

This Ph.D. would not have been plausible or possible without the strong foundation and high standards all my past teachers have set for me. Thank you for believing in me.

Lastly, there are many more individuals that have in some way made my experience here at Texas A&M. Dr. Ra'Sheedah Richardson, other Graduate Teaching Consultants, and staff at the Center for Teaching Excellence: thank you for being my teaching escape. I thank Dr. Teri Reed and Dr. Magda Lagoudas for constant engineering education support. Finally, to the faculty and staff in the department of Biomedical Engineering, thank you.

CONTRIBUTORS AND FUNDING SOURCES

Contributors

This work was supervised by a dissertation committee consisting of Professor Akhilesh Gaharwar (advisor) and Professors Michael McShane and Roland Kaunas of the Department of Biomedical Engineering and Professor Jamie Grunlan of the Department of Mechanical Engineering.

The data analyzed for Chapter 5 was partially provided by Professor Kayla Bayless. The analyses depicted in Chapter 5 were conducted in part by Dr. David Howell, post-doctoral associate in Dr. Kayla Bayless' laboratory, of the Department of Health Sciences and will be published in 2018.

All other work conducted for the dissertation was completed by the student independently.

Funding Sources

This work was made possible in part by NIH Grant Number (DP2 EB026265, R03 EB023454) and NSF Grant Number (CBET 1705852). Its contents are solely the responsibility of the authors and do not necessarily represent the official views of the NIH or NSF.

NOMENCLATURE

PEG	Poly (ethylene glycol)
PEG-DTT	Poly (ethylene glycol)-dithiothreitol
PEG-DA	Poly (ethylene glycol) diacrylate
GelMa	Gelatin methacrylate
nSi/XLG/Laponite	Laponite XLG
UV	Ultra-violet
GF	Growth factor(s)
VEGF	Vascular endothelial growth factor
FGF	Fibroblast growth factor
PDGF	Platelet derived growth factor
ATR	Attenuated total reflection
NMR	Nuclear magnetic resonance spectroscopy
G’	Storage modulus (Pa)
G”	Loss modulus (Pa)

TABLE OF CONTENTS

Page

LIST OF FIGURES

Page

LIST OF TABLES

Page

1. INTRODUCTION

1.1 Introduction to Extrusion-based Printing

Additive manufacturing is a process in which layer by layer materials are deposited on a surface to construct complex three-dimensional objects.[1] Recognizing that the body is composed of complex anatomical and physiological three-dimensional tissues and organs, recent advances have occurred within the realm of biomanufacturing. Various additive manufacturing techniques can be used to construct anatomical structures with increasing degrees of complexity. While tissue engineering aims to create bio-functional replicas of full scale human organs and tissues ex vivo,[2] there remains an overall lack in manufacturing techniques that fully recapitulate complex anatomical structures.

Current biomedical technologies have mimicked certain cell behaviors such as cell spreading,[3, 4] cell-cell crosstalk,[5, 6] and extracellular matrix secretion ex vivo,[7, 8, 9] developments are forthcoming to replicate tissue structure and function. Traditionally tissue engineering combines support material, cells and bioactive cues to create tissue mimics. Most common support materials are composed of hydrogels as they replicate the native extracellular matrix properties such as stiffness and hydration degree.[10, 11] Manufacturing hydrogels has been limited to cast methodologies wherein low viscosity solutions are constrained via molds and subsequently crosslinked to form mechanically rigid structure. However, recent advances in both additive manufacturing and in hydrogel chemistry has permitted free-from fabrication of self-supporting structures.[12]

Due to high water content, hydrogels lack the mechanical ability to hold shape without being constrained (i.e. hydrogel precursor solutions are Newtonian fluids).[13, 14] However, manufacturing technique such as Laser-Induced Forward Transfer or Inkjet Printing may be used to construct three-dimensional shapes.[12, 15, 16] Hydrogels with higher viscosities can be used for direct-write three-dimensional printing and have shown promise to localize scaffolds in specified areas.[17, 18, 19] Given the complex physiology and anatomy of organ systems, precise location of cells, scaffolds, and cues are necessary. Overall, shape customization results in complex structures that facilitate nutrient supply and waste removal.[20] Recent investigations have implemented injectable scaffolds for repair of ischemic heart tissue,[21, 22, 23] damaged cartilage,[24, 25, 26] and as skin grafts[27, 28]. In addition, hydrogels are often used to study cell-material and cell-cell interactions.[3, 4]

Hydrogels are an emerging class of materials in the additive manufacturing. Traditional materials for 3D printing include metals,[29] ceramics,[30] and thermoplastics.[31] Biomedical engineers can utilize processes and techniques developed through the aforementioned materials and apply them to use with cell-laden hydrogel precursor solutions, also called bioinks. Hydrogels chemistries and fabrication techniques development are critical for continued progression in tissue engineering, elucidating the combined effects of material chemistry and mechanical deposition on cell viability, proliferation, and differentiation. Regardless of manufacturing procedure used, fundamental relationships between hydrogel composition and cell interactions in both two-dimensional and three-dimensional microenvironments should be carefully characterized. Further material characterization in terms of swelling, degradation, and flow properties gives rise to the material's use as an bioink.

Herein, we describe characteristics necessary for bioinks, characterization techniques, and their relationship to the direct-write bioprinting process. Advanced readers may find reviews papers concerning hydrogel types and overall uses more advantageous[11, 32] or other reviews on specific bioinks formulations the readers are referred reviews by Malda et al.[33] and Chimene et al.[34]

1.2 The Bioprinting Process

Bioprinting combines the biological aspects of cell culture with the mechanical processes of printing. In doing so, the interface between cell culture, material science, and mechanical fabrication must be reconciled for development of appropriate hydrogel precursor solutions. Cell culture involves the continued proliferation of cells using established protocols. Most cell culture protocols seed cells on two-dimensional tissue culture polystyrene, contrary to physiological three-dimensional environment. Contrary, material science examines material stiffness, crack propagation, and phase diagrams of materials for example. Careful control of material chemistry determines material stiffness and further dictates the processing capability of the material.

To begin the bioprinting process (Figure 1-1), cells are cultured to approximately 70% confluency before being passaged. During the passaging stage, rather than plating cells onto well plates, the cells are suspended in hydrogels to be used for printing, creating a bioink.[35, 36] During this process, cells are distributed throughout the hydrogel bioink via pipetting or gentle swirling. Homogeneous distributions ensure that each printed layer has inherent bioactivity and provided mechanically homogenous constructs. After bioinks are prepared, they are loaded into syringes or extrusion

barrels in preparation for printing. Material properties, such as yield stress, are critical to control for both cell incorporation and for the ability of the 3D printer to extrude the material. Once the syringe/barrel is loaded, the print commences, depositing cell-laden bioinks in specific areas. Crosslink chemistry, including thermo-gelation, determines how the hydrogel will be cured to form a stable structure and upon print completion constructs are placed in media for nutrient supplementation. Prior to printing, computer aided design (CAD) files are used to design the final printed construct. CAD files are converted to g-code files which is the code which 3D printers used to determine how fast the print should proceed and when materials should be deposited. CAD software provides an array of tools to create complex and anatomically relevant structures.

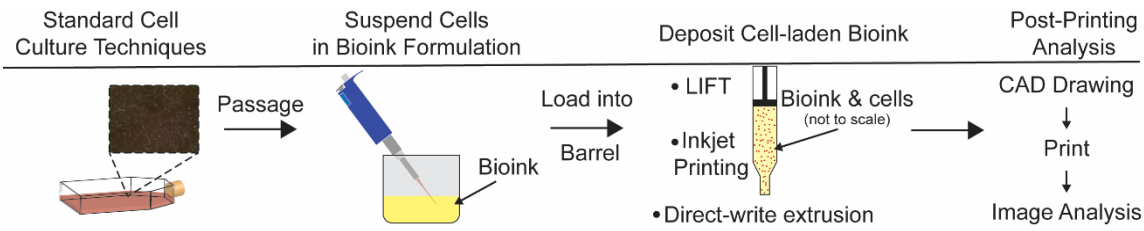

Figure 1-1. Bioprinting process. Various cells types are cultured to confluency, suspended within the bioink, printed, and analyzed.

Throughout the process, coordinating cell-material interactions, mechanical aspects of materials, and maintaining sterility govern the ability to successfully bioprint. Throughout each stage of the bioprinting process various techniques can be used to measure each of these aspects. For example, flow sweeps can determine if a material has potential to be injectable and cytotoxicity assays indicate if a material has favorable interactions with cells. The proceeding sections will examine techniques and relationships in the bioprinting process.

1.3 Pre-Printing Considerations

Current hydrogel creation relies heavily on external structures and support for formation prior to crosslinking. Here we focus on characterization of hydrogel bioinks used for bioprinting, such as gelatin,[37, 38, 39, 40, 41] alginate,[42, 43] poly (ethylene glycol),[44, 45] and chitosan,[46] and the cell interactions with materials. Bioprinting involves more complex design criteria as compared to typical hydrogel formulations: bioinks (hydrogel precursors) must be transported through a needle and able to retain its shape upon exit. Appropriate choice of polymer will maintain cytocompatibility along with achieving the necessary mechanical requirements for 3D printing. Several factors must be taken into consideration for quality bioink formulation. In the proceeding section, polymer molecular weight, flow profile, and cytotoxicity will be discussed (Figure 1-2). Each of these parameters can influence the ability of the bioink to behave appropriately to produce viable tissues.

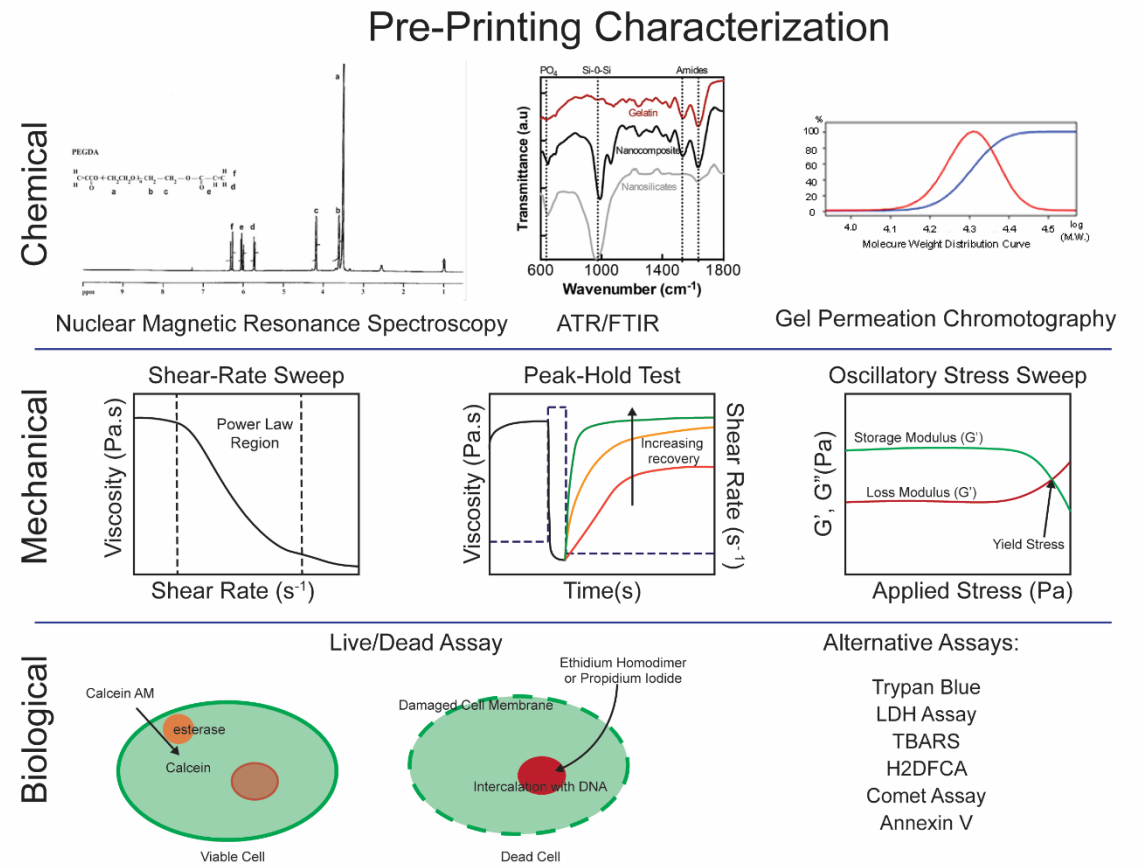

Figure 1- 2. Pre-printing parameter considerations. NMR, ATR/FTIR, and GPC can be used for chemical quantification. Various rheological tests examine the bioink's ability to be printed. Biological assays to measure cell viability should be used as an initial indicator for use as bioink.

1.3.1 Molecular Weight Determination: NMR, ATR/FTIR, GPC

Polymer molecular weight, crosslinking mechanism, and side-groups dictate functionality of the polymer as a bioink and subsequent compatibility. High molecular weight polymers are typically viscous due to an increase in chain entanglements, being useful to suspend cells. Polymer molecular weight further influences flow behavior of the bioink. Biologically, cell-bioink interaction can be broadly measured by the cytotoxicity of the material. These techniques can be

used to quantify the bioprinting process and the determine the interplay between material chemistry/properties and cell behavior during the printing process.

Bioink composition should support cell integration (viability and proliferation) via control over stiffness,[47, 48, 49] mesh size,[50, 51] crosslinking mechanism, and shielding cells from shear stress during extrusion.[42] Both synthetic and natural polymers offer advantages for cell integration and control over material parameters. Molecular weight and crosslinking density remain the two most critical physical characterizations that influence cell behavior regardless of polymer source. Naturally derived polymers often exhibit high molecularly weights while synthetic polymers can be carefully controlled during the synthesis.[52, 53] As an example, gelatin or methacrylated gelatin (Gelma) presents many cell binding sequences, facilitating strong material-cell interactions. Gelatin's inherent bioactivity is a result of denature bovine or porcine collagen (typically hooves and skin products). Gelatin production result in high molecular weight chains with broad distribution. Most manufacturers sell gelatin by "Bloom strength" which reflects the average molecular weight of the polymer. Higher bloom strength indicates stiffer gels. Conversely, poly (ethylene glycol) (PEG) manufacturing process results in finely tuned molecular weights ranging from <500 to >1000000 Da, controlling mesh size and nutrient diffusion. Due to the chemical formula ($-CH_2-CH_2-O-$) of the PEG backbone, it is often considered a "stealth" or "bioinert" molecule that does not illicit a foreign body response.[54] However, PEG needs to be chemically modified in order to crosslink to form stable hydrogels. Both dimethacrylated and diacrylated PEG have been among the most widely studied model hydrogels.[55] More recently, click chemistry has emerged as a viable crosslinking mechanism for PEG hydrogels. Regardless, nuclear magnetic

resonance spectroscopy or attenuated total reflectance is used to verify the terminal end groups of the polymer and molecular weight of the polymer.

Nuclear magnetic resonance spectroscopy (NMR) quantifies molecular systems based on its molecular structure, assuming the sample is pure. NMR experiments measure the energy transfer between base energy and higher energy level once a magnetic field is applied.[56] Radio frequencies are used to detect the energy emission from high to base levels.[57] Specifically, ^{1}H NMR is often used within polymer systems to determine molecular weight and end functional groups.[58] For example, diacrylation of poly(ethylene glycol) can be quantified based on the unique chemical signature.[50] Chemical signatures, or shifts, are governed by the surrounding electrons, the more electro-negative a nucleus is, the higher the resonant frequency. In addition, determination of polymer molecular weight can be completed using NMR.[59, 60] For molecular weight analysis, standardization of the backbone is accomplished compared to the predicted manufacturer's value. For example, in PEG MW=3,350 Da, there are approximately 76 repeat (-O-CH_2-CH_2-) segments resulting in 304 H's in the backbone. By standardizing the δ=3.45 ppm peak, the overall molecular weight and end group functionality can be determined.[61]Molecular weight influences cell behavior due to the amount of swelling a hydrogel may undergo resulting in nutrient supplementation and waste removal. Swelling and degradation of hydrogels is commented further in the post-printing considerations. For the printing process, higher molecular weight polymer bioinks can offer stress-shielding wherein cells are not exposed to the high shear stresses due to being entangled within the polymer. Subsequently, cell viability post-printing remains high.[42]

Similarly, attenuated total reflectance spectroscopy (ATR) can measure end groups and polymer backbone.[62] ATR uses infrared beam, rather than magnetic field, for determination of sample characteristics. As the beam interacts with the sample, small changes occur to its exiting angle due to an evanescent wave that exudes from the sample. Computer systems subsequently generate infrared spectrum for interpretation. NMR and ATR provide information about polymer backbone and end-groups which is pertinent to bioink formulation. End-groups can determine crosslinking mechanism that must be employed. Acrylate end groups have historically been common as the provide facile method for creation of covalent crosslinks. However, additional crosslinking methods are becoming more widespread.

Along with NMR, gel permeation chromatography (GPC) is used for molecular weight determination. The advantages of GPC over NMR are that molecular weight distribution rather than a single molecular weight can be obtained and that weights above 35,000 Da can be measured. Gel permeation chromatography is a form of size exclusion chromatography that specifically measures the elution time of a polymer compared to a known standard. Higher molecular weight polymers cannot travel through the beads packed into the column, eluting faster than smaller molecular weight polymers. As such, polymer dispersion index (PDI) can be found using GPC.[63, 64] Polymer molecular weight is critical to control as it dictate bioinks flow characteristics and resulting mechanical and biocompatibility properties. Having low PDI, suggest that the polymer is all similar length, resulting in consistent mechanical properties. Due to processes variations, natural polymers are typically more disperse than synthetic polymers. Increasing polymer molecular weight, crosslink density, or concentration can improve the printability of the solutions at the coast of limited cell migration and a reduction in nutrient diffusion.

1.3.2 Rheology of Bioinks

As bioinks must be extruded through needles, the ability to flow is of utmost importance. Rheology is the mathematical study of how matter flows when external force is applied. Studies are beginning to understand the correlation between the rheology of bioinks and the subsequent shape fidelity. The data that is often presented lacks the contextual relationship of the rheology to the printed results. Here, we present an understanding of the various rheological tests that are available, their ability to predict a bioink's potential, and the parameters that are often lacking in current studies.

Rheology is completed using either a stress or a strain controlled rheometer resulting in numerous parameters that are of importance for measuring flow of material. Rheometers either apply a specific displacement or apply a specific force, both of which can either be applied in oscillation (back and forth) or in rotation (unidirectional). For whichever parameter is applied, the other is measured (e.g. apply force, measure displacement). Using instrument geometric constraints, parameters such as storage (G'), loss (G"), and viscosity (η) are calculated and reported. Storage modulus is a measure of the elastic energy within the sample while loss modulus is a measure of the viscous portion or dissipated energy within the sample. Both storage and loss modulus are calculated while performing oscillatory measurements. Viscosity, calculated via rotational tests, measures the materials resistance to flow. Typically, bioink papers contain an oscillatory stress or frequency sweep to demonstrate the storage and loss modulus along with a rotational shear-rate sweep to determine viscosity.[65] Storage and loss modulus most accurately correspond to once the bioink has been extruded and final material properties. Viscosity should be used to describe the

ability of the bioink to flow through the reservoir, needle, and onto the printing surface. After extrusion, a bioink must quickly recovery or be crosslinked as to not spread on the printing surface. Being able to recovery is often deemed being thixotropic. Alternatively, printing surface can also be modified to increase the contact angle with the material therefore decreasing the amount of spreading that will occur.

Once the bioink is loaded into the barrel, a certain amount of stress, deemed yield stress, must be overcome to allow the material to flow. Yield stress is the minimum stress that must be placed on the material for flow to occur. Uncrosslinked hydrogel precursors are typically weakly bound together through electrostatic forces. When stress is applied above the yield stress, these bonds are broken permitting the material to flow. For example, gelatin is a thermo-responsive hydrogel that above ~37°C has weak hydrogel bonding due to high chain motility. When a stress is applied it can easily be extruded through the needle. High yield stresses pose process difficulties in cell incorporation and in the work required for the 3D printer motor. Along with gelatin, other hydrogels such as a self-assembling peptide[66, 67] and colloidal systems[68, 69] have been developed that incorporate yield stress as an important design consideration.

For direct-write extrusion bioprinting, high viscosity is necessary to ensure the bioink does not separate and prevents collapse of structures. Viscosity can be controlled by polymer molecular weight, degree of branching, concentration, and addition of rheological modifiers. Generally, an increase in these parameters results in an increase in viscosity across all shear rate. This is illustrated in Table 1-1 which presents a short list of commonly used polymer for bioinks. Conversely, lower crosslinking concentration within hydrogel matrix aids in cell proliferation,

migration, and tissue formation by facilitating nutrient diffusion and waste removal. Importantly, the viscosity of a hydrogel bioink can directly influence the resulting shape fidelity such as drooping and spreading.

Table 1-1. Common polymers, viscosities, and crosslinking mechanism for Bioinks

Polymer	Concentration	Crosslinking mechanism	Viscosity Range (Pa·s)	Reference
methacrylated hyaluronic acid/methacrylated gelatin	6-12%	UV	0.1-10000	70
PEG-DA + Laponite	10% PEG-DA, 4% Laponite	UV	1200	71
Sodium alginate	3-5%	Ionic	0.6-6.4	72
GelMa	3-5%	UV	75-2000	73
Hyaluronic Acid	1.5	Temperature	22	74

Shear-rate sweeps are most commonly used to predict viscosity as this test accurately determines viscosities across ranges of shear-rates that the bioink will experience. Steady state shear-rate is reached for each of the measurements within a shear-rate sweep therefore it precisely determines the bioink's ability to deform. Shear-rate sweeps are often ran from low shear-rate ($<10^{-3}$ s^{-1}) to high shear rates ($>10^{2}$ s^{-1}), mimicking the bioink going through the needle. For bioinks, having

high viscosity at low shear rates and low viscosity at high shear rates is imperative for the extrusion process. Materials that exhibit this characteristic are called “shear-thinning”. Often characteristic shear-rate versus viscosity graphs are presented with lack of details and lack of applied mathematical equations. Models have been developed that can describe a material’s ability to shear-thin. Classically, the power-law model has been applied to materials where no low shear-rate or high shear-rate viscosity plateau is observed. The power law index can describe the degree of shear-thinning a solution exhibits. When n=1, the solution is Newtonian; n<1 shear-thinning; n>1 shear thickening. Relatively few studies report equation fitting to the shear-thinning curves that are presented. While graph interpretation informs readers that materials are shear-thinning, equation fitting may bring broader understanding to data and a material’s ability to extrude through needles. For example, Blaeser et al have examine alginate hydrogels for use as bioinks that and have quantified these using Power-law rheology equations.[42] Through the application and study of the flow consistency index, they have concluded that n of approximately 0.3-0.4 has appropriate flow profile. In addition, they examine the yield stress as a critical parameter that dictates cell fate during the printing process. Other work completed by Aguado et al suggests that un-crosslinked hydrogel modulus is important for cell delivery.[75] Uncrosslinked bioink viscosity and storage modulus are analogous measurements with the viscosity measuring resistance to flow while storage modulus is an interpretation of hydrogel stability.

Viscosity influences bioinks’ ability to flow on the printing surface. In addition, surface tension between needle material and bioink should be considered in designing a 3D printing system. An increase in surface tension will decrease the bioinks ability to shear thin while an ideal frictionless system will aid in ability to extrude. Currently limitation in bioink development is increasing the

viscosity of the solution. Viscosity of the bioink determines if a droplet or continuous strand of hydrogel will form. Low viscosity solutions, such as 20% gelatin methacrylamide, tend to form droplets that much either be forcefully expelled or allowed to form large enough droplets until gravity causes them to separate from the nozzle.[76] However, fillers such as nanosilicates[77] or hyaluronic acid[76] can be added to GelMA such that a filament rather than a droplet formation. Filament formation allows for high-fidelity 3D structures to be formed rather than a puddle.

Many researchers will use shear-thinning information to predict a bioink's ability to be 3D printed. We would like to make the important distinction of being able to be injected versus 3D printed: 3D printing requires bioink to stabilize or localize as a given point while injection requires inks to be shear-thinning. Once the bioink has exited the needle, there are little to no shear-rates induced on the material. More accurate rheology test predictions for 3D printing applications, researchers are encouraged to calculate the shear-rates experienced throughout the 3D printing process, program rheometers to induce specific shear-rates and examine the viscosity recovery. Notably, Li et at. have taken this approach for alginate hydrogel containing graphene oxide.[78] Recovery time of 30s was deemed appropriate and percentage recovery was measured as a comparison between unsheared and post sheared samples. Researchers often use uncrosslinked samples during the extrusion process eliciting viscosity as the defacto measurement of choice via a rheometric viewpoint. Additionally, thixotropic loops (increasing shear rate following by a decreasing shear rate in a set amount of time) describe the internal structure rebuilding time. A perfectly Newtonian bioink will have overlapping curves for both the increasing and decreasing shear rates, indicating little internal structure and is a non-ideal candidate as a bioink. A difference in loading and unloading curves indicate the degree of thixotropy within the context of the test (i.e. if the test was

completed using a one minute loading and one minute unloading curve, the thixotropy is specific to that time frame). Thixotropic loop tests can be difficult to interpret and often require specialized "cup and bob" geometry for the rheometer to obtain reliable results.

Oscillatory thixotropy measurements further elucidate bioink stability during printing process. To complete oscillatory thixotropy measurement, an amplitude sweep must first be conducted to determine where the bioink's linear viscoelastic region. Storage modulus and loss modulus should be independent to applied stress or strain (both of which are amplitudes). Outside of the linear region the bioink is dependent on higher order harmonics, requiring more advanced knowledge for interpretation of data. A yield point where the storage modulus decreases below the loss modulus (G'<G") is exhibited typically at amplitudes above 10^1 Pa or between 50-1000% strain. Oscillatory thixotropic tests apply an amplitude below the yield point in order to illustrate that G'>G", an increase in amplitude is applied such that G">G' illustrating the process through the needle, lastly the original amplitude is applied and G' is expected to increase quickly to the original value. Traditionally researchers have tested multiple cycles although the 3D printing process requires only one application of high amplitude (bioink travelling the length of the needle).

Overall, recoverable, low-shear viscosity dictates print fidelity. Often bioinks lack recoverability resulting in structures printed with lower resolutions and accuracies than other additive manufacturing techniques. When shear-thinning behavior, yield stress, and recoverability are examined holistically, high fidelity prints may be achieved. In conjunction with the bioink's flow behavior, internal shear stress can influence cell viability. Mechano-transduction of cell-material

interface and the mechanical stress placed on cells continues to be a hurdle for 3D bioprinting constructs.

Concurrent with viscosity, shear stress is exerted on the material during the printing process affecting cell adhesion, proliferation, and overall cell viability.[42, 75] Cells suspensions in high viscosity bioinks have been used to increase viability.[75] Stress-shielding occurs to cells being entangled within the bioink and the stress being placed on the material rather than the cell. Higher viscosity bioinks tend to have higher viability due to lack of differences in the positive pressure gradient.[75] Along with viscosity, geometric constraints of the printing apparatus can influence shear stress: large deposition needles (small gauge number) reduces the shear stress while simultaneously reducing resolution of the 3D print and lower volumetric flow rates decrease the shear stress. There is no universal induced mechanical stress that all cell types express negative markers. For example, at 1 Pa of induced shear stress, articular chondrocytes significantly change morphology and metabolic activity;[79] however, human mesenchymal stem cells can only withstand shear stresses on the range of $1x10^{-5}$ – $1x10^{-4}$ Pa before significant upregulation of mRNA expressions of osteocalcin, Runx2, and alkaline phosphataste.[80] The printing process subjects cells to complex chemical (trypsin/EDTA) and mechanical (printing) stress. Current techniques to study cell viability as a function of shear stress rely on 2D culture with varying the flow rate of media above the cells. Short term, high shear stress, with cells suspended in a moving medium is less studied though cells appear to be resilient to the printing process.[81, 82]

Within the afore discussion concerning assessment and measurement techniques for 3D bioprinting, bioinks such as GelMa,[76, 77] alginate,[42, 43] and PEG[44, 45] were focused on. Along with

these materials, peptides,[83, 84, 85] PCL,[86, 87, 88] kappa carrageenan,[89, 90] and others[91, 92, 93] have been used for 3D printing applications. Gelatin (subsequently GelMa) is often used due to its inherent bioactivity, ability to bind adherent cells, and thermo-responsiveness. Xavier et al have used GelMa based scaffolds to 3D printed complex shapes[77] and Billet et al have used GelMa scaffolds for deposition of HepG2 cells.[81] Gelatin based hydrogels can be easily fabricated, offer cell binding sites, and are re-constructed through collagenase. Alginate is often used due to its non-immunogenicity, ability to shear-thin, and quick crosslinking in CaCl2 solutions.[94]Alginate is often used due to its non-immunogenicity, ability to shear-thin, and quick crosslinking in CaCl2 solutions.[94] Blaeser has extensively investigated alginate across several compositions (0.5-1.5 wt/vol%) and printing pressures (0.5-1.5 bar).[42] Cells were >60% viable at shear stress >10 kPa while nearing 100% viability with shear stress <5 kPa. Bioinks containing poly (ethylene glycol) are of importance due to the bioinert, non-fouling nature of PEG-based hydrogels. [95] Raphael et al have developed self-assembling peptide hydrogels, offering advantages in cell growth and migration compared to synthetic hydrogels.[35] Overall, an abundance of hydrogel formulations have been developed in order to study the effect of particular chemistries on cell viability, proliferation, and migration.

1.3.3 Extracellular Matrix Considerations

Concurrent with the mechanical considerations in the pre-printing process, biological considerations should be considered to aid in cell adhesion, proliferation, and/or differentiation. Physiologically, the extracellular matrix is a complex network of proteins (collagen, elastin, laminin and fibronectin), glycoprotein and proteoglycans that in conjugation create a three-dimensional structure that provides cells structural support biochemical support.[96] The mechanical

stiffness and elasticity of the ECM varies from on tissue type to the next, primarily due to change in the compositions of the ECM (in particular elastin and collagen) and the stiffness can differ by several order of magnitudes. For example the elastic modulus of soft brain tissue lies in the range of tenths of a kilopascal (kPa) while that of calcified bone is measured in the range of megapascals (MPa).[97] The change in the composition of the ECM in diseased tissue, particular in case of cancer metastasis is well-documented.[98, 99, 100, 101] The ECM protein collagen also contains RGD residues that act as the site of action for the integrin and hence play an important role in cellular adhesion. The process of cell adhesion onto the ECM is itself a complex biochemical process that has be lined to other cellular event such as cell differentiation, cell migration, cell cycle.[102]

Both the ECM mechanical properties and cell adhesion are of paramount importance while selecting biomaterial constructs. The main goal of a synthetic ECM is to provide adequate sites to the cell for binding as well as a 3D architecture and mechanical stiffness similar to native tissue. Careful bioink selection allows for the generation of 3D architecture that faithfully mimics the native tissue, while allowing for variation in the overall mechanical stiffness and chemical properties by changing the polymeric composition of the hydrogel.

Hydrogel literature is rich with various compositions of hydrophilic polymers for studying cell processes and interactions that may be candidates as bioinks. Naturally derived polymers, such as gelatin and alginate, have been well characterized in crosslinking-mechanism and mechanical properties (as a formed hydrogel).[40, 103, 104, 105] Gelatin based hydrogels have elucidated cell binding mechanics, promoted angiogenesis, and used for biodegradable hydrogels. Gelatin is an attractive polymer due to the thermo-gelation crosslinked mechanism by which strands of gelatin hydrogen

bond to each other forming stiff matrix. Facile temperature manipulation of 3-D printer apparatuses promotes the use of gelatin, alginate, and kappa carrageenan as natural bioinks. Alternatively, synthetic polymers such as poly (ethylene glycol), poly (lactic acid), or polycaprolactone have been extensively modified to achieve appropriate crosslinking mechanisms and to increase viscosity of solutions for bioprinting application. Polymers used as bioinks must meet the needs of both being able to mechanically deform and re-form and also provide an environment for cell proliferation.

Most commonly, cell-bioinks interactions are measured *via* two-dimensional seeding of cells on the bioink surface. While useful, these techniques fail to fully capture the complex interactions when cells are encapsulated with three-dimensional matrices. The 3D encapsulation of cells within hydrogels represents an increasingly important and popular technique for culturing cells and towards the development of constructs for tissue engineering. This environment better mimics what cells observe *in vivo*, compared to standard tissue culture, due to the tissue-like properties and 3D environment. In designing new bioinks for direct write extrusion bioprinting, initial cell screenings continue to use established methods to determine cell-material interactions.

1.3.4 Cytotoxicity Considerations

Estimation of cellular toxicity is an essential part of understanding the effect bioink-cell interaction and how the cells are stimulated by the material they are being encapsulated inside. It is also important to estimate the effect of any degradation product being created while the hydrogel is degraded. The use of nanoparticles to modify rheology of the polymeric systems also created challenges in terms of toxicity to cellular systems. Unlike polymeric components of hydrogels,

whose behavior when interacting with cells is well documented, nanoparticles can interact with the cells in many different ways, such as interaction with proteins in cytosol, effecting on mitochondrial activity and generation of Reactive oxygen species(ROS). Hence it is paramount to identify the concentration dependent effect the nanoparticles have on the cells, before we use them for printing applications. These factors are also important for understanding the effects of polymer crosslinking agents on overall cellular viability.

The major drawback of these assays is that they focus only on the cell viability and do not consider factors such as cell differentiation, formation of cell signaling molecules or secretion of proteins. Advanced genetic testing such as sequencing of mRNA may also be sued to identify the effect of hydrogel components on cells, but this process is both expensive and time consuming in most cases. Table 2 summarizes different tests for cytotoxicity and methods of detection.

Table 1-2. List of common assays to measure cell viability

Reagent	Site of action	Method of Detection	Reference
Trypan blue	Cytoplasm	Trypan blue is excluded by live cells with intact plasma membranes, while dead cells are stained blue	106
LDH	Extracellular space	Release of LDH Lactate dehydrogenase cytosolic enzyme into external environment indicates	107, 108, 109

Table 1-2. Continued

Reagent	Site of action	Method of Detection	Reference
TBARS	Cytoplasm	Estimation Lipid peroxidation due to ROS generation by quantification of Malondialdehyde present in cells.	110, 111
Calcein-AM and Ethidium Bromide	Cytoplasm	Fluorescent probes Commonly used together in the form of Live/Dead Viability assay. Live cells are able to exclude Ethidium bromide, while dead cells do not show fluorescence for calcein.	112, 113

Table 1-2. Continued

Reagent	Site of action	Method of Detection	Reference
H2DFCA	Cytoplasm	The cell-permeant 2',7'-dichlorodihydrofluorescein diacetate (H_2DCFDA) (also known as dichlorofluores *cin* diacetate) is reduced to its fluorescent form inside cells I the presence of Reactive oxygen species(ROS)	114, 115
Comet assay	N/A	DNA fragmentation is viewed by Single cell gel electrophoresis.	116, 117
Annexin V	Membrane	Early apoptosis detection, due to movement PS into the outer membrane of the plasma membrane	118

1.4 Post-Printing Analysis

Upon establishment of cytocompatibility between bioink composition and cell type of interest, the bioink can by printed into complex shapes and morphologies. Post-printing there are additional considerations for biological and mechanical components of the constructs. Mechanical characterizations often do not include cells during the testing. Cells may act as deficits in the crosslinked network compared to pure bioink compositions. Regardless, many bioinks began due to the crosslinked mechanical properties exhibiting ideal physiological parameters. Analysis relies on mechanics, optical qualification, and measuring cell adhesion and proliferation (Figure 1-3).

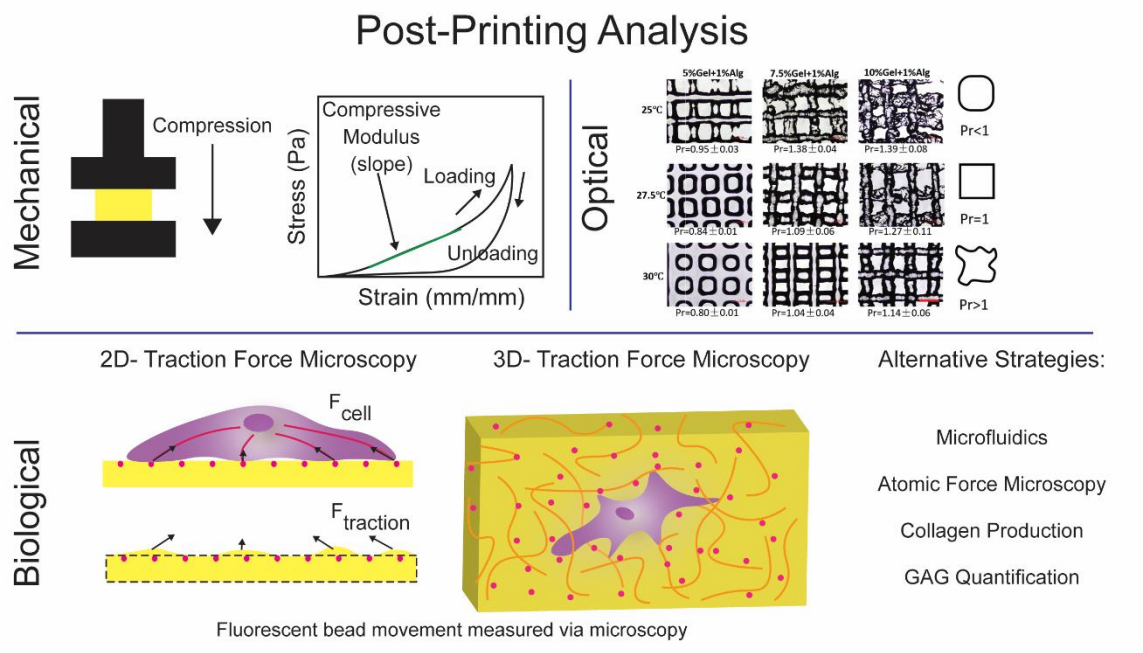

Figure 1- 3. Post-printing analysis. Compression is often used as a measure of tissue compatibility. Prints are measured optically to determine printability. Biological metrics of printed inks rely mainly on cell adhesion forces. Optical portion of figure reprinted with permission from [136] "Ouyang, L.L.; Yao, R.; Zhao, Y.; Sun, W. Effect of Bioink properties on printability and cell viability for 3D bioplotting of embryonic stem cells. *Biofabrication* 2016, *8* (3)"

1.4.1 Mechanical Considerations

1.4.1.1 Compression and Shear Modulus

Compressive and tensile modulus are classical methods to study a material's ability to withstand deformation. While often interchanged, compressive modulus is limited in that a material can only compress 100% while tensile (Young's Modulus) can be theoretically indefinite. Native tissue moduli are well characterized therefore composing a material to match should, in essence, provide mechanical stability.[119, 120, 121] Bioinks composed of synthetic polymers typically have higher moduli compared to natural polymers. Regardless, both types of bioinks tend to exhibit lower modulus once 3D printed. The printing process deposits layers of material that must adhere to each other for strong mechanical properties. The delamination of the layers due to low adhesion provide and defect for crack propagation.[122, 123] Compression testing standardizes the force applied to the sample and the distance the sample is compressed. Stress (Pa) and strain (mm/mm or dimensionless) are plotted and the loading slope is calculated to quantify the compressive modulus. Compression testing of cast bioinks ensures that the material does not have void space within the tested samples (assuming no bubbles present and the sample is cleanly removed from the substrate it was crosslinked onto). Cast bioinks typically have low polymer alignment since the material is allowed to conform to the surrounding mold. However, due to the layer by layer deposition of material in the 3D printing process, void spaces can develop or polymer may align ultimately producing lower compressive modulus. Ideally the printed sample has 100% layer to layer adhesion and contact. In using a circular gauged needle though there will be some space due to a geometric mismatch. From these spaces, cracks propagate, decreasing the compressive modulus.

1.4.1.2 Swelling and Degradation

Once the bioink is crosslinked and placed in either implanted or placed in media, swelling of the structure occurs. Swelling can influence post-printing mechanics: an increase in fluid maximizes the distance between crosslink points.[124] Swelling can also be beneficial as it allows for diffusion of any entrapped therapeutics and cellular waste products.[125] Bioinks composed of natural polymers such as gelatin will both swell and degrade due to enzymes present in the extracellular matrix. Gelatin hydrogels have been used for bioinks previously and in accelerated degradation with application of collagenase (5 U/mL) showed a mass loss of 65% within 11 hrs.[126] Synthetic bioinks must be designed to be degraded on time-scales appropriate to applications. Poly (lactide-co-glycolide) compositions are often used to regulate the degradation profile of the formed hydrogel or nanoparticles[127, 128] and for drug incorporation.[129, 130] Specifically, therapeutic release profiles can be modulated via encapsulation into PLGA nanoparticles with varying amounts of lactide and glycolide to allow for appropriate release times.[130] Alternatively, PEG has been modified with poly (lactic acid) end groups (PLA) to modulate network degradation[131, 132] and cell adhesion[133] and proliferation.[134] For full recapitulation of native tissue, degradation is a key feature of developed bioinks that must continue advancing.

1.4.1.3 Image Analysis

Pre-printing rheology is an important tool to determine bioink's potential for printing and the material's innate ability to deform and recover. Post crosslinking, image analysis of bioprinter inks provides additional information concerning spreading of bioinks. Several methods have been employed for to analyze the quality of the extruded bioink. The 3D printing process begins in

designing a print construct in a computer aided design program (AutoCAD, Solidworks, etc.). Depending on the design method, using the programmed dimensions of the construct and comparing to printed construct can be used. Light microscopy or μCT have been used to image printed constructs.[71, 135] Ouyang et al. have devised a system of images and equations to quantify the "printability" of the bioink.[136] Three classes of printability were established (under gelation, proper gelation, and over gelation) to describe the morphology of the extruded samples. Proper gelation bioinks exhibited smooth surface with regular grid pattern; under gelation bioinks flowed together creating circle pattern rather than square; over gelation bioinks had irregular grid pattern. Mathematically, printability was defined as $Pr = \frac{\pi}{4}\frac{1}{C} = \frac{L^2}{16A}$ where C is the circularity of the print, L is the length and A is the area. Pr values <1 indicate poor fidelity with spreading and large, curved corners. As the Pr approaches 1, the print is "exactly as it should be," with precise angles, smooth prints, and exact deposition of material. As Pr increases, the bioink became jammed or "crinkly"/rough. Ridges began to form, cracks became prominent, and the overall print was poorly constructed. Mathematically defining quality 3D prints is an important milestone for bioprinting literature.

1.4.2 Techniques to Monitor Cell-Material Interactions

Extracellular mechanics are influential to cell behavior.[137, 138, 139] Interactions between materials and cells can be carefully monitored through biological and mechanical methods. Pre-printing consideration of cytotoxicity can prompt a bioinks to be further investigated. While cytotoxicity is integral for understanding cell viability, mechanical forces due to adhesion or fluid shear stress

can also elucidate cell material interactions. Several techniques have been developed to study the influence of mechanics on cell adhesion.

1.4.2.1 Traction Force Microscopy

Traction force microscopy (TFM) is used to determine a single cell's traction force, or force that the cell pulls on the material. Typically, cells are cultured on a clear polyacrylamide gel functionalized with adhesive ligands and fluorescent beads are embedded just below the gel surface.[140] When the cell attachment occurs the cells generate a traction force that moves the fluorescent bead and movement is quantified by measuring the displacement of the fluorescent bead. This technique has been used to compare the cellular traction forces generated by human metastatic breast, prostate, and lung cancer cell lines and their non-metastatic cell line analogs. the traction forces of the metastatic cell lines was found to be higher.[141] With post-printing seeding of cells, TFM could be used to determine where cells are adhering to the bioink and subsequent movement. However, this requires an optically clear bioink and a flat surface on which to image. Alternatively, vinculin staining to monitor focal adhesion points elucidate cell binding.

1.4.2.2 Microfluidics

Cell adhesion post exposure to shear-rates can be studied through microfluidics which also monitor spreading and migration. The techniques aims to mimic the hemodynamic stress that cells exposed to within the body due to continuous fluid flow and does not fully replicate cells suspended in a bioink undergoing shear-stress. This system has many advantages such as fluid manipulation and control, miniaturization and low fluid intake. It also allows for dynamic culturing of cell adhesion studies. The balance between shear-stress forces generated by the fluid flow determines the cell

adhesion and the adhesion forces between membrane bound receptors and their ligands.[142] Previous research has established that cells in microfluidic environment have morphology and growth rates similar to that of Petri dishes.[143] Specifically, microfluidic channels has also been used to understand the difference in adhesion properties of blood cells and how they differ in case of sickle cell. [144] Post-shear cell viability of encapsulated cells has been of interest to several groups.[42, 71, 75] Within these experiments, observation of overall cell viability it performed using one of the cytotoxicity (most commonly Live/Dead assay) from Table 2.

1.4.2.3 Atomic Force Microscopy

AFM probe techniques involves measurement of how strongly a cell is adhered to the surface of the bioink. Immobilization of individual cells to the AFM cantilever occurs and then withdrawn at constant speed to free the cell from its binding site. The cantilever deflections during this process are recorded as force-distance curves and the highest forces is the cells adhesion strength. The techniques can used for measurement of both cell-cell adhesion forces and cell-matrix adhesion forces.[145] The limiting factor of using AFM in bioinks is that the cell must be on the surface of the printed construct. Fully 3D encapsulated cells cannot be sensed by the AFM probed without destruction of the printed construct.

1.4.2.4 Three-Dimensional Traction Force-Quantification (3D-TFM)

Alternative to the AFM and TFM, three-dimensional traction force quantification can be used to understand the cell behavior in 3D cultures. Fluorescent beads are embedded within the bioink prior to cell incorporation. Rheological properties can be changed due to the addition of the bead component and care should be taken to maintain consistent parameters. However, this method

allows us to better understand and predict the cell behavior within the bioink. Fraley et al[146] used this techniques to track the movement of focal adhesion proteins in the 3D matrix and establish their role in cell motility. 3D-TFM is a modification to TFM and does not require that cells be on the exterior of the sample being analyzed. Optically clear samples are preference due to the ability to clearly visualize the fluorescent beads.

1.4.2.5 ECM production and Estimation

Along with visualization of cells within or seeded on bioinks, quantification of deposited matrix and protein quantification enhances the understanding of how cell are behaving once encapsulated. The production of extracellular matrix (ECM) by cells is an important cellular event. In case of escalated cells, it becomes essential for cells to produce ECM to facilitate further proliferation over the scaffold. Native ECM is composed of various components such as proteins (collagen, elastin, and fibronectin) and GAGs (heparan sulphate, chondroitin sulphate etc). Hence, it is important to quantify the production of ECM components in case of 3D printed scaffold whose is to mimic the 3D architecture of the native tissues. Various methods can be employed for determining the individual components as listed below.

1.4.2.5.1 Collagen Production

Collagen is the most abundant protein within the human body and is an important ECM component. The most common methods for collagen estimation is the quantification of hydroxyproline in a sample buy dissolving the sample in Hycholoric acid followed by neutralization and further reaction with reagents such as chloramine T[147]. This method has a distinct drawback of being rather tedious and is effected by type of samples. Hence, simpler

colorimetric methods have been developed using dyes such as Sirius Red F3BA, which bind the specifically to collagen and show no specific binding with elastins[148]

1.4.2.5.2 GAG Quantification

There are five types of animal GAGs heparan sulfate (HS), chondroitin sulfate (CS), dermatan sulfate (DS), keratin sulfate (KS), and hyaluronan (HA), of which heparin is the most studied. There are two commonly used techniques for the quantification of GAGs, namely the Alcian Blue assay carbazole assay. The latter work on the principle of acid digestion of the polysaccharide followed by reaction with the carbazole to give a coloured product[149].However this methods has a distinct tendency to overestimate the concentration of the GAGs due to interference pH buffer components such as chloride ions (present in PBS)[150]. Alcian bye assay relies on the ability of sulfated GAGs to bind the cationic dye 1,9-dimethylmethylene blue[151] and hence is better suited for the quantification.

With both collagen and GAG quantification, standardization to the number of incorporated cells informs how active the cells are and if they are proliferating. Bioink properties should support similar amounts of the protein and GAG production and 2D controls.

1.5 Conclusions and Future Directions

Current analysis techniques for printing polymeric bioinks are widespread with little standardization within the field while cell-bioink interactions are well established. Increasingly, intricate architectures across several scales have been constructed though there remains an overall

lack of bioink formulations are methodology for predicting usefulness of a polymer as a bioink. Clinical application of direct write extrusion bioprinting requires bioinks that can be organized to replicate tissue organization, support cell proliferation and differentiation, and degrade at physiological time scales. The rheological properties of hydrogels and bioinks interact with the biological performance of the bioink, dictating the need for novel analysis techniques to monitor cell/material interactions during the printing process. Optimization of the rheological properties, specifically yield stress, may permit homogeneous cell incorporation and further optimization of the printing process can prolong the printing time. Often high resolution is sought in 3D printing, though recent studies suggest the high precision may not be necessary.[152, 153]

Overall, there is a lack of fundamental rheological understanding coupled with lack of biological techniques developed specifically for direct write 3D bioprinting. The forthcoming works aims to at least partially overcome the mechanical characterization in developing bioinks while continuing to utilize present biological techniques. First, a model bioink is formulated consisting of poly(ethylene glycol) and Laponite XLG.[71] Rheological characterization and relationships to literature are well formulated and established within the PEG/Laponite work. From there, modification to the bioink formulation via addition of Gelma and changing the PEG-backbone are completed. Gelma addition permit better cell binding and spreading within the bioink as measured via staining and microscopy. Modifying the PEG-backbone to be more hydrolytically susceptible modulated degradation times via an increase in ester hydrolysis. Lastly, Laponite XLG is investigated as a therapeutic delivery vehicle within collagen matrices as a potential angiogenic device. Taken together, the forthcoming works present advances in understanding the mechanics

governing bioinks and their subsequent macroscopic properties, ability to modulate adhesion, degradation, and therapeutic delivery.

2. NANOENGINEERED COLLOIDAL INKS FOR 3D BIOPRINTING*

2.1 Introduction

Nanoengineered biomaterials from polymer and nanoclays continue to generate interest in biomedical and biotechnological applications due to their ability to act as a barrier in controlled release devices and their support in tissue scaffolds.[154, 155, 156] Swelling clays are layered mineral sheets with isomorphous substitution in the inner layer that results in a permanent positive edge and negative face charge.[157] Due to the large variation in natural clays, Laponite® has become a model system with controllable features during the manufacturing process. Laponite are two-dimensional (2D) nanomaterials, 30-50 nm in diameter and 1-2 nm in thickness.[158] The hydration of Laponite and internal arrangements result in macroscopic solutions ranging from low viscosity solutions to highly ordered colloidal gels and Wigner glasses.[158] At low salt concentrations ($< 10^{-4}$ mM) Laponite (and other clays) remain stable in solution and interact with each other in a "house-of-cards" structure.[159, 160] However, with addition of salt, change in pH, or addition of polymer, the phase diagram and subsequent interactions are more difficult to determine. In order to determine precise interactions, various techniques are often used such as dynamic light scattering[161, 162], small angle neutron[163], or x-ray scattering.[160] Analogous to these techniques is viscosity characterization *via* shear rheology which further elucidates the internal structure as

---

macroscopic properties of the material.[164] Additional complexity of Laponite's internal structure occurs with polymer interactions such as gelatin,[165] kappa-carrageenan,[89] pluronics,[166, 167, 168] poly(N-isopropylacrylamide),[169, 170, 171] and poly(ethylene oxide)s[164, 172, 173, 174] due to adsorption/desorption of polymer, additional charge interactions, and ability of both polymer and Laponite to hydrate. Here, we investigate the rheological effect of adsorption/desorption of poly (ethylene glycol) (M_w=3400 Da) on Laponite at various concentrations and the potential for colloidal suspensions as three-dimensional printing inks.

Previously Nelson *et al* have investigated PEO (-CH2-CH2-O-) with low concentrations of Laponite *via* SANS and DLS measurements[164, 174] and rheological work completed by Schmidt *et al* with low concentrations of Laponite.[172, 175] Ruzicka *et al* have suggested that above concentration of 3% Laponite, a gel forming structure will result; however, this has not been widely investigated with the addition of polymer chains.[158, 176] Earlier work has extensively elucidated the interactions between poly (ethylene glycol/oxide) and Laponite.[164, 174, 177, 178, 179] Quickly desorbing/adsorbing PEG chains onto Laponite changes PEG-Laponite behavior which can be modeled as various fluids such as Newtonian or Bingham Plastic depending on the concentration of each component. Here, we aim to control these interactions for extrusion and bioprinting applications. Colloids show promise for three-dimensional (3D) printing applications since they can be precisely tuned to meet various parameters such as shear-thinning and recovery time.

3D printing materials have long been limited to thermoset polymers wherein polymer chemistry dictates their thermo-responsiveness.[180, 181, 182] Due to the temperatures at which they must be processed, these polymers often have limited biomedical applications both in their structure and in their ability to extrude living cells. Colloids and hydrogels can overcome the temperature and structure barriers present in current thermoset 3D inks. “Bioinks”, as they are often named, must be able to support cell viability (cytocompatible), recover quickly for printing, and have crosslinking mechanisms that are compatible with tissues.[34] Hydrogel precursors are often too fluidic to be considered for printing applications and crosslinked hydrogels are too brittle to deform through a needle without fracture. High viscosity colloid systems and nanocomposites fulfill the requirements of a bioink at rest. However, to be a printable system it must first shear-thin followed by a quick rebuilding of internal structure.[77, 183] Polymer/clay nanocomposites have previously been demonstrated as shear-thinning.[104, 184, 185] As such we further investigate the rheological implications between model clay and polymer system of poly(ethylene glycol) and Laponite for use in 3D bioprinting and cell delivery.

2.2 Materials and Experimental Procedure

2.2.1 Materials

Laponite XLG, procured from Byk Additive and Instruments was dried in the oven at 100°C for 4h to ensure limited environmental water swelling of particles. Poly (ethylene glycol) was dried before acrylate modification using procedures previously reported.[186] In short, 20 g PEG (3.4kDa) was dissolved in dichloromethane along with triethylamine (Sigma). Acryloyl chloride (Alfa Aesar) was added dropwise to the solution on ice and stirred for 24 hours. After washing, the

solution was precipitated into diethyl ether and dried over vacuum. ^{1}H NMR *300 MHz, $CDCl_3$, δ): 3.62 (s, 297H; -OCH_2CH_2), 5.81 (dd, 2H, J= 10.5 and 1.2 Hz; -$CH=CH_2$), 6.40 (dd, 2H, J = 17.3 and 1.5 Hz; -$CH=CH_2$) confirmed diacrylation of PEG3.4kDa.

2.2.2 Synthesis of PEG Laponite Colloids

The desired amount clay and PEGDA was dispersed into 18 MΩ water (pH=7.4) and vortexed vigorously for at least 2 minutes. For rheological time sweeps, samples were immediately loaded and tested. For all other experiments, the solutions were allowed to sit for 24 hours before use as determined by the initial time sweep. Samples were carefully loaded onto a Peltier plate base as to not disrupt internal structure formation. Once geometry was lowered, samples were allowed 15 minutes to equilibrate.

2.2.3 Rheological and Mechanical Characterization

A Discovery Hybrid Rheometer 2 (DHR-2) (TA Instruments) with attached 40 mm parallel plate at gap height of 0.25 mm and 25°C was used for all experiments. Pre-cursor solutions of PEG and PEG/XLG were used for all experiments unless otherwise noted. Rotational time sweeps were executed for 18 hours at 1Pa, 1Hz to determine aging time and dynamics of solutions. Rotational shear rate sweeps were executed between 10^{-6}-10^{3} (s^{-1}) to determine the yield stress and the power law region. Power-law parameter n (flow behavior index) was calculated using TRIOS software (TA Instruments). Rotational time sweeps were executed at three different shear rates (s^{-1}) in sequential order: 10^{-2} (60 s), 3000 (5s), 10^{-2} (120s) to determine shear recovery of solutions. Time

to 80% recovery was manually observed/calculated.[183] Oscillatory shear stress sweeps between 10^{-1}-10^{3} were performed at 1 Hz and frequency sweeps between 10^{-2}-10^{2} were performed at 10 Pa to further validate yield points and investigate dependence on frequency. Increasing stress was applied to the samples (1, 10, 50, 100, 300, 500, 1000 Pa) and storage modulus was monitored to further verify yield stress. Creep experiments were conducted by applying 50 Pa stress for 5 min followed by 15 minutes of recovery (no applied stress). Data from creep experiments were evaluated by attempted fitting of the creep region with the Burger model: $J_c(t) = J_0 + J_1\left[1 - \exp\left(-\frac{t}{\tau}\right)\right] + t/\eta$ $J_C(t)$ is the compliance of samples measured by the instrument at time *t*. J_0 is the instantaneous compliance and J_1 is the retarded compliance corresponding to Maxwell and Kelvin-Voigt elements respectively. τ is the retardation time and η is the Newtonian viscosity. Ultra-violet curing of samples at 7 mW/cm^2 occurred, and subsequent oscillatory frequency and stress sweeps as described above were conducted on cured hydrogel samples. An ADMET eXpert 7600 Single Column Testing System equipped with 25 lb load cell was used for compression testing of 3D printed and cast (bulk) hydrogel. Strain rate of 1 mm/min was used to compress the samples 50% of original height. The compressive modulus was calculated and plotted to compare bulk versus 3D printed structures. Print fidelity was calculated as: $\left(\frac{Actual\ Print}{Programmed\ Print} - 1\right) * 100$

2.2.4 *In vitro* Studies

Murine preosteoblasts (NIH MC3T3 E1-4, ATCC) were grown in alpha modified MEM (Hyclone, GE Lifesciences), supplement with 10% fetal bovine serum, and passaged at 80% confluency. Passages 4-6 were used for all experiments. After passaging, counting was completed and cells

were re-suspended and aliquoted into Eppendorf tubes at 10,000 cells per mL solution. Solutions were gently pipetted or mixed to achieve a homogeneous cell distribution. To visualize cells encapsulated within bioinks, cells were incubated at 37 °C with 2 μM Cell Tracker Green Dye (ThermoFisher) in 1X PBS for 30 minutes prior to passaging. Cell imaging was performed using a (SteREO Discovery.V8, Carl Zeiss) microscope after extrusion. Images were processed and analyzed in ImageJ (NIH) to quantify localization of extruded samples.

2.2.5 3D Printing

PEG-Laponite constructs were fabricated utilizing a HYREL System 30M 3D printer. The PEG-Laponite colloid was loaded into a HYREL VOL-25 extruder (HYREL L.L.C., Norcross, GA) equipped with a luer lock adapter and 23 gauge, 5 mm long blunted stainless steel needle (Jensen Global Inc, Santa Barbara, CA). Once connected to the printer, constructs were modeled in Solidworks 3D CAD Design, exported as an STL file, and imported into Slic3r version 1.2.9. Overall, this process converts the Solidworks design into layer-by-layer instructions for the printer, or G-code. The G-code files are then imported into HYREL's proprietary software (Repetrel Rev2.828) and printed at room temperature onto glass slides. Upon completion, glass slides were placed under a UV lamp and photo-crosslinked for 150 seconds at an intensity of 25 mw/cm^2

2.2.6 Statistical Methods

The data is presented as the means ± standard deviations of the experiments (n=3-5). Statistical analysis was performed via one-way ANOVA with post-hoc Tukey's test using GraphPad Prism

(version 6.01). Levels of significance were assigned as * = $p<0.05$, ** = $p<0.005$, *** = $p<0.0005$, and **** = $p<0.0001$.

2.3 Results and Discussion

2.3.1 Colloidal Bioink Synthesis

Laponite XLG has a complex phase diagram that ranges from sols and gels to attractive and Wigner glasses.[158] Being a synthetic clay, the production process of Laponite precisely controls its size, shape, and chemical make-up, therefore it has been used as a model clay system. However, groups such as Ruzicka *et al.* and Yoshi *et al.* continue to investigate various aspects of Laponite exfoliation, nematic order, and structure through means such as dynamic light scattering[164], rheology[172], and SANS/SAXS.[166, 174] The addition of polymer, regardless of molecular weight, results in ongoing adsorption and desorption of polymer to clay platelets which may alter the phase diagram boundaries of Laponite. We aim to use the reported internal "house-of-cards" structure of Laponite as a suitable matrix for three-dimensional printing.[158] Gel forming solutions of poly(ethylene glycol) (10% wt./vol, 3.4 kDa) occurred with concentrations above 4% Laponite after 24 hours. Over longer periods of time (months), solutions containing 2% Laponite will form a gel but can easily be disturbed and liquefy, and subsequently must undergo aging once more. Mourchid *et al*, Ruzicka *et al*, and others suggest that Laponite XLG form a "house-of-card" structure upon exfoliation or hydration of particles.[159, 176] This internal structure has been previously studied *via* dynamic light scattering.[187] The build-up of structure resulted in an increase in solution viscosity which can be useful for three-dimensional printing applications (Figure 2-1a). Time sweeps (1Hz, 1 Pa) indicated that there is a delay in PEG-Laponite XLG gel formation at

initial time points as indicative of increasing storage modulus (Figure 2-1b). This may be due to competition between Laponite and PEG becoming fully hydrated or rapid adsorption and desorption of PEG to the Laponite particles.[179] Samples containing 6% Laponite were removed for graph clarity. At longer time points (18+ hrs) the shear storage modulus (G') was concentration dependent based on how much space was filled within the solution and by how much water adsorbed to the surface of the Laponite.

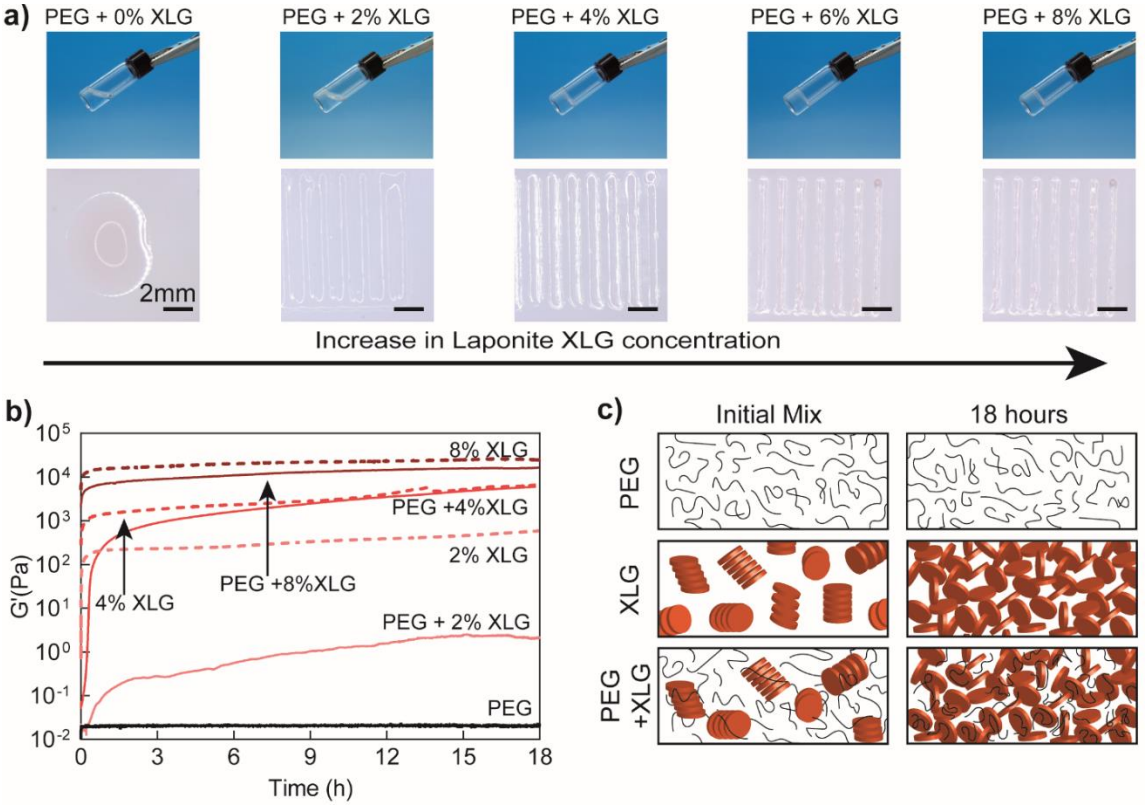

Figure 2-1. Synthesis of PEG-Laponite colloidal solution. (a) Viscosity increases at rest with increasing Laponite XLG concentration; Changes in print quality with increase of Laponite XLG concentration; (b) Time sweep of solutions of PEG/Laponite, PEG, and Laponite; (c) schematic of internal structure formation of PEG, Laponite, and PEG/Laponite solutions

PEG concentration was kept constant at 10% wt./vol while Laponite XLG concentration was varied. Here we observed that PEG solutions containing 2% wt./vol Laponite XLG did not form a strong internal structure after 18 hrs. In addition, at any given concentration of Laponite XLG, the addition of PEG either decreased the storage modulus or increased the time for storage modulus plateau to occur. Nuclear magnetic resonance spectroscopy (NMR) analysis by Lorthioir *et al.* suggests that PEG/Laponite systems are dynamic yet have strong local constraints that slow down segmental motions of the PEG backbone[179] suggesting the observed decrease in storage modulus is most likely due to intermolecular motions of PEG ad/desorbing from the surface of Laponite XLG. Solutions seemingly underwent a shift from tactoid sheets and random polymer configuration to a disconnected "house-of-cards" with PEG adsorbed on the surface (Figure 2-1c). Particles underwent what is known as jamming transition during which movement is restricted since there is no physical space within the solution thus lowering the amount of free energy required to remain in suspension.[177, 178, 188] A flocculation was avoided by balancing the colloid electrostatic repulsions and attractive van der Waals forces.[189]

2.3.2 Addition of Laponite to PEG results in Shear-thinning Bioink

After the time-aging of solutions occurred, the solutions were still able to flow with an applied stress or an induced shear rate.[172] Subsequently, the solution was broken down with an increase in shear rate (Figure 2-2a). Previous studies suggest that there are two flow regions of Laponite with an induced shear rate: plug-like flow and Newtonian-like flow. [190]

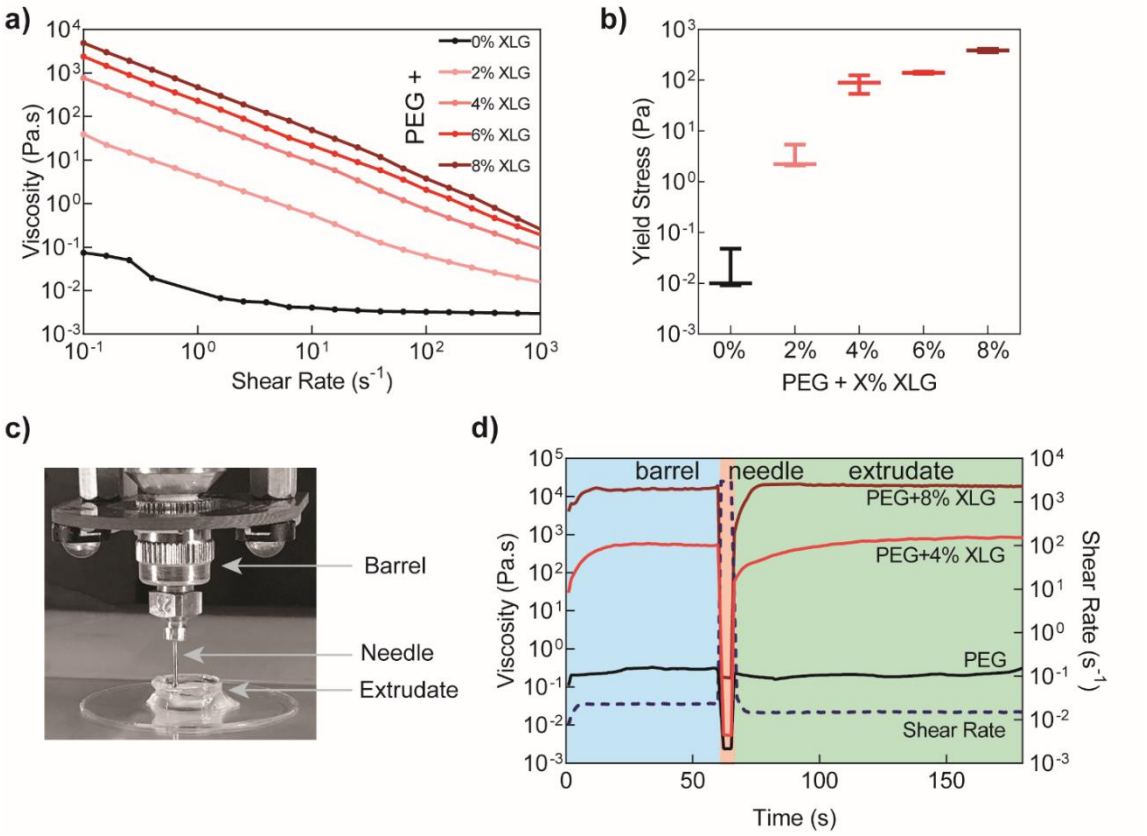

Figure 2-2. Laponite induces shear-thinning characteristics to PEG solution. (a) Shear Rate Sweep of PEG/Laponites suspensions; (b) yield stress quantification of PEG/Laponite concentrations; (c) illustration of extrusion through a syringe barrel, needle, and onto print-bed; (d) peak hold experiments to mimic flow during extrusion/printing.

During and after the transition of flow types, it is suggested that the internal network is broken into smaller blocks that freely move as solid bodies within a fluidic matrix. Thus, PEG/Laponite XLG materials must overcome a yield stress before they can be smoothly extruded or printed (Figure 2-2b). Several fluid models can be used to describe PEG/Laponite XLG systems such as Herschel-Bulkley model or shear-thinning model. During printing application, shear-rate is determined according to equation 1: $\dot{\gamma}=\frac{3n+1}{4n}*\frac{4Q}{\pi R^3}$. Where *n* is the shear-thinning index, Q is the volumetric flow

rate and R is the radius of the annulus. It was determined that shear-rates experienced in typical printing parameters (Q = 300 µL/min, R = radius of gauged needle) are between 10^{-1}-10^{3} s^{-1}. The shear-thinning index is determined by power law fitting of the viscosity vs shear rate curve as described in equation 2: $\eta = K\dot{\gamma}^{n-1}$. Where η is viscosity, *K* is the flow consistency index (defined as the viscosity when shear-rate is 1 s^{-1}), and *n* is the shear-thinning index. Table 2-1 summarizes the *K* and *n* values.

Table 2-1. Summary of Power-law parameters for PEG/Laponite XLG solutions.

	PEG (10% wt./vol) + X % (wt./vol) Laponite XLG				
	0	2	4	6	8
n	0.96 ± 0.02	0.22 ± 0.10	0.20 ± 0.16	0.22 ± 0.27	0.29 ± 0.05
K	0.0029 ± 0.0003	6 ± 1	60± 34	149± 24	169 ± 43

Addition of Laponite XLG decreased *n* due to disruption of balance between the van der Waals and electrostatic forces. *K* increased due to a close packed "house-of-cards" structure where the repulsion forces are balanced with attractive forces. There was a denser packed "house-of-cards" (edge to face platelet orientation) internal structure[191] of samples containing 6% and 8% Laponite XLG when compared to 2% and 4% containing samples, which resulted in an overall increase in viscosity across all shear rates (Figure 2-2a). The power law index can describe the degree of shear-thinning a solution exhibits. When n=1, the solution is Newtonian; n<1 shear-thinning; n>1 shear thickening. With any addition of Laponite there was a significant decrease in *n* compared to PEG solutions, suggesting that Laponite is the cause of shear-thinning. With an induced shear, Laponite orients itself parallel to the direction of flow.[172] It is suggested that due to electrostatic

charge, two parallel Laponite particles repel each other therefore gliding over each other to produce a shear-thinning fluid. While numerical values are not significantly different, it is hypothesized that larger or more numerous sections of the PEG/4-8% Laponite solutions are flowing within the medium and have not fully broken up.[190] Previous work has analyzed shear-induced flow of clay nanoparticles (3% wt./vol), supporting a decrease in viscosity with an increase in shear rate.[172, 190, 191, 192]

Injection and extrusion based direct write 3D printing materials must first meet the criteria for shear-thinning, which describes the change from soft-solid/gel to fluid/low viscosity ($\eta < 100$ Pa.s). Once material has exited the end of the deposition needle, re-building time of the internal structure can predict the amount of localization versus spreading and its ability to be used in 3D printing. As such, unidirectional flow through a syringe and needle (Figure 2-2c) were modeled using rheometry (Figure 2-2d). Rheometry was used to quantify the solution's "printability" by observing the change in viscosity with a change in shear rate. During initial stages, solutions are in a barrel and experience low shear rate ($<10^0$ s^{-1}). Once solutions enter the needle shear-rates increase to upwards of 10^2-10^4 s^{-1} depending on volumetric flow rate. Once exited, the flow stops and the material must quickly regain viscosity—viscosities above ~10^2 Pa.s were desirable as they have previously been reported as printable.[75, 193] The viscosity change over time, induced by changes in shear rate (Figure 2-2d), can indicate how quickly a solution rebuilds (thixotropy) thereby elucidating its usefulness as an ink. PEG behaved as a fluid across all shear rates and variation in the viscosity measurement was attributed to surface tension between solution and the upper geometry. Solutions containing Laponite XLG underwent rapid breakdown and rebuild.

Recovery of 80% of initial viscosity was considered significant. Increasing Laponite XLG concentrations decreased the recovery time due to incomplete destruction of internal "house-of-cards" structure (Figure A1). In solutions containing greater concentrations of Laponite XLG, larger sections of polymer/clay mixture exist and therefore can quickly agglomerate compared to 4% containing samples. Balance between solution yield stress, ability to shear-thin, and structure rebuilding must be optimized for injection and printing applications.

2.3.3 Laponite Increases Mechanical Stability of Colloidal Bioink

PEG/Laponite XLG mixtures can be described both as highly viscous fluids and as soft solids. As such, we continued investigating *via* oscillatory rheometry with stress and frequency sweeps to determine shear storage modulus (G') and any dependency on stress or frequency of uncrosslinked samples. PEG behaved as a Newtonian fluid with an increase in applied frequency (Figure 2-3a). With an increase in frequency, the storage modulus increased as the PEG solution responded to increasing frequency. Formation of an internal structure *via* the addition of Laponite XLG negated all frequency dependencies of the fluid. Increased storage modulus was observed and attributed to an increase in fill volume/decrease of free space for water movement. Increasing Laponite XLG concentration increased G' in a similar fashion to the increased viscosity. Further, frequency sweeps were used to determine the linear viscoelastic region for samples. Stress sweeps (Figure 2-3b) were used to verify trends in yield point (though yield point was determined *via* rotational tests as previously discussed). Oscillatory stress sweeps resulted in cross-over points (G'<G") of 6.48 ± 2.07, 35.25 ± 17.56, 147.61± 18.82, 297.13 ± 79.62, and 544.37 ± 74.89 Pa for samples that contained 0, 2, 4, 6, and 8% Laponite respectively. Again, with increasing concentrations of

Laponite XLG an increase in storage modulus was presented. Solutions with 8% wt./vol Laponite were statistically significant ($p<0.0001$) compared to all other compositions for both frequency and stress sweeps (Figure 2-3c). As further verification of yield stress, an increasing amount of stress was applied to uncrosslinked PEG/Laponite samples (Figure 2-3d). Rapid breakdown of structure occurred once applied stress was above the yield stress. Storage modulus recovery for PEG solutions was nonexistent while PEG/4% Laponite solutions recovered 50.3% of storage modulus and PEG/8% Laponite solutions recovered 58.7% of the storage modulus. Storage modulus remained > 500 Pa for all recovered samples. The effect of Laponite on the viscoelastic properties of PEG precursor solutions is most evident through creep experiments. By fitting the creep curves of samples with Burger's model,[194] J_0, J_1, τ, and η were obtained (Figure 2-3e). Representative creep curves highlight the recovery for samples containing Laponite XLG as compared to PEG. The PEG compliance curve showed high compliance but no recovery. Compliance is inversely proportional to modulus which corroborated data presented in Figure 2-3a&b. Samples of PEG/ 4 & 8% Laponite XLG exhibited recovery due to possible polymer bridging of Laponite XLG particles which are able to store accumulated strain in the sample and then release as elastic recovery upon relaxation (cessation of applied stress).[195] Storage modulus and viscosity both indicate if a material can support itself without external support material. In particular, viscosity recovery after shear dictates the ease of incorporating cells for use as bioinks. Quick material recovery suggests incorporation of cells may need to be pipetted multiple times. As such, 4% Laponite XLG samples were chosen for printing applications as it balances the viscosity recovery and storage modulus.

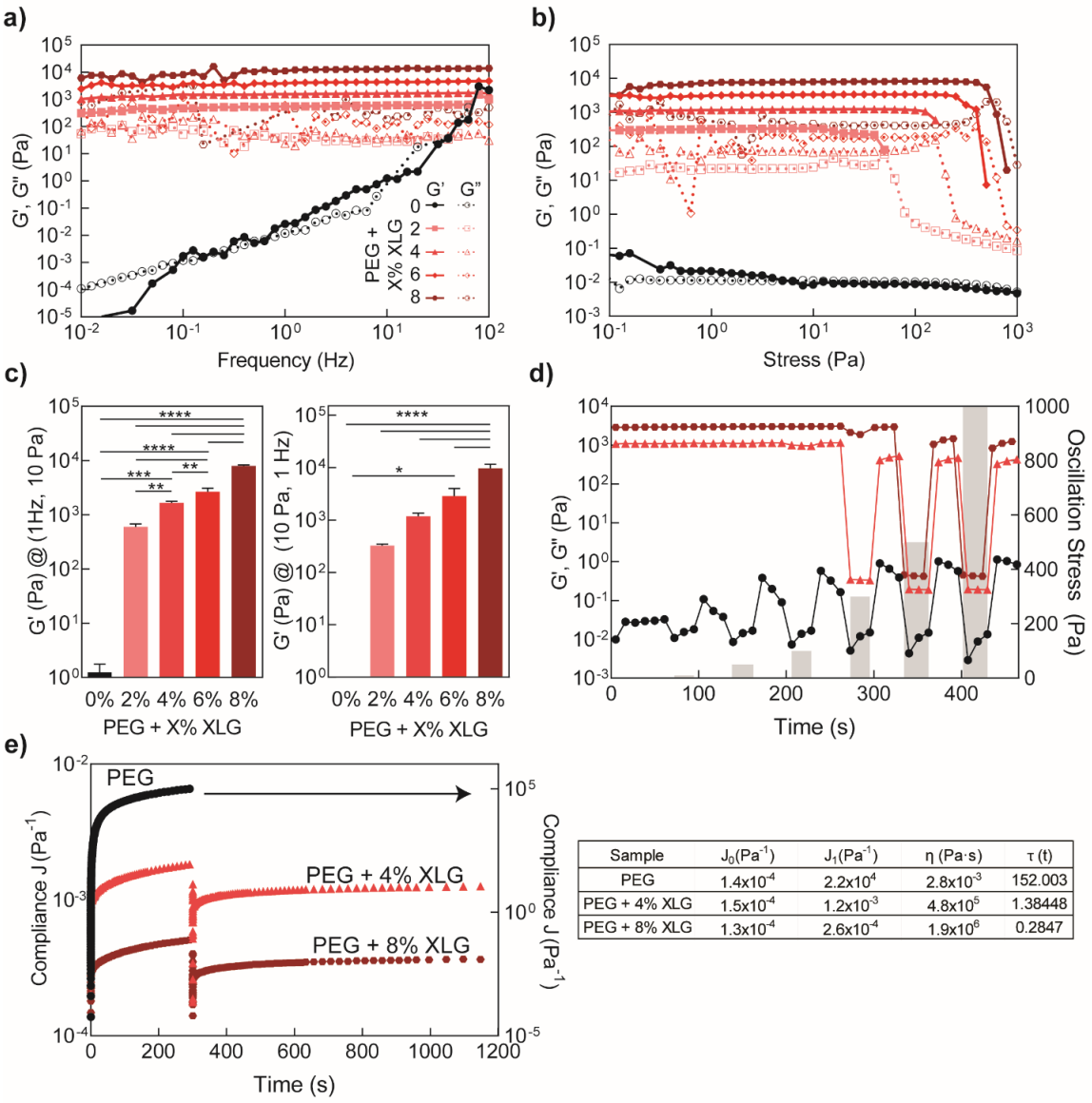

Sample	J_0(Pa^{-1})	J_1(Pa^{-1})	η (Pa·s)	τ (t)
PEG	1.4×10^{-4}	2.2×10^{4}	2.8×10^{-3}	152.003
PEG + 4% XLG	1.5×10^{-4}	1.2×10^{-3}	4.8×10^{5}	1.38448
PEG + 8% XLG	1.3×10^{-4}	2.6×10^{-4}	1.9×10^{6}	0.2847

Figure 2-3. Rheological sweeps of uncrosslinked PEG/Laponite suspensions (a) Frequency sweeps from 10^{-2}-10^{2} Hz; (b) stress sweeps from 10^{-1}-10^{3} Pa; (c) storage modulus at 1Hz from samples; storage modulus at 10 Pa from samples. For all data, * indicates $p<0.05$, **$p<0.005$, ***$p<0.0005$, ****$p<0.0001$ (d) Increasing applied stress with monitored storage modulus; (e) Representative creep and recovery curves for PEG/Laponite solutions. PEG plotted on right y-axis (as indicated by arrow), PEG/4% & 8% are plotted on left y-axis.

2.3.4 3D Bioprinting Using Colloidal Bioinks

Localization of cells and therapeutics is of utmost importance for biomedical applications. Within literature, shear-thinning has been the focus for printing applications as it will dictate a material's ability to flow through a needle.[196, 197, 198, 199] Once the material has exited the needle the shear forces placed on the material cease and recovery (Figure 2-2d) will indicate final placement of extrudate compared to the material's ability to shear-thin. Therefore, the materials we developed have the potential for printing applications. To demonstrate bioprinting applications, murine pre-osteoblasts were incorporated into PEG/4% Laponite and printed to create a circle and crosshatch shapes (Figure 2-4a &b). Printed constructs of PEG/4% Laponite achieved heights up to 23 layers tall without support material or collapse. Low amounts of spreading occurred for PEG/4%Laponite solutions as predicted through the peak hold tests (Figure 2d). Localization of cell delivery occurred with PEG/4% Laponite samples compared to PEG and phosphate buffered saline solution (PBS) samples as measured *via* cell tracker experiments (Figure A2). The amount of spreading (print fidelity) as indicated by the separation of the red and white lines indicate that PEG/4% Laponite samples have more precise local delivery and shorter recovery time compared to PEG or PBS. There was a statistically significant difference ($p<0.0001$) between PBS and PEG/4% Laponite printed structures as well as between PEG and PEG/4% Laponite in terms of print fidelity.

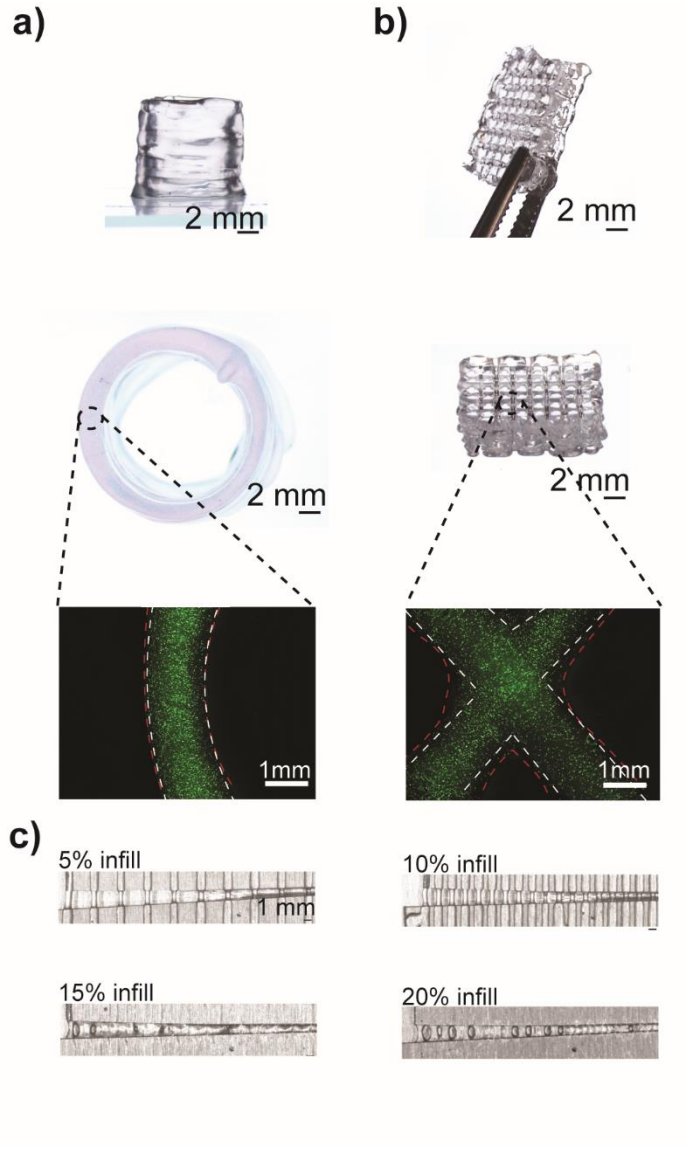

Figure 2-4. Bioprinting of colloidal inks. (a) 3D printed circle of PEG/4% Laponite with preosteoblasts and cell tracker images (b) 3D printed crosshatch structure of PEG/4% Laponite with preosteoblasts and cell tracker images. Note: For both (a) and (b) white dashed lines represent the programed print path and red dashed lines represent the 3D printed contruct. (c) PEG/4% Laponite bridging gaps up to 2.5 mm.

PEG/4% Laponite resulted in structures 7.78 ± 19.75% larger than designed while PEG structures spread 413.1 ± 76.84 % and PBS spread 376.4 ± 47.27%. The lack of spreading permitted PEG/4%

Laponite bridging a gap of 2.5mm across a variety (5-20%) of infill density (Figure 2-4c). While PEG/6% and 8% Laponite samples have higher storage modulus (Figure 2-3c) and viscosity (Figure 2-2a), inhomogeneous incorporation of cells was observed due to high yield stress and quick recovery times. As cells were added to the solution, they were unable to flow within the solution as it presented itself as a solid object rather than a viscous colloid. For PEG/4% Laponite, live/dead (Figure A3) indicated that across several volumetric flow rates (500, 1000, 2000 μL/min) there was no difference in viability immediately post injection. Two-dimensional seeding of pre-osteoblasts on PEG/Laponite hydrogels and subsequent proliferation have previously been reported.[200, 201, 202, 203] In addition, long term cell viability, up to three weeks, within PEG-based hydrogels has been demonstrated with osteoblasts, chondrocytes, HUVECs, and β-cells in previous studies.[204, 205, 206, 207] To facilitate long-term cell viability, the macro-porous structure can be controlled through changing the density of the crosshatch layer, as demonstrated in Fig 4b, aiding nutrient administration and waste removal. Printing of solutions is a macroscopic physical representation of the rheological properties of uncrosslinked solutions. Printed structures exhibited low sagging and precision in deposition. Cell tracker and live/dead images coupled with printing images indicated that PEG/Laponite rheological properties meet the requirements necessary for bioprinting.

2.3.5 Covalently Crosslinked Colloidal Bioinks

In the 3D printing process, the uncrosslinked hydrogel is extruded until print completion and subsequently exposed to ultraviolet light for crosslinking to occur. 3D printed structures using colloidal bioink showed high mechanical stiffness and could sustain mechanical deformation

(Figure 2-5a). Compressive modulus of print and cast hydrogels were compared and no difference was observed as determined with a Student's t-test. Printed structures may develop anisotropy due to particle alignment.[36] However anisotropy was observed in PEG/Laponite, suggesting that the internal "house-of-cards" Laponite structure was conserved during extrusion. Oscillatory shear experiments of crosslinked hydrogels were used to determine viscoelastic properties. Hydrogels were UV crosslinked and subjected to oscillatory shear stress (1Hz) and frequency sweep (1 Pa) experiments, and the materials' response in terms of elastic moduli (G') and viscous moduli (G") were measured. All hydrogels were found to have a large viscoelastic plateau within the range measured. Interestingly, PEG hydrogels were not dependent on frequency (Figure 2-5b) compared to uncrosslinked samples (Figure 2-3a). Prior to UV crosslinking an internal network was not present within PEG, after UV crosslinking covalent bonds are formed between PEG chains therefore storing energy put into the system. Covalent bonds require more energy to break compared to electro-static attractive forces that dominate in uncrosslinked samples leading to stability across frequency and stress ranges. Internal structure was not broken down within crosslinked hydrogels during a stress sweep; however, it is noted that the viscous modulus (G") is highly variable suggesting internal rearrangement of polymer and Laponite structure. Further stress sweep experiments (Figure 2-5c) suggested that upon crosslinking the samples do not mechanically yield within the experimental range and there is no decrease in storage modulus. Again, the presence of covalent crosslinking prevented yielding of the material as covalent bonds are much stronger compared to weak electrostatic interactions occurring in uncrosslinked colloids. These results, when coupled with the uncrosslinked flow parameters, suggest that PEG/Laponite samples are effective both in extrusion/printing applications and as a stable matrix once crosslinked.

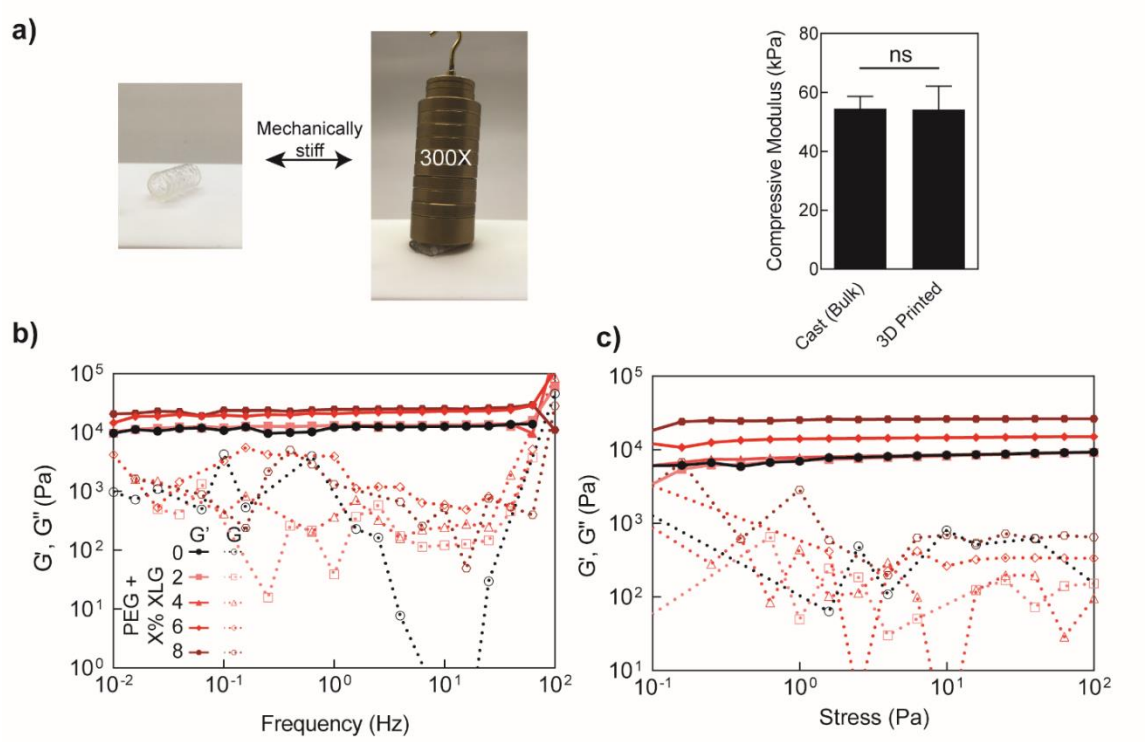

Figure 2-5. Covalently crosslinked PEG-Laponite network. (a) Covalently crosslinked 3D printed structure using PEG/Laponite bioink shows high mechanical stiffness and elasticity. Compressive modulus of PEG/4% Laponite for cast and 3D printed constructs. Rheological sweeps of crosslinked PEG/Laponite suspensions (b) Frequency sweeps from 10^{-2}-10^{2} Hz; (c) stress sweeps from 10^{-1}-10^{3} Pa

2.4 Conclusions

This study has investigated the rheological modification of PEG precursor solutions *via* incorporation of Laponite XLG clay nanoparticles. PEG/Laponite XLG form internal "house-of-cards" structure, influencing fluid flow and ability to print and reform structures. Laponite XLG addition to PEG reduced the flow behavior index and reduced the recovery time of solutions from infinite (Newtonian fluid) to seconds which is more appropriate for bioprinting applications.

The rheological behavior of the samples was found to be dominated by the behavior of Laponite network, independent of PEG addition. Recovery time of samples was controlled by the PEG:Laponite ratio and ability of Laponite XLG to interact with itself to form "house-of-cards" structure. Rapid adsorption or excess of PEG prohibits necessary charge-charge interactions between Laponite particles, concentrations of Laponite below 4% wt./vol with 10% wt./vol PEG (3.4 kDa) are unable to recover quickly. For practical applications, electrostatic repulsion and van der Waals attractive forces must be balanced. PEG presents a special situation due to the extensive literature available supporting strong interactions between Laponite and polymer. The present study combines rheological properties with application to show that appropriate concentrations of PEG/Laponite suspensions can be used as an appropriate bioink. While this work gives unique insight into the macroscopic use of PEG/Laponite as a bioink, structural information is obtained from previous work by others.[164, 172, 174, 208, 209, 210] We believe the present study complements both colloidal literature and biomedical literature in balancing colloidal forces and methods of study with appropriate cellular assays to optimize bioinks. We have proposed linear PEG/Laponite interactions and subsequent rheological profile for bioink characterization to determine critical parameters necessary for bioinks before more complicated systems are developed.

3. ELASTOMERIC CELL-LADEN NANOCOMPOSITE MICROFIBERS FOR ENGINEERING COMPLEX TISSUES[*]

3.1 Introduction

Complex tissue structures are difficult to mimic from a biomedical engineering perspective due to the complexity associated with its native structure at multiple length scales. Often, biomaterials are developed as stand-alone implants with bulk properties and interdependent biophysical properties such as bio-adhesivity and/or mechanical strength. As biomaterial design progresses, biomimetic design can address some of the challenges needed to engineer complex tissue.[211, 212, 213] The need to mimic the tissue architecture along with the ability to control or enhance cell adhesion and proliferation is a challenge to traditional tissue engineering approaches. Many complex tissues such as bone, muscle, tendon and ligament have microarchitectures that have not yet been efficiently recapitulated using existing biomaterials.

Hydrogel chemistry and fabrication has quickly morphed into a paradigm for tissue engineering since its inception.[214, 215] Mechanically robust synthetic systems are often sought and studied, while naturally occurring polymers are often inadequate to fully meet the mechanical requirement for implantation. Poly (ethylene glycol) (PEG) has demonstrated biocompatibility in a wide variety of

[*] Reprinted with permission from "Peak, C. W.; Carrow, J. K.; Thakur, A.; Singh, A.; Gaharwar, A. K. Elastomeric Cell-Laden Nanocomposite Microfibers for Engineering Complex Tissues. *Cel. Mol. Bioeng.* **2015,** *8* (3), 404-415." Copyright 2015 by Springer.

biomedical applications spanning drug delivery to tissue engineering.[32, 215, 216, 217] However, due to its inert chemical composition, PEG in its pure form has limited applications as a scaffolding material.[3, 218, 219] In order to fully take advantage of the PEG network, supplementary additives are used. Natural polymers, like gelatin, enable cell-driven degradation to augment migration throughout the matrix and also provide unique amino-acid sequences for mediated binding to the substrate.[220, 221, 222] However, gelatin cannot covalently crosslink in networks; therefore, gelatin methacrylate (GelMA) is used.[222] GelMA provides advantages in processing when compared to collagen semi-interpenetrating hydrogels or polymer backbones that use degradable or biologically relevant sequences.[223, 224, 225] We have focused on incorporating gelatin within PEG hydrogels to modulate cell adhesion and improve the biomaterial degradation characteristics. This is an advantage over current methods due to the simplicity of design.

Recently, there has been significant interest in manufacturing bioadhesive hydrogel matrices, [226, 227] including nanocomposite hydrogels[228, 229, 230] that offer unique advantages over conventional single polymer hydrogels. For example, to design a bioactive hydrogels for bone regeneration, bioactive nanoparticles such as hydroxyapatite, synthetic silicates or bioactive glass can be incorporated with in polymeric matrix. Recently, we have reported that synthetic silicates, a class of ultrathin nanomaterials, incorporated within gelatin hydrogel can up regulate production of osteo-related proteins and deposition of mineralized extracellular matrix.[231, 232, 233] In addition, we have also reported that silicates when incorporated into a poly(ethylene oxide) (PEO) matrix can control cell adhesion, spreading and proliferation[234, 235] Due to their unique shape and surface charge characteristic, silicate nanoparticles interacts with gelatin[233, 236] and PEG[237] resulting in shear-thinning and viscoelastic network. [186, 202, 238, 239] Silicate loaded hydrogels are biocompatible

and biodegradable under *in vivo* conditions and can be used for a range of biomedical and biotechnological applications. [233, 236] Recently, using Michael-addition based reactions and silicate nanoparticles and gelatin, we have recently reported an interpenetrating network (IPN) that enabled independent control over adhesive ligand availability and tissue stiffness for tumor cell engineering.[229]

Here, we engineer a multicomponent semi-IPN hydrogels as elastomeric microfibers with enhanced cell adhesion characteristics. By combining PEG with silicates nanoparticles, elastomeric and mechanically stiff microfibers can be engineered that allow mimicking viscoelastic characteristic of native tissues. The addition of gelatin to PEG/silicates nanocomposite provides additional control over degradation properties. By designing this multi-component system, we propose to engineer cell adhesive biomaterials with elastomeric properties.

3.2 Materials and Methods

3.2.1 Materials

Synthetic silicate nanoparticles (Silicates) (Laponite XLG) were obtained from BYK-Chemie GmbH (Wesel, Germany). Poly (ethylene glycol) (M_W = 10 kDa), Gelatin (300 g Bloom, type A) from porcine skin, and methacrylic anhydride were purchased from Sigma-Aldrich (St. Louis, MO). Acryloyl chloride and triethylamine were purchased from Alfa Aesar (Ward Hill, MA). Poly (ethylene glycol)-diacrylate (PEG) and gelatin methacrylate (GelMA) were synthesized as previously described [220, 240]. For proliferation studies, preosteoblast cell type MC3T3-E1 Subclone 4 were used (ATCC®CRL-2593). Fluorescent cell types for encapsulation visualization were a

transfected green fluorescent protein (GFP) NIH 3T3 from Cell Biolabs (San Diego, CA) and a red fluorescent protein (RFP) transfected osteosarcoma (MOSJ, donated by the Kaunas Lab, Biomedical Engineering Department, Texas A&M University).

3.2.2 Nanocomposite Formulation

Stock solution of 8% (w/v) silicate was prepared in milliQ water by vigorous agitation at 4 ºC. Ciba® IRGACURE® 2959 (Ciba Specialty Chemical, USA), UV photoinitiator (PI), stock solution of 0.6% (w/v) was prepared in milliQ water. The nanocomposite prepolymer solution were fabricated by vortexing silicate stock with PI stock and dissolving in 5% PEG (10 kDa) and 1% GelMA. Vortexing and centrifugation ensure proper mixing of solution. The nanocomposite prepolymer solution was injected in 10X phosphate buffer saline (PBS) using glass micropipette (Drummond) of different diameters to obtain physically crosslinked microfibers. These microfibers were subjected to ultraviolet (UV) radiation (320-500 nm) (Omnicure S200, Lumen Dynamics, Canada) for 10 seconds at an intensity of 8 mW/cm^2. PEG and PEG/GelMA solutions do not form fiber structures when placed in PBS or media.

3.2.3 Chemical Characterization

Attenuated total infrared reflection (ATIR) was performed using Bruker vector-22 FTIR spectrophotometer (PIKE technologies, USA) on all hydrogel compositions. Zeta potentials and hydrodynamic size of PEG, PEG/GelMA, PEG/Silicates, and PEG/GelMA/Silicates precursor solutions were determined in ultrapure water (Milli-Q) using a 633 nm laser in a Malvern ZEN3600 (Malvern Instruments, U.K.). Scanning electron microscopy (SEM) images of the

lyophilized hydrogels were obtained using a SEM, FEI Quanta 600 FE-SEM, USA fitted with Oxford EDS system) at an accelerating voltage of 20 KV.

3.2.4 Nanocomposite Hydration and Degradation

Nanocomposite samples were placed in 1.5 mL Eppendorf tubes and weighed. Each sample was frozen, lyophilized and weighed. Comparing the wet weight to dry weight, hydration degree was calculated. Accelerated degradation was performed in presence of collagenase Type II (Worthington Biochemicals, USA) solution (5 units/mL) in PBS at 25^{o}C while shaken. Comparison of fully hydrated wet weight to collagenase treated wet weight determined the % mass remaining.

3.2.5 Biological Characterization

For cell spreading, preosteoblasts were seeded onto UV sterilized bulk polymer compositions in a 96-well plate at a density of 10,000 cells/mL. At each time point, cells were washed in PBS, fixed with 2% glutaraldehyde for 12 minutes at room temperature, permeated with 0.1% Triton X-100 for 5 minutes, then incubated with rhodamine phalloidin for 20 minutes at 37°C followed by DAPI for 5 minutes. The samples were removed from the wells and inverted onto glass coverslips for fluorescence imaging. Cell area was calculated using software ImageJ (NIH, Bethesda, MD) and normalized with number of cell nuclei. For encapsulation, prepolymer solutions were physically mixed with a concentrated cell pellet of interest. The solution was then collected in a 1 mL syringe and extruded into media, in which the fibers would maintain shape due to physical crosslinking. UV light was then utilized for further crosslinking as previously explained. An additional cell type

could be added to the surface of the fibers via adding a cell suspension dropwise to a petri dish containing media and fibers with encapsulated cells. Encapsulated preosteoblast viability was evaluated using Calcein AM and Ethidium Homodimer staining (Life Technologies, Carlsbad, CA). Cell cycle analysis was performed using the BD Accuri C6 Flow Cytometer and propidium iodine (PI) stain following manufacture's protocol. In short, cells seeded on each composition were trypsinized at two separate time points and fixed in cold 70% ethanol. Cell pellets were formed and washed in PBS, followed by incubation in a PI staining solution at 37℃ for 30 minutes. Cells were stored at 4℃ until analysis. Focal adhesion studies were performed by encapsulating mouse embryonic fibroblasts expressing vinculin fused to eGFP (vinculin T12) in PEG hydrogels.[241, 242] Vinculin localization was imaged using fluorescence microscopy.

3.2.6 Mechanical and Rheological Analysis

An ADMET eXpert 7600 Single Column Testing System equipped with 25 lb load cell was used for compression testing. Strain rate of 1 mm/min was used to compress the samples 50% of original height. The compressive modulus was calculated and plotted versus the sample composition. An Anton Paar MCR 301 rheometer was used for mechanical testing. Parallel-plate geometry (10 mm diameter) with a gap height of 400 μm was used for ultraviolet (UV) rheology. The UV light was turned on after 30 seconds with an intensity of 8.437 mW/cm^2. Stress was set constant at 1 Pa and strain constant at 1 Hz. Viscosity of precursor solutions were measured at a gap height of 400 μm.

3.2.7 Statistical Analysis

Determination of statistical significance between multiple groups was completed via analysis of variance (ANOVA) with Tukey method. Significant p-values were considered <0.05 unless otherwise noted. All analysis was completed in GraphPad Prism (San Diego, CA).

3.3 Results

The nanocomposite hydrogels were fabricated by mixing prepolymer solution containing PEG, GelMA, and Silicates (Figure 3-1). Using ionic interactions, covalent crosslinking chemistries, and viscosity, we have been able to extrude fibers of various sizes ranging from 0.2-1 mm. By using various strengths of PBS (1-20x) we found that 10X PBS forms the most ionically stable hydrogels. Therefore, for all sample preparation, 10X PBS was used. Hydrogels were mechanically stable and could be assembled into knots and other complex geometries simply using tweezers.

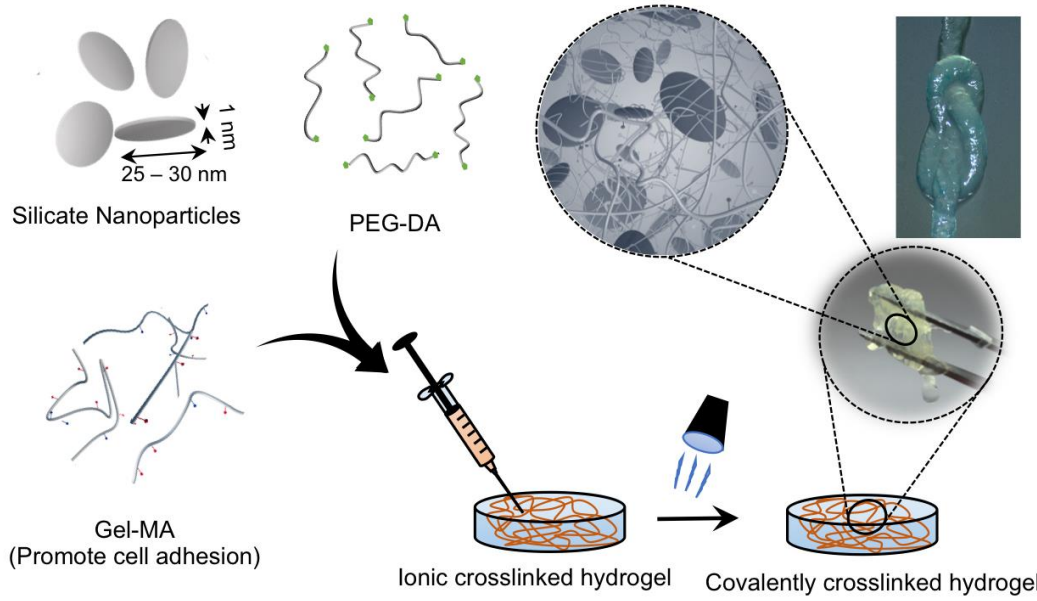

Figure 3-1. Synthesis of nanocomposite microfiber hydrogels via ionic and covalently crosslinking. Silicate nanoparticles are combined with PEG and Gel and injected into PBS to obtain ionically crosslinked microfibers. UV crosslinking for 10s results in formation of covalently crosslinked network. Covalently crosslinked microfibers are mechanically stiff and elastomeric to form a knot.

3.3.1 Physical Characterization of Nanocomposites

The pre-polymer solution of PEG and PEG/GelMA remained liquid at room temperature (25 °C) (Figure 3-2a). Addition of silicates to these pre-polymer solutions resulted in formation of highly viscous solutions. The interactions between silicate and polymers were investigated using electrophoretic measurements and DLS. The zeta potential of pre-polymer solution of PEG and PEG/GelMA was -5±0.4 and -7.1±0.6 mV, respectively and silicates was -28.7±2.4 mV. The addition of silicates to prepolymer solutions resulted in a decrease in zeta potential of PEG and PEG/GelMA to -24.2±1.2 and -27±1.9 mV, respectively (Figure 3-2b). We next determined the effect of silicate on size. The hydrodynamic diameter of silicates was ~56nm, and the addition of PEG and PEG/GelMA prepolymer to silicates increased the hydrodynamic size of silicates to ~65

nm and ~72 nm respectively (Figure 3-2c). These findings suggest that polymer coats the silicate nanoparticles before crosslinking. Silicates naturally exfoliate when placed in prepolymer solution and result in an increase in viscosity of precursor solutions. With an increase of shear rate, we observed a decrease in viscosity for all compositions (Figure 3-2d); addition of silicates increased the viscosity when compared to non-silicate containing compositions. The shear-thinning characteristic was used to fabricate microfibers with required diameter. The ionic interactions between silicates present on the microfibers and ions present in PBS, result in formation of ionic complex, stabilizing the surface of microfibers. After exposing the prepolymer solution to UV, covalently crosslinked network was formed, indicated by the increase in G' (Figure 3-2e).

PEG is a hydrophilic polymer and covalently crosslinked hydrogels contains around 97% water. The hydration degree of PEG hydrogels decreases with the addition of GelMA and silicates (Figure 3-3a). We observed that when collagenase solution was added into fully hydrated samples, there was a decrease in wet weight for samples containing GelMA (Figure 3-3b). We observed no significant difference in weight for samples not containing GelMA (PEG and PEG/Silicates). A significant degradation was observed in PEG/GelMA/Silicates hydrogels. Within 4 hours, the hydrogels network dissociated to smaller fragments and within 12 hours, PEG/GelMA/Silicates hydrogels was completely dissociated.

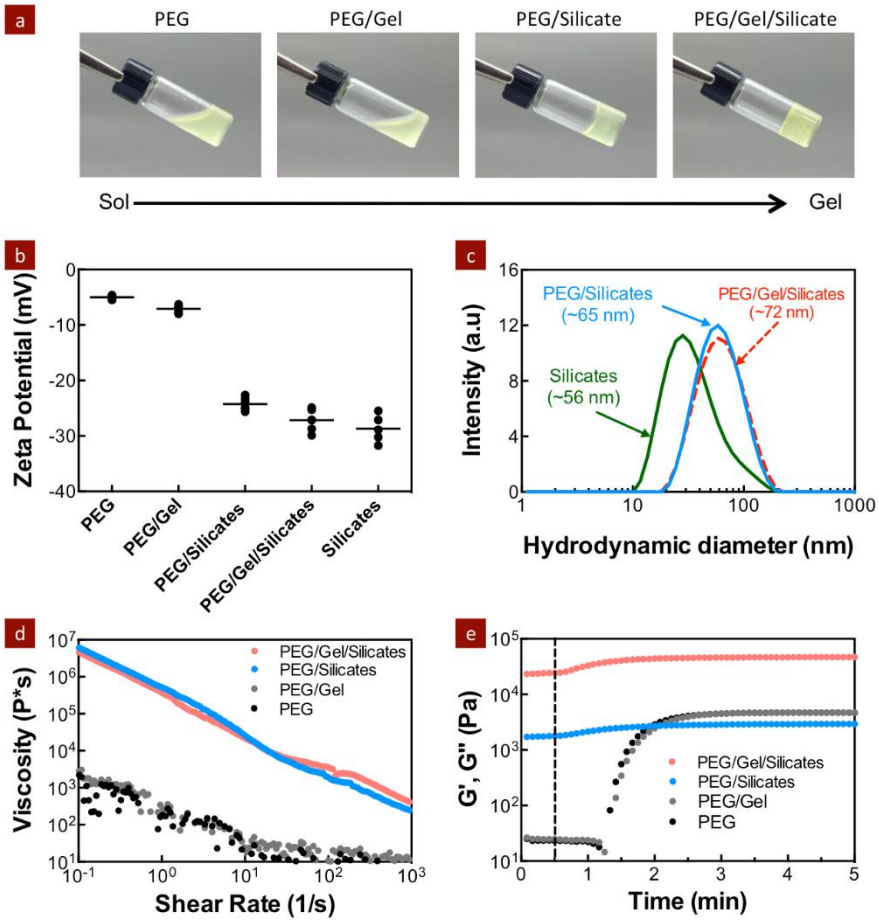

Figure 3-2. Shear thinning characteristic of prepolymer solution. (a) Viscosity of pre-polymer solution increases due to addition of silicate nanoparticles. (b) Zeta potential and (c) dynamic light scattering of pre-polymer solutions indicate that silicates strongly interacts with PEG and PEG/Gel. (d) Shear-thinning characteristic of prepolymer solutions was investigated by monitoring viscosity with respect to shear rate. (e) UV rheology of precursor solutions indicates that addition of silicate result in stronger network.

The addition of silicates or GelMA to PEG has no effect of the mechanical stiffness (Figure 3-3c). However, the compressive modulus was significantly increased for PEG/GelMA/Silicates to 6.5±1 kPa compared to PEG (1.7±0.1 kPa), indicating synergistic effect of silicates and GelMA. All the hydrogel network sustain serve compression loading and unloading cycle indicating elastomeric behavior. The addition of silicates and GelMA, result in significant increase in ultimate stress at

50% compression. The FTIR spectra indicate the presence of gelatin and silicate in nanocomposite hydrogels (Figure 3-3d).

The microstructure of PEG, PEG/GelMA and PEG/GelMA/Silicates indicated that addition of GelMA or silicates enforced formation of porous and interconnected network (Figure 3-4a). The nanocomposite fibers (PEG/GelMA/Silicates) also showed formation of highly porous and interconnected network (Figure 3-4). The average pore size of nanocomposites was ~17.6 μm. The uniform distribution of silicates within nanocomposite hydrogels was determined using EDX mapping of silicon and magnesium. No aggregation of silicates was observed within the hydrogel network indicating strong interaction between polymer and nanoparticles.

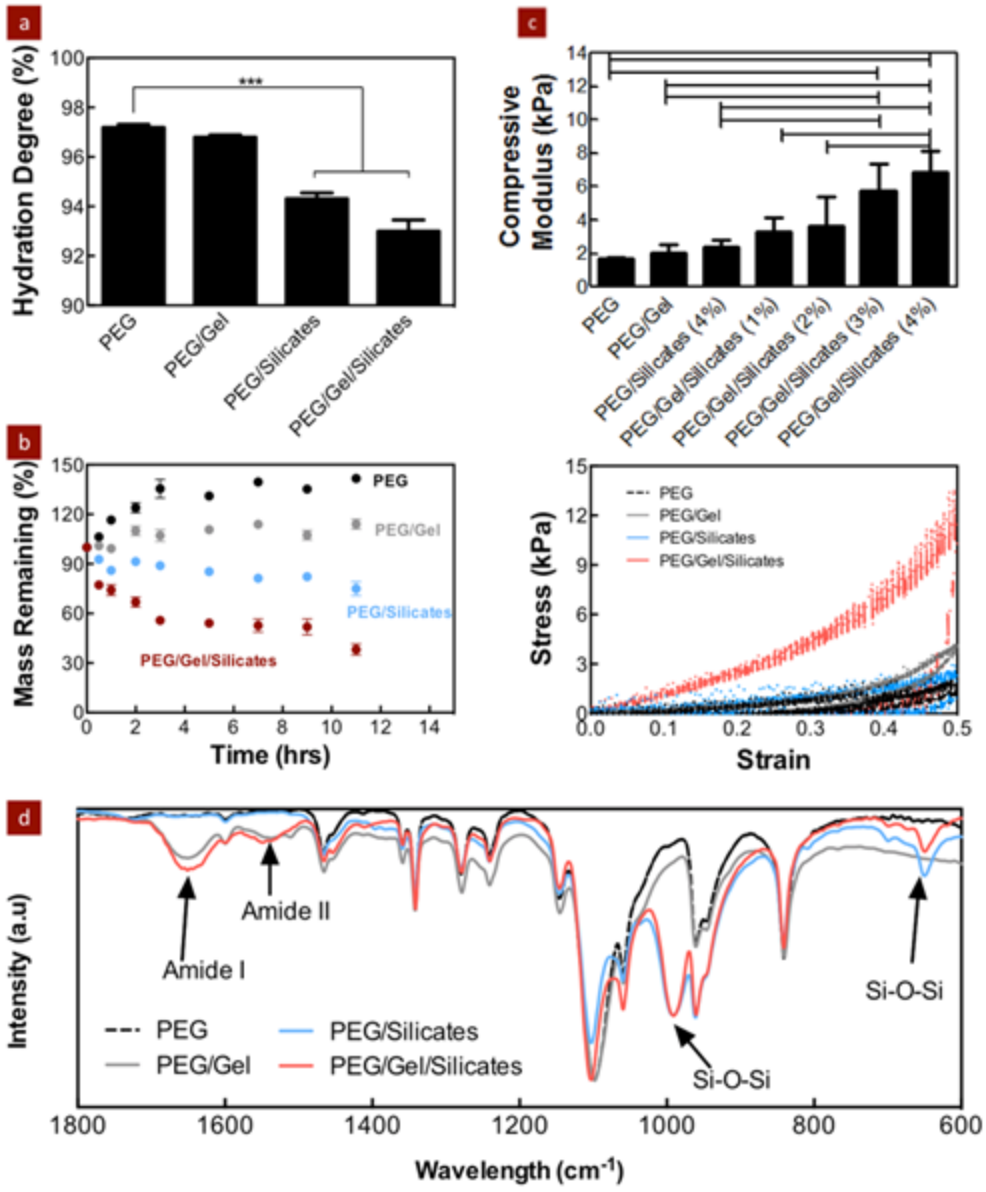

Figure 3-3. Physical stability of nanocomposite hydrogels. (a) Hydration degree (%) of PEG, PEG/Gel, PEG/Silicates, and PEG/Gel/Silicate hydrogel samples are shown. The addition of silicates result in a significant decrease in the saturated hydration degree due to the strong interactions between silicate and polymer chains (***$p<0.005$). (b) Degradation study of PEG/Gel and PEG/Silicates/Gel. (c) Compressive moduli of hydrogel samples indicate addition of silicate to PEG/Gel hydrogel result in 3-fold increase in modulus. Representative compression curves for all compositions are also shown. (d) FTIR analysis of lyophilized nanocomposite samples indicate presence of Amide I (1650 cm^{-1}), Amide II (1530 cm^{-1}) and Si-O-Si peaks (1030 and 650 cm^{-1}), indicating presence of gelatin and silicate.

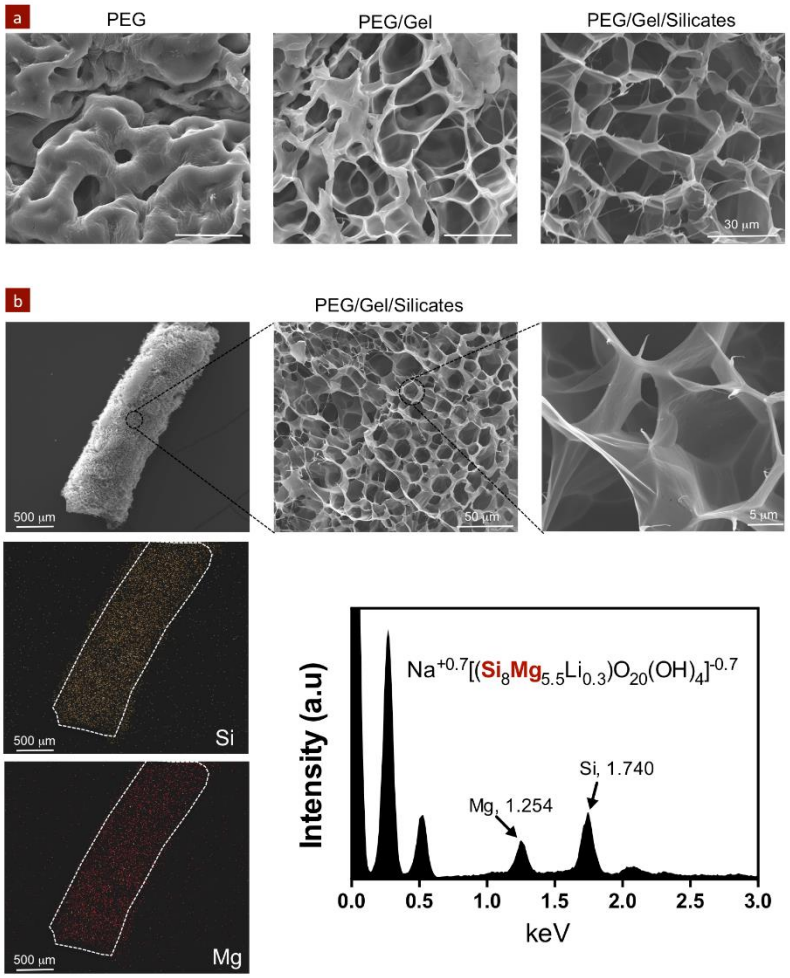

Figure 3-4. Microstructure characteristics of nanocomposite fibers. (a) Representative SEM images for PEG, PEG/Gel and PEG/Gel/Silicates. (b) PEG/Gel/Silicate microfiber show highly porous and interconnected network at different magnification. EDX mapping of silicon (Si) and magnesium (Mg) within PEG/Gel/Silicate fiber indicate uniform distribution of silicate nanoparticles within the hydrogel structure

3.3.2 Cell-nanocomposite Interaction in 2D Microenvironments

Cellular adhesion to biomaterial scaffolds plays a vital role in the survivability, proliferative capacity and development of new tissues. To examine the biological impact of incorporated silicates as well as natural polymer, we introduced a variety of model cell types into two-dimensional (2D) and three-dimensional (3D) microenvironments. We hypothesized that the

inclusion of GelMA and/or silicate enables enhanced survival and proliferation via an interactive cellular environment to improve upon the "blank slate" matrix provided by PEG. To investigate cell-silicates interactions, we evaluated cellular adhesion and spreading on bulk polymeric hydrogels (Figure 3-5a). Cells did not adhere to PEG surfaces, as no cell binding sites were present. Interestingly as we introduced the silicates to PEG, cellular adhesion and spreading significantly improved and was comparable to PEG/GelMA/Silicate. These findings suggest that silicate enables cell spreading which could possibly be attributed to the presence of magnesium in silicates that supports integrin clustering and the ability of silicate nanoparticles to sequester serum proteins.

Since PEG is inert, it provided negligible proliferative support and cells remained in the stationary phase (G_0) as demonstrated by cell cycle analysis (Figure 3-5b). After one hour of interaction with the bulk material, cells showed no variation in cell cycle distribution; although, inclusion of the bioactive nanosilicates altered cellular behavior toward a mitotic state (G2/M) as early as 3 hours post seeding on hydrogels (Figure 3-5b). The amount of silicates included did not induce DNA damage as expected, which was verified by no arrest in the S-Phase of the cell cycle at all of the three time points tested. Interestingly, the most dramatic trend appeared at 3hr in which, the MC3T3 cells shifted significantly to a proliferative state. Additionally, flow cytometry analysis of apoptotic cells confirmed that a PEG sample motivated a greater percentage of the cell population to an apoptotic state, while those including silicate nanoplatelets maintained notably lower levels of apoptotic cells.

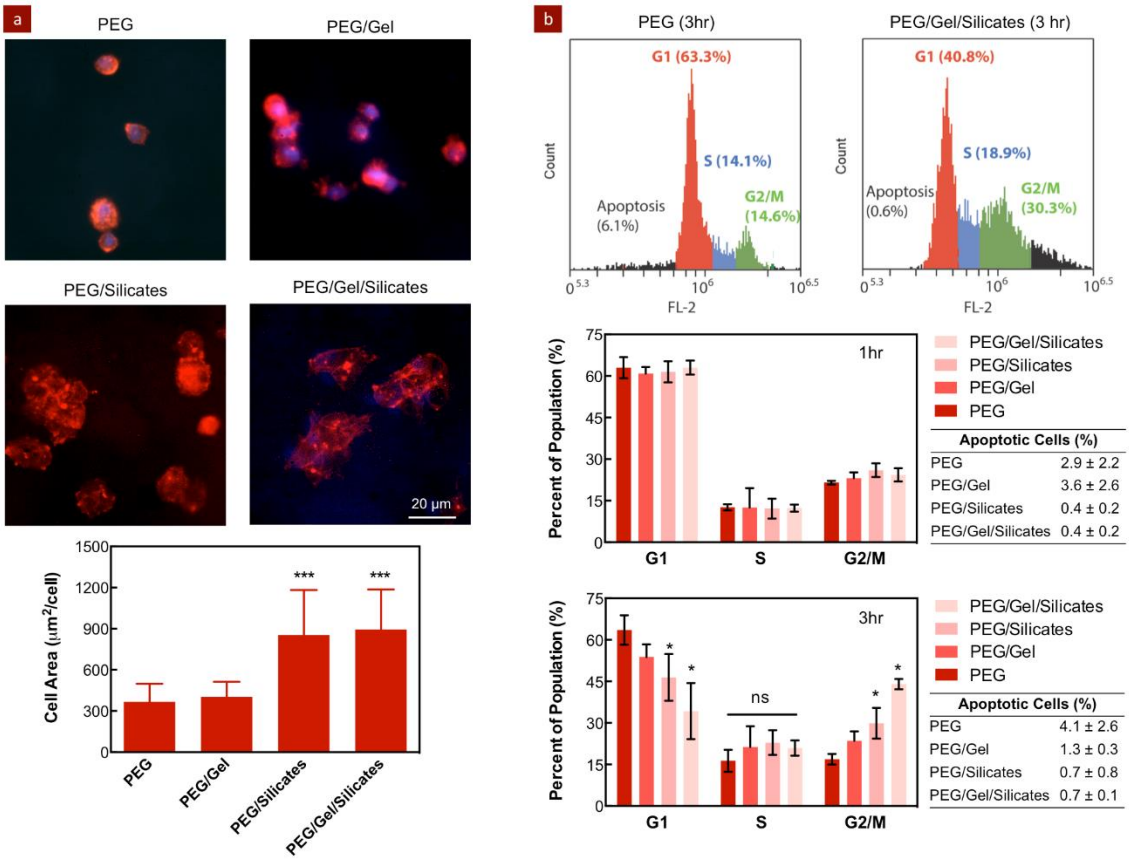

Figure 3-5. Cellular adhesion, spreading and proliferation on nanocomposite hydrogels. (a) Cell adhesion and spreading on hydrogel compositions. (b) Cell cycle analysis of adherent cells at 1 hr and 3 hr indicate addition of silicate promote cellular proliferation and reduces cell apoptosis.

The mitotic trend that emerged over 3 hours suggested that the cellular compatibility of the PEG/Silicate and PEG/GelMA/Silicate constructs were superior to that of the PEG samples. RGD sequences within the natural polymer promote cellular adhesion and subsequent cellular spreading, likely leading to the augmentation of cell numbers. We would expect this to account for the apparent increase in apoptotic cells as presented by flow cytometry, considering the relatively low concentration of the natural polymer and therefore RGD sequences. Electrostatic interactions between the surface of the nanoparticle and proteins may also provide anchor sites for cell binding events, an additional mechanism for cellular attachment and augmentation of cell survival.

Likewise, migration throughout could be mediated by these sites in addition to those enzymatically cleavable locations within the GelMA backbone. This aspect can be interesting to investigate the formation of tissue structure by seeding multiple cell types.

3.3.3 Cell-nanocomposite Interaction in 3D Microenvironments

Cellular adhesion in 3D microenvironment plays an important role in normal functioning of cells including proliferation, survival and production of ECM. Cells were encapsulated within the microfibers and viability was assessed to evaluate the effect of fiber formation process on cells. The result indicates that most of the cells encapsulated within fiber survive the fabrication process and very few apoptotic cells were observed (Figure 3-6a). Due to the small diameter of the fibers (≤500 micron), diffusion of vital nutrients was not hindered, and therefore cells within the core of the fiber were live. Furthermore concerns regarding shear stresses placed on cells during extrusion and UV exposure for crosslinking showed no adverse effect on cell viability. An important criteria for material selection was low viscosity. The precursor solutions were injectable even with a higher viscosity due to its shear-thinning characteristic. We believe the shear thinning effect was caused by the surface charge and alignment of exfoliated silicate nanoparticles, enabling flow past each other.[243] This property was useful in encapsulating cells, engineering complex geometry and for minimally invasive therapies.

To demonstrate the capabilities of this system for engineering complex tissue, a proof-of-concept multicellular culture was investigated (Figure 3-6b). RFP MOSJ cells were encapsulated within PEG/GelMA/Silicates microfibers and GFP-labeled preosteoblast cells were seeded on the

microfiber surface. The presence of both GelMA and silicates enabled sufficient binding of GFP labeled preosteoblast cells to the surface of the fiber surrounding the encapsulated REP MOSJ cells. After 1 hr, GFP-labeled cells adhered on the surface of microfibers. The majority of adhered cells demonstrated spreading on the fiber surface within 24 hr. These results suggest that if let to proliferate, these cells would coat the surface and begin to form a stable shell around the secondary cells within. We further examined the localization of cell adhesion and focal adhesion protein vinculin in cells encapsulated inside these hydrogels. As indicated in Figure 3-6b, enhanced spreading and localized focal adhesion spots were observed in PEG/GelMA/Silicate hydrogels compared to PEG hydrogels.

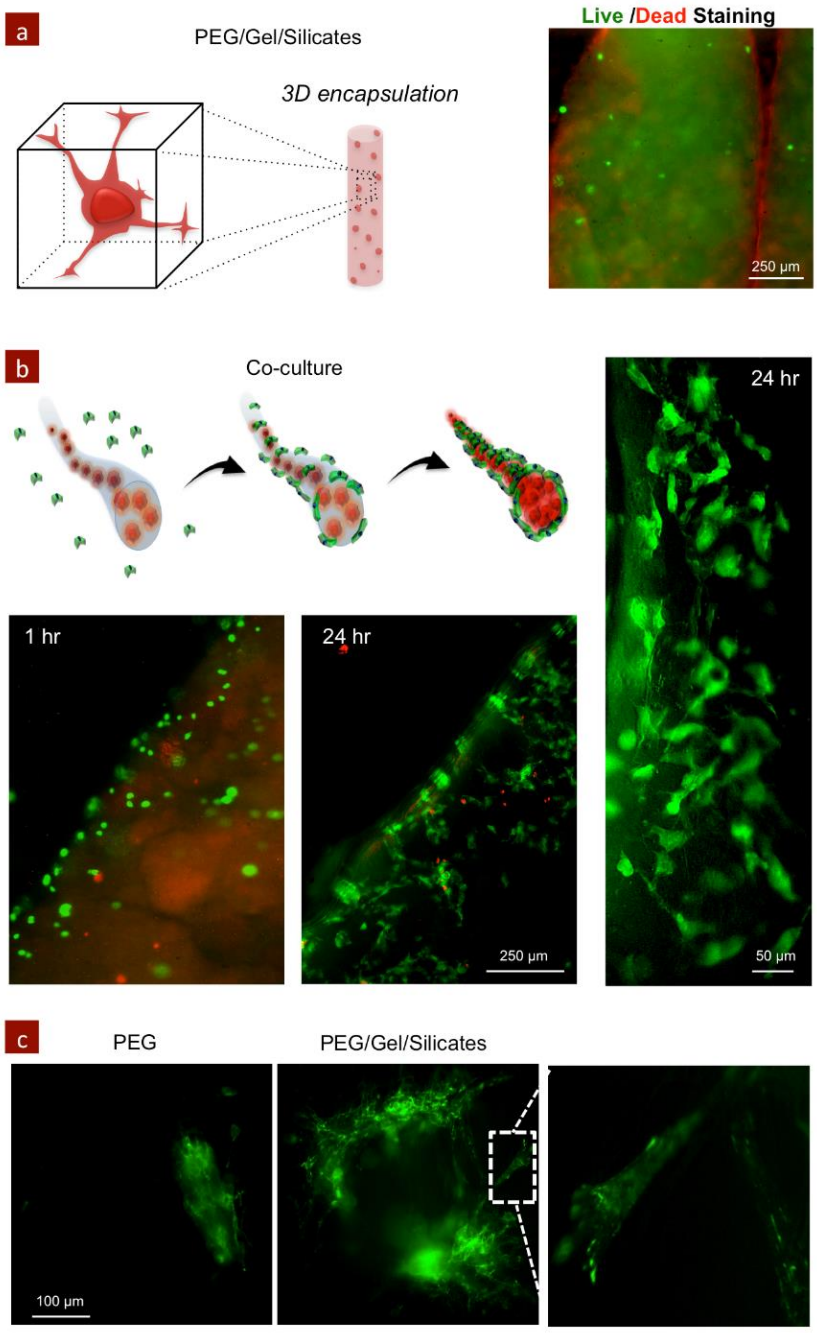

Figure 3-6. Engineering multicellular structures. (a) Live/Dead assay of PEG/Silicates and PEG/Gel/Silicates fibers containing fibroblast cells. (b) Co-culture of preosteoblast cells (green) on microfiber surface and RFP mosJ cell (red) inside the microfibers. (c) Expression of vinculin of encapsulated cells demonstrating cell adhesion.

Furthermore, the method of hydrogel polymerization does not appear to cause a decrease in cell survivability or proliferation. In our initial mechanical studies, fibers were extruded in 10X PBS. The variable of osmotic shock was mitigated by extruded fibers in standard cell culture media. This procedure permitted immediate nutrient flow around the cells incorporated into the fiber. We believe this method is a viable method to include cells into hydrogels that can be later processed in to complex architectures.

With the development of complex tissue scaffolds, nutrient exchange was of utmost importance.[244] It is possible to control the diameter of the fibers by changing the microcapillary diameter during the fabrication process. Smaller diameter fibers (<0.5 mm) were able to support cellular proliferation. Additionally, we have quantified the degree of swelling in bulk hydrogel compositions. The addition of silicate inhibited the uptake of water into the PEG/GelMA/Silicates hydrogel and was significantly different ($p<0.001$) from PEG and PEG/GelMA hydrogels. This can potentially be attributed to the silicates being fully exfoliated before PEG and GelMA were added. Cells were encapsulated in precursor solutions and then extruded in either PBS or media. The small fiber diameter facilitated fast and efficient nutrient transport. Pore size further facilitates nutrient exchange. With regard to degradation, we believe that the low percentage of GelMA is biodegraded through collagenase solution and left over is PEG and silicates. GelMA has multiple covalent binding sites for PEG and as the GelMA was biodegraded, we observed the network physically disassembling. For implantation, this property is important as to facilitate natural tissue ingrowth.

3.4 Conclusion and Future Direction

We demonstrate the fabrication of nanocomposite microfibers with tunable cell adhesion characteristic to engineer complex tissues structures. Spatiotemporal control over multiple cell types is needed. The addition of GelMA and silicates to PEG render development of physically and covalently crosslinked network with tunable cellular characteristics. Overall, the presented data suggest a promising future for the use of microfibers in cellular and drug delivery devices, ex vivo cell culture. Further investigation is needed to understand the PEG/GelMA/Silicates interactions during the polymerization. According to previously published reports, PEG chain can either interact with silicate surface or form crosslinked network.[237] The addition of GelMA appears to influence the mechanical properties, therefore, there must be a different interaction between PEG, GelMA and Silicates. Further studies must be completed to fully understand the interactions. We foresee the potential for a variety of investigative directions with these materials. The supplementation of bioactive natural and synthetic materials into the PEG matrix lends itself to the incorporation to a variety of biological agents, specifically those found in physiological environments with similar architectures. Endothelial cells provide a model of functional growth around a tubular polymer structure.[245, 246] These endothelialized fibers could be subsequently arranged within a GelMA network with a secondary cell type for more complex tissue organization. In a parallel study, the silicates could be functionalized with a deliverable drug or protein, enabling controlled release from within the embedded fibers. This system could be utilized for a vascular diffusion model in which cells embedded within the GelMA hydrogel could be tracked for migration kinetics or demonstrate spatiotemporal responses to the included agents within the fibers. Future studies will focus on tailoring the degradation of these fibers with the growth and formation of a functional cellularized conduit.

4. THERAPEUTIC DELIVERY VIA 3D PRINTING VISCOUS BIOINKS*

4.1 Introduction

Hydrogels are an integral component for tissue engineering strategies that aim to recapitulate natural tissues and function. Polyethylene glycol (PEG) based hydrogels have been evaluated in microfluidics,[247, 248] scaffolds for tissue repair,[55, 249] and disposable devices as well as cell scaffold matrixes. While PEG's bio-inert nature is advantageous due to low protein adsorption,[250] and minimal immunogenicity,[251] modifications of physical properties via changes in chain length, end groups, and biofunctionality enhance its usefulness as tissue engineered scaffold. In addition, modification of the degradation profile of PEG enhances the likelihood of adopting PEG as it does not require removal if the matrix is implanted. One such method, has been the introduction of hydrolysable crosslinkers[252] and backbones.[131, 132] To this end, PEG-dithiothreitol (PEGDTT) has previously been developed as a degradable cell scaffold.[253] However, low viscosity of PEGDTT limits the usefulness to pre-cast hydrogels. As tissue engineering progresses from cast hydrogel matrixes to precision deposition *via* three-dimensional printing, PEG based precursor solutions do not meet the complex mechanical requirements for 3D printing.[71, 78]

Injectable and printable polymer hydrogels with tunable physical properties can be used for a variety of bioprinting and precision deposition processes (i.e. precise delivery of therapeutics).

---

* C.W. Peak, J. Chen, K.A. Singh, M. Adlouni, A.K. Gaharwar, Submitted to *Biofabrication*, March 2018

Methods to enhance printability in an hydrogel precursor solution include changes in molecular architecture,[254] addition of additives such as nanoparticles,[255] and/or complete re-design using thermo-responsive hydrogels.[256] Specifically, the combination of synthetic polymers, such as PEG, and nanoparticles give rise to an interesting class of nanocomposite hydrogels that can support cell growth, withstand physiological loadings, and may have enhanced printability compared to polymer hydrogels by themselves.[11, 71, 257, 258, 259] In addition, these nanocomposite hydrogels can be used as vehicles for precision therapeutic delivery due to their unique rheological profile. Earlier we have used nanosilicates to form a shear-thinning hydrogel composed of kappa-carrageenan for stem cell delivery.[89] Addition of nanosilicates modified the shear-thinning ability and recoverability of kappa-carrageenan precursor solutions permitting use for printing applications. We have also included nanosilicates with PEG-DA and gelatin methacrylate.[77, 126] Likewise, carbon nanotubes are also used to control the rheological properties of alginate hydrogel precursor solutions.[78] Often ,theological analysis of hydrogel precursor solutions is for deposition of cell-laden materials.[75] However, hydrogel precursor solutions can similarly be examined for precision deposition of therapeutics.

Combination of a degradable polymer with nanoparticle to produce a shear-thinning, printable hydrogel precursor solution with therapeutic holds promise for precision therapeutic delivery.[11] Hydrogel degradation characteristics and subsequent mesh size influence therapeutic diffusion and delivery to surrounding tissues.[260] Developed methods for fabrication of degradable hydrogels rely on the ester linkage in hydrogel backbone to modulate the degradation rate of the hydrogel. Previous studies have varied PEG compositions to examine *in vivo* degradation profiles.[261, 262] For example, PEG has been modified with poly (lactic acid) end groups (PLA) to modulate network

degradation[131, 132] and cell adhesion[133] and proliferation.[134] Inclusion of more hydrolytically labile ester groups, as compared to the ether present in PEG backbone, presents an established strategy for degradation.[54, 263] Di-acrylated PEG presents a facile approach for modifying the backbone through which a Michael-like reaction can occur between acrylate and thiol groups present in dithiothreitol. Through precise control of initial reactants, the acrylate crosslinking functionality can be preserved while creation a hydrolytically labile ester. Controlling polymer chemistry, addition of nanoparticles, and therapeutics can facilitate fabrication of 3D printable therapeutic hydrogel precursor solutions.[71, 89, 264]

Herein we describe a simple approach to create a hydrolytically labile, PEG-based nanocomposite that exhibits a rheological profile suitable for precision delivery and 3D printing. This approach permits the inclusion of therapeutics such as vascular endothelial growth factor (VEGF) and fibroblast growth factor (FGF) for the precision deposition of therapeutics. Laponite XLG, a synthetic clay nanoparticle composed of complex polyions, that imparts shear-thinning properties when combined with PEG-based hydrogels.[126] Synthesis of hydrolytically labile PEG was achieved through Michael-like addition of dithiothreitol via step growth polymerization. By stoichiometrically imbalancing the reaction towards PEG-diacrylate, the acrylate functionality of the resulting macromer was preserved and the resulting hydrogel solutions were UV curable. Through combining PEGDTT with Laponite and the inclusion of growth factor, precision deposition of hydrogel solutions was possible, resulting in a facile method for therapeutic patterning.

4.2 Materials and Experimental/Procedure

4.2.1 Materials

Laponite XLG, procured from Byk Additives and Instruments, was dried in the oven at 100°C for 4h to ensure limited environmental water swelling of particles. Poly (ethylene glycol) was dried before acrylate modification using procedures previously reported.[186] In short, 20 g PEG (3.4kDa) was dissolved in dichloromethane along with triethylamine (Sigma). Acryloyl chloride (Alfa Aesar) was added dropwise to the solution on ice and stirred for 24 hours. After washing, the solution was precipitated into diethyl ether and dried over vacuum. ^{1}H NMR *300 MHz, $CDCl_3$, δ): 3.62 (s, 297H; -OCH_2CH_2), 5.81 (dd, 2H, J= 10.5 and 1.2 Hz; -$CH=CH_2$), 6.40 (dd, 2H, J = 17.3 and 1.5 Hz; -$CH=CH_2$) confirmed diacrylation of PEG3.4kDa. PEG-Dithiothreitol (PEG-DTT) was synthesized as reported by Cereceres *et al.*[265] PEG3.4kDa was dissolved in dichloromethane with triethylamine. DTT was dissolved in dichloromethane and added dropwise to the solution. Molar ratio of reactants were as follows PEG:DTT:TEA::3:2:0.9 to ensure a acrylate terminated macromer. Elman's assay was used to measure free thiol groups after reaction completion. ^{1}H NMR *300 MHz was used to approximate macromer molecule weight, using DTT backbone as the standard.

4.2.2 Sample preparation

The desired amount Laponite XLG (4% wt/vol) and polymer was dispersed into 18 MΩ water (pH=7.4) and vortexed vigorously for at least 2 minutes. Due to previously reported degradation profile for PEG-DTT, PEG3.4kDa was added into the polymer mix at 25% increments though total

polymer concentration was kept constant at 10% wt/vol. Samples were identified as percentage (%) of PEG-DTT and with or without Laponite XLG (+ XLG). As such, 10 experimental samples were used for evaluation of: compressive modulus and swelling. At the conclusion of swelling experiments evaluation was conducted to reduce the number of samples for rheology, therapeutic incorporation, and cell studies. Samples were photocrosslinked *via* the inclusion of 0.3% wt/vol IGRAcure2959 and exposure to 365 nm UV light for 90 seconds at an intensity of 7.0 mW/cm^2.

4.2.3 Hydrogel Swelling

PEG-DTT nanocomposite samples were cut into 5 mm circles (1 mm thick) and allowed to swelling in 1mL PBS at 37°C for 1, 3, 5, 7, 14, or 21 days with PBS replaced daily for the first 7 days and every-other day thereafter. Weight measurements were taken before swelling (W_0) and after swelling (W_s). Comparing the wet weight to dry weight, swelling was calculated according to the following equation:

$$Swelling\ \% = \frac{W_s - W_0}{W_0}$$

Mechanical Analysis. An ADMET eXpert 7600 Single Column Testing System equipped with 25 lb load cell was used for compression testing. Strain rate of 1 mm/min was used to compress the samples 50% of original height. The compressive modulus was calculated and plotted versus the sample composition. All samples were used for mechanical testing to ensure proper synthesis and trends with inclusion of PEG were being observed.

4.2.4 Rheological Analysis

A Discovery Hybrid Rheometer 2 (DHR-2) (TA Instruments) with attached 40 mm parallel plate at gap height of 0.25 mm and 25°C was used for all experiments. Pre-cursor solutions of PEG-DTT ± Laponite XLG were used for all experiments unless otherwise noted. Rotational shear rate sweeps were executed between 10^{-3}-10^{3} s^{-1} to determine the power law region. Power-law parameter n (flow behavior index) and K (flow consistency index) were calculated using TRIOS software (TA Instruments). Rotational time sweeps were executed at three different shear rates (s^{-1}) in sequential order: 10^{-2} (60 s), 3000 (5s), 10^{-2} (120s) to determine shear recovery of solutions.[71] Time to 80% recovery was manually observed/calculated.[183] Oscillatory shear stress sweeps between 10^{-1}-10^{3} performed at 1 Hz and frequency sweeps between 10^{0}-10^{2} performed at 10 Pa to further validate yield points and investigate dependence on frequency.

4.2.5 Therapeutic Incorporation

Bovine serum albumin was used as a model protein. Laponite XLG were allowed to exfoliate for 24 hours. Albumin was added to the solution such that final concentration was 140ng/1 mL. After overnight incorporation, polymer was added to the solutions and 100 µL gels were formed. Samples were placed in 1 mL of PBS at 37 °C and supernatant removed at 1, 2, 3, 4, 6, 9,12, 24, 48, 72, 96, 120, and 168 hour time points. Using microBCA kit (Thermo-Fischer), albumin release was measured. Similarly, fibroblast growth factor and vascular endothelial growth factor (FGF and VEGF respectfully) were incorporated into hydrogel samples for *in vitro* testing.

4.2.6 Therapeutic Release, Staining and Imaging

To test therapeutic efficacy, migration of HUVECs through 8 um transwell inserts was monitored. Samples containing 40 ng/mL VEGF and 400 ng/mL FGF were UV crosslinked and cut out to obtain 8 mm circles, 1 mm thick. Positive control consisted of exogenously delivery VEGF (0.5 uL/mL) and FGF (2 uL/mL), negative control was no sample and no growth factor. Experimental negative control were composed of PEGDTT and PEGDTT/Laponite. HUVECs were seeded on top of transwell at a density of 10,000 cells/mL and allowed to adhere. Wells were then inserted into appropriate treatments, allowed to proceed for 24 hours, then fixed with 10% neutral buffered formalin. Subsequently cells were treated with 1X Triton X for 30 min, washed with PBS and then DAPI was added for 5 min. Cells were washed and Phalloidin was added for 20 min. All well were them imaged under a Nikon Eclipse TE2000-S Microscope at 20X. Afterwards, gold plating of wells was completed and a JEOL (JCM-5000: Benchtop SEM) scanning electron microscope (SEM) was used to visual deposited extra cellular matrix.

4.2.7 3D Printing

PEG-DTT ± nanosilicates constructs were fabricated utilizing a HYREL System 30M 3D printer. Solution was loaded into a HYREL VOL-25 extruder (HYREL L.L.C., Norcross, GA) equipped with a luer lock adapter and 23 gauge blunted stainless steel needle (Jensen Global Inc, Santa Barbara, CA). Once connected to the printer, constructs were modeled in Solidworks 3D CAD Design, exported as an STL file, and imported into Slic3r version 1.2.9. Overall, this process converts the Solidworks design into layer-by-layer instructions for the printer, or G-code. The G-code files are then imported into HYREL's proprietary software (Repetrel Rev2.828) and printed

at room temperature onto glass slides. Upon completion, glass slides were placed under a UV lamp and photo-crosslinked for 150 seconds at an intensity of 25 mw/cm^2.

4.2.8 Statistical Analysis

Determination of statistical significance between multiple groups was completed via analysis of variance (ANOVA) with Tukey method. Significant p-values were considered <0.05 unless otherwise noted. All analysis was completed in GraphPad Prism (San Diego, CA).

4.3 Results and Discussion

4.3.1 PEGDA-Dithiol Reaction and Hydrogel formation

Polyethylene glycol diacylate (PEG-DA) was reacted overnight with dithiothreitol resulting in a hydrolytically labile macromer (Figure 4-1). The reaction of PEG-DA with DTT in DCM was efficient as measured by Ellman's assay, which showed 99.4% of all thiols having been consumed in the reaction. Michael addition reaction between thiol and acrylate groups are widely used as summarized by Nair *et al.*[266] Specifically, we used a base-catalyzed (triethylamine) Michael addition that facilitates the reaction between the thiol (DTT) and electron-deficient vinyl group (acrylates on PEG). Complete or nearly complete consumption of DTT is highly important within this reaction; DTT has been used to reduce disulfide bonds in proteins and deprotect thiolated DNA.[267] The reaction of PEG-DA with DTT forms a stable macromer (Figure 4-1). Modification of this facile synthesis yields many macromer compositions that dictates degradation rate, mechanical properties (compressive modulus), and swelling properties.[253, 268, 269]

We have used a low molecular weight PEG-DA (3,350 g/mol) prior to addition of DTT as this molecular weight can be cleared by the body via the kidneys.[270] Hudalla *et al* have investigated the PEG to DTT ratio and demonstrated the synthesis process.[253] While Hudulla presents a synthesis in PBS, Cereceres presents a similar synthesis as the one present here.[265] It is suggested by Hudalla that reaction reaches completion within 60 minutes, but due a difference in solvent (dichloromethane as compared to PBS) it was allowed to complete overnight yielding PEG-DTT with 95% acrylation as verified through NMR (Figure 4-1, inset). Using NMR and Caruther's equation, PEG-DTT molecular weight is estimated to be between 8,000-12,000 Da.

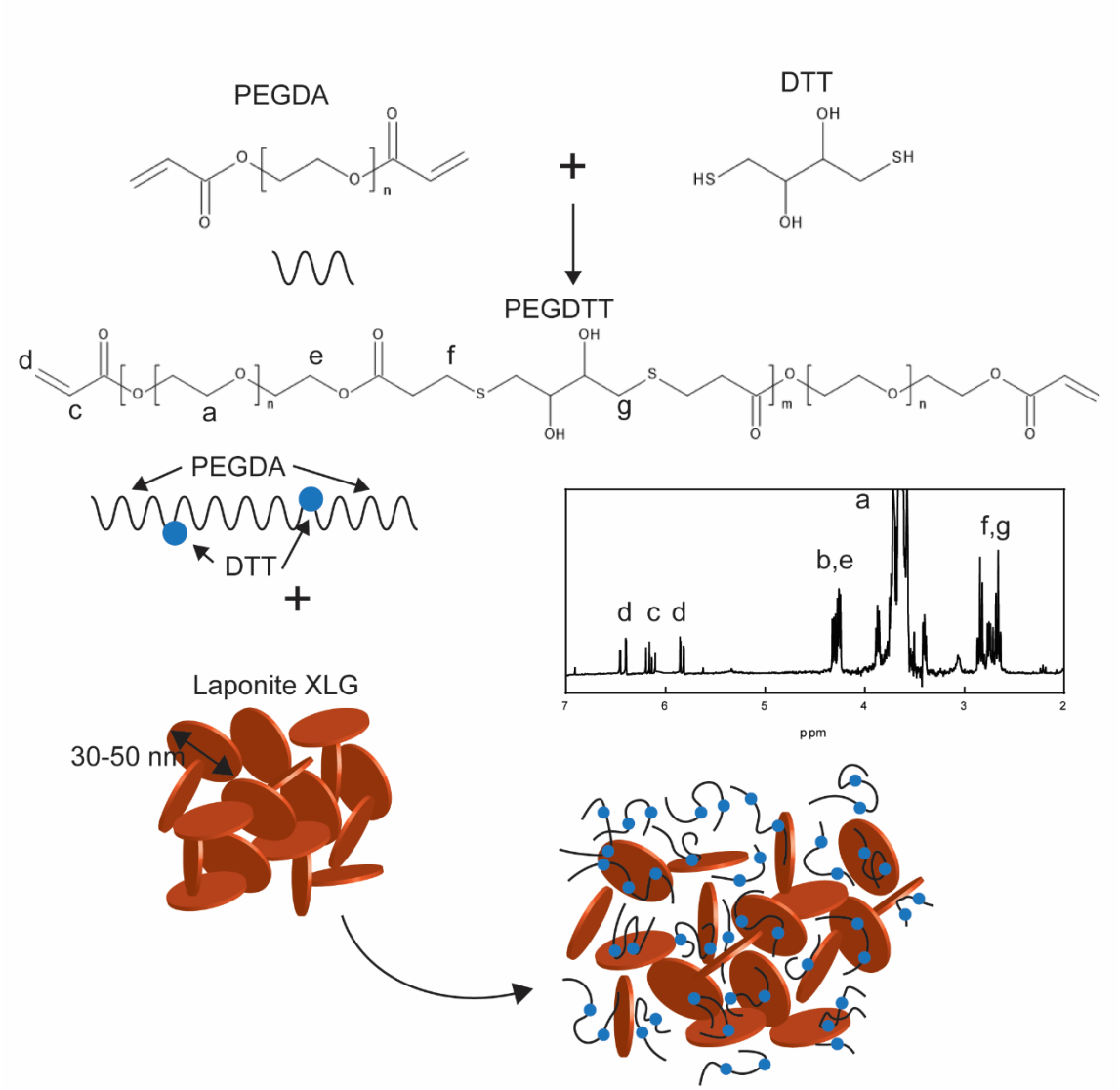

Figure 4-1. Synthesis schematic of PEG-DTT. A Michael-like addition reaction between poly(ethylene glycol) diacrylate and dithiothreitol to form hydrolytically labile linkages into the polymer chain. Blue dots represent DTT linkages. Confirmation of PEG-DTT synthesis via NMR spectroscopy (peaks labeled). Laponite XLG inclusion creating a nanocomposite hydrogel precursor that can be subsequently crosslinked.

The control for this reaction was achieved by careful dropwise addition of DTT to the PEG-DA to allow for complete Michael addition to the PEGDA chains and *via* a stoichiometric imbalance in favor of PEG-DA was to ensure acrylate terminated macromer. Once dried, combination with Laponite XLG (4% wt./vol) results in a nanocomposite hydrogel. To the best of our knowledge,

there have been no reported nanocomposite hydrogels using PEGDTT as the macromer. Laponite XLG has been used with other PEG hydrogel compositions to modulate cell adhesion and mechanical properties.[271] Nanocomposite hydrogels are created by exfoliating a double concentration of Laponite XLG in IGRAcure solution and then the addition of PEGDTT. After 3 min of UV exposure (365 nm, 7 mW/cm^2) hydrogels are created for subsequent testing.

4.3.2 Swelling and Degradation of PEG-DTT Nanocomposite Hydrogels

PEGDTT degrades at the β-thio ester linkage created during the Michael addition and swells considerably due to entropy decrease surrounding free chain movement. Depending on the original molecular weight of PEG used in the reaction and the ratio of PEGDTT, swelling and degradation of hydrogels can be controlled. Here, we focus on one composition of PEG-DTT with a 3:2:PEG:DTT ratio and the addition of Laponite XLG to the matrix. PEG-DA was incorporated into PEG-DTT hydrogels at 10% intervals with final polymer weight (Figure B-1) to investigate modulation of hydrogel swelling and degradation. PEGDTT degraded at an appreciable time scale (7 days) and was further investigated. Previous studies with Laponite XLG demonstrate the hydrogels will not swell has much as those not containing Laponite XLG.[272] This is suggested due to interactions among the polymer and nanoparticle, hindering swelling of polymer chains. It has been proposed that Laponite XLG acts as a physical crosslinker within the hydrogels which generally limits the swelling ability of the material.[167]

PEGDTT hydrogels containing Laponite XLG behave similarly in that the swelling percentage at any given day is less than that of pure PEGDTT hydrogels (Figure 4-2a). Overtime, PEGDTT hydrogels continue to swell and degrade, becoming completely absent from solution by day 21. As the PBS is replaced, free chains are removed from the samples thereby reducing the swollen weight of samples. Conversely, PEGDTT/Laponite hydrogels do not swell as much but degrade faster than PEGDTT samples. Due to the chemical composition and cation balance of Laponite XLG, solutions of the particle will naturally exhibit a pH of 9.4 as described by Thompson and Butterworth.[273] Given that esters are hydrolytically labile, basic solutions exacerbate susceptibility due to large hydroxide concentration. This is a likely explanation for the decreased time interval needed to observe complete dissociation of PEGDTT/Laponite hydrogels. The ionic structure of Laponite XLG (Figure 4-2b) evolves with increasing time from having sodium cation adsorbed on the surface of the particle to balance the oxygens that are covalently bound to the silicon to having sodium cation freely in bulk solution. Sodium cation is in its lowest energy state when surrounded by 5-6 water or hydroxide molecules.[274] Through osmotic pressure, the sodium diffuses away from the surface of Laponite, leaving exposed oxygen with two electrons pairs.

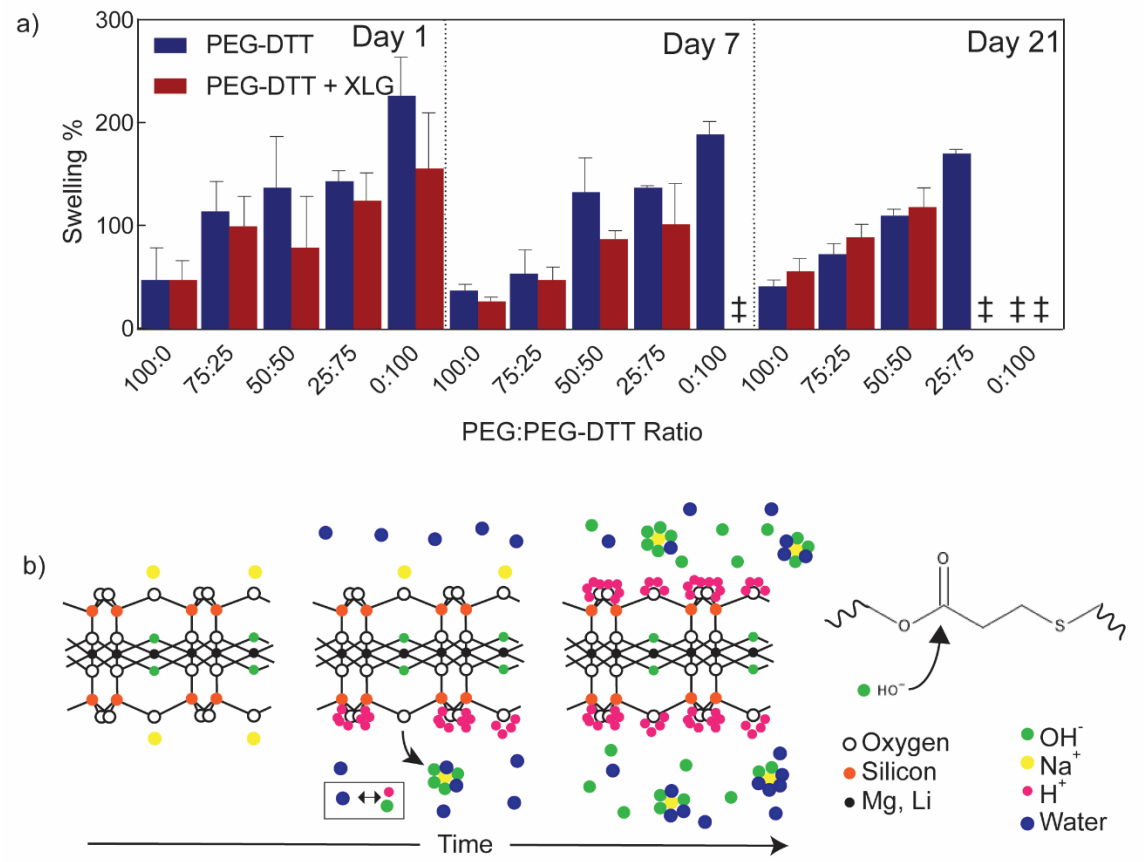

Figure 4-2. Swelling of PEG-DTT hydrogels and potential mechanism of degradation (a). Changes in swelling of PEG-DTT and PEG-DTT/Laponite hydrogels was monitored over 21 days (‡ indicates complete dissolution of hydrogel). (b) Proposed mechanism of nanoparticle induced degradation of PEG-DTT. Adsorbed sodium cation gradually releases from Laponite surface resulting in the solution achieving a pH of 9.4 which accelerates PEG-DTT degradation.

Stabilization of Laponite particles occurs through disassociation of water, forming hydrogen and hydroxide ions. Hydrogen ions will quickly adsorb onto the surface of the particle creating a stable Stern layer.[275] The hydroxide anions will surround the sodium cation present in solution. For every sodium cation released, 4-8 hydrogen ions are needed to stabilize Laponite.[276] This imbalance creates a surplus of free hydroxide ions caused pure Laponite solutions to evolve in pH and rest at 9.4.[273] Equilibrium pH of Laponite resting at 9.4 caused a decrease in time for PEG-DTT samples to decompose. PBS buffered the solution and prolongs the degradation time compared to pure

water. When samples were swollen in water, complete sample degradation occurred in <24 hrs. Hudalla and Paralato have rested their samples in water overnight to remove salts from gels in order to obtain pure wet and dry weight measurements of samples.[253, 268] Due to the quick erosion time our samples experience in water, we are unable to remove the dissolved salt that may be resting in our samples. Swelling corresponds with degradation as they are simultaneously occurring.

4.3.3 Mechanical stability of Precursor solutions and crosslinked hydrogels

PEGDTT/Laponite hydrogels hold potential as a therapeutic delivery vehicle and as a 3D printable hydrogel. To verify its application as an injectable or printable delivery matrix, stress and frequency sweeps, shear-rate sweeps, and peak-hold viscosity tests were performed. PEGDTT/Laponite samples will be used as delivery vehicles as an un-crosslinked precursor solution. Injectability of precursor solutions through a needle is a crucial parameter for 3D printing. High viscosity at low shear rate elucidates if the hydrogel will flow freely when placed on a surface.

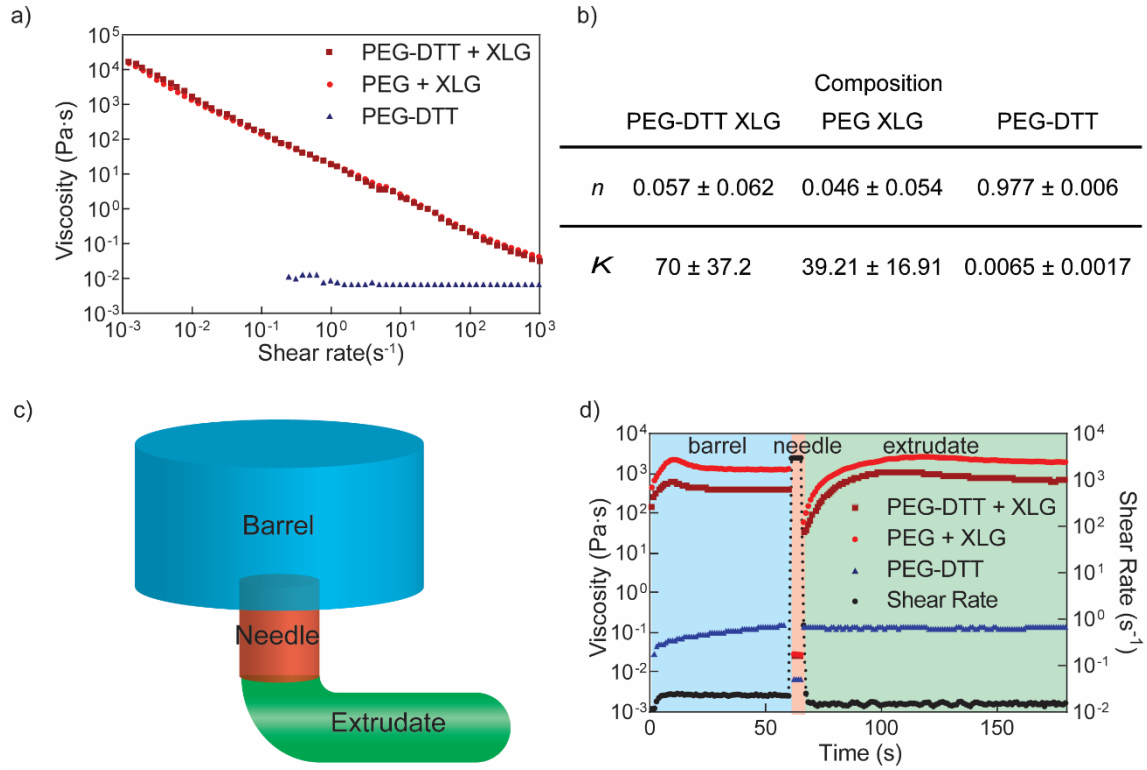

Figure 4-3. Rheological sweeps of PEG-DTT/Laponite precursor solutions and crosslinked hydrogels (a) Shear-rate sweep from 10^{-3}-10^{3} s^{-1} indicating Laponite inclusion influences shear-thinning ability; (b) Power-law parameters for uncrosslinked hydrogels; (c) schematic of printing process through barrel, needle, and on printing bed; (d) peak hold experiments to mimic flow during extrusion/printing

Ideally, hydrogel precursor solutions should have a decrease in viscosity with an increase in shear rate. PEGDTT is a low viscosity solution across all tested shear rates (Figure 4-3a). The addition of Laponite increases low shear rate viscosity while maintaining low viscosity at higher shear rates. Power-law rheological models were fit to these data and the inclusion of Laponite decreases *n* from ~1 (Newtonian fluid) to ~0.05 Pa·s (Figure 4-3b), suggesting that Laponite is the cause of shear-thinning behaviors. Shear-thinning elucidates if a material can extrude through a needle but to maintain structure once deposited the hydrogel must be able to recover. Solutions were exposed to sequential shear-rate holds to mimic the rates experienced within the printing apparatus (Figure

4-3 c &d). The recovery of samples containing Laponite was observed while PEGDTT by itself remained fluid. Taken together, these data suggest that PEGDTT/Laponite can be used for precision deposition and printing applications.

Storage modulus (G') and loss modulus (G") of PEGDTT/Laponite hydrogels was determined via stress and frequency sweeps. Storage modulus is a measure of the elastic, or recoverable energy, in the sample while loss modulus is the viscous, or dissipated energy, in the sample. Laponite XLG is gel forming at concentrations above 3% wt./vol when using low ionic solvent.[158] PEG-DTT dissolved well in aqueous environments and appears fluidic. With an increase in applied oscillation frequency, PEGDTT storage modulus increased as a result. Addition of Laponite results in the solution becoming stiffer and more gel-like as indicated by G'>G". Both PEG/Laponite and PEGDTT/Laponite responded similarly to applied oscillation frequency and within a linear viscoelastic region throughout the testing parameters (Figure 4-4a). Oscillation stress further demonstrated that Laponite containing samples are within the linear viscoelastic region. Here, yield stresses were apparent with PEG/Laponite having a higher yield stress than PEGDTT/Laponite. Yield stresses were 71.26 ± 11.55 and 64.21 ± 14.69 Pa for PEG/Laponite and PEGDTT/Laponite respectfully and are not statically different (Figure 4-4b).

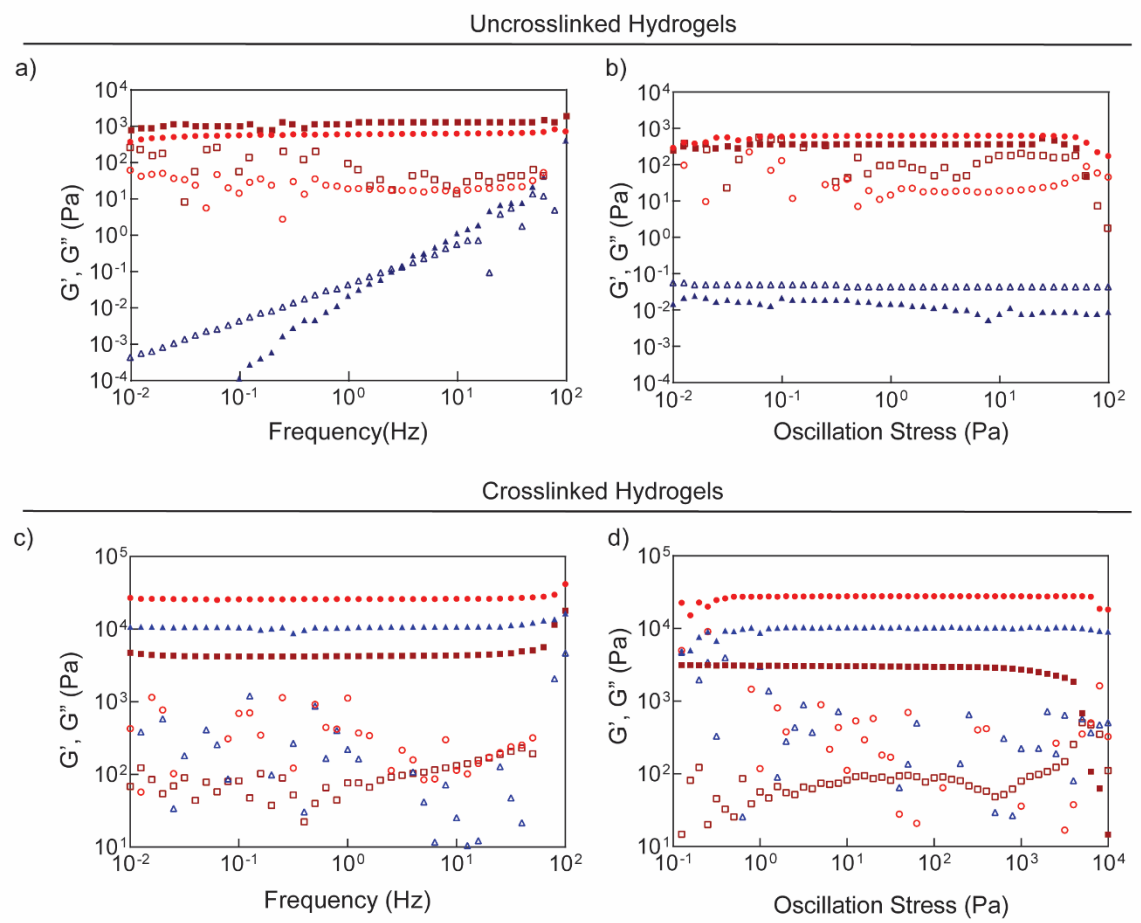

Figure 4-4. Frequency and oscillatory stress sweeps for uncrosslinked and crosslinked samples. Note: maroon squares=PEG-DTT/XLG, red circles=PEG/XLG, blue triangles=PEG-DTT, full colored shapes indicate storage modulus (G'), open shapes indicate loss modulus (G") (a) frequency sweeps of uncrosslinked precursor solutions (b) stress sweeps of uncrosslinked precursor solutions (c) frequency sweeps of crosslinked hydrogels (d) stress sweeps of crosslinked hydrogels

In the extrusion process, hydrogel precursors will be exposed to UV light once injected or printed. Stress and frequency sweeps (Figure 4-4 c & d) of crosslinked hydrogels increase due to covalent crosslinking that occurred through UV light exposure. Prior to crosslinking, the precursor solution remained stable through Laponite-Laponite interactions. Terminal acrylate π-bonds are converted to δ-bonds during crosslinking, increasing the overall stiffness of the hydrogel and making it such that they no longer freely flow. PEGDTT/Laponite has a lower modulus (G') than PEGDTT which

is contrary to literature. However, inclusion of Laponite immediately exposes PEGDTT to a basic environment. While the basic environment is critical for modulation of the degradation, it adversely affects storage modulus. Storage modulus of crosslinked PEGDTT/Laponite remained higher than of un-crosslinked PEGDTT/Laponite Crosslinking is a necessary step for prolonged localization of PEGDTT hydrogels.

4.3.4 Model Therapeutic incorporation and release

Rheological profile of PEGDTT/Laponite gels demonstrates their potential as a local therapeutic delivery vehicle. Localization methods predominately rely on pre-cast hydrogel molds and implantation into specific regions. Further, methods for released therapeutic have predominately used the degradation of poly(lactic-glycolic acid) (PLGA) as releasing mechanism.[130] This system combines localization of therapeutic with a potential release mechanism. Due to the adsorbed sodium cation on the surface of Laponite XLG, ion exchange can occur for stabilization and release of therapeutics (Figure 4-5a). Bovine serum albumin (BSA) was used as a large glomerular protein model that can be released from the Laponite containing samples. Pre-exfoliated Laponite XLG and BSA were thoroughly mixed overnight, allowing cation exchange to occur. Albumin replaces the sodium cation in the interlayer space, creating a Laponite-protein conjugate. Overtime, both ionic and biological cations replaced the adsorbed therapeutic of interest, allowing for a potentially delayed release. As a mimic, PBS was used as a sink solution for release of BSA; the release was monitored for 7 days. Release curves (Figure 4-5b) suggested that there is no difference in addition of Laponite to PEG-DTT for delay of protein

release (release rate for PEGDTT=0.009458 hr^{-1}, PEGDTT/XLG=0.009080 hr^{-1}). Several studies have demonstrated that addition of Laponite XLG delayed release of therapeutic due to competition between cations that stabilize the Laponite.[277, 278] However, due to the creation of the basic environment and decrease in degradation time, it is suggested that the overall mesh size over time is increasing with addition of Laponite XLG. Increase mesh size allows more cation exchange and interaction between the adsorbed protein and surrounding solution, suggestive of an increase in release-rate. Further, PEG molecular weights below 15kDa showed low amounts of release of entrapped protein[279]; therefore, it is expected that degradation of PEGDTT hydrogel will control the release of BSA. The faster degradation rate of the entire PEGDTT/Laponite hydrogel seemingly counteracts any benefit from Laponite XLG/protein interactions. However, the inclusion of Laponite XLG is crucial for precision deposition of therapeutics. Increasing PEGDTT concentration or decreasing the macromer molecular weight could increase the overall time for releasing protein since more covalent crosslinks would be present, resulting in a decrease in mesh size. Alternatively, an increase in Laponite XLG concentration should delay release of therapeutic at the increase of overall faster degradation of PEGDTT hydrogel.

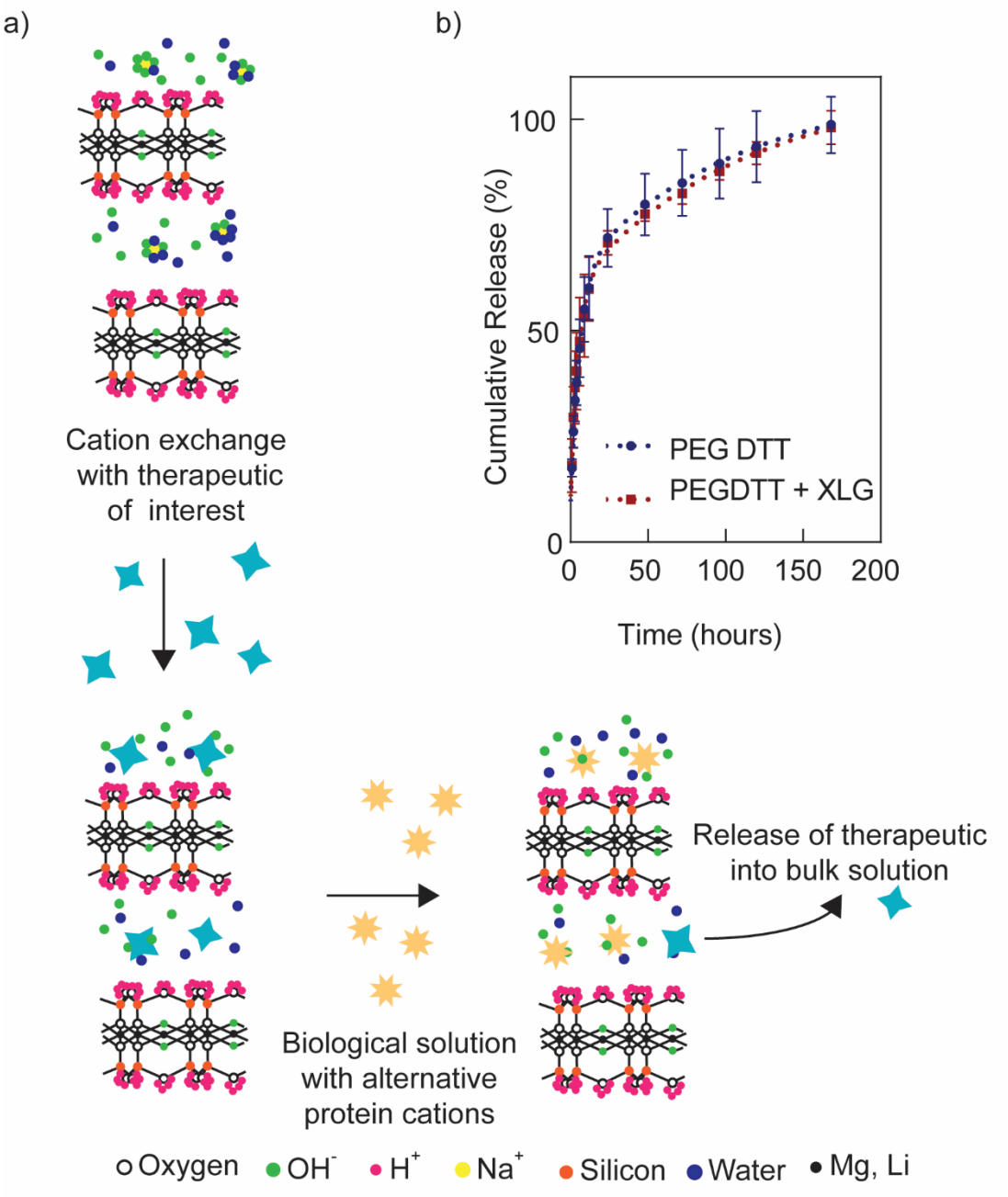

Figure 4-5. Therapeutic incorporation and release (a) Cation exchange of therapeutic of interest (bovine serum albumin or growth factors) with biological cations (b) Release curve of bovine serum alumin from PEG-DTT and PEG-DTT/Laponite hydrogels

4.3.5 Therapeutic efficacy and bioprinting advanced anatomical structures

Albumin release studies and rheology characterizations suggest that PEGDTT/Laponite are useful for precision therapeutic delivery vehicles. Albumin was used as a model protein for release study. Of biological importance are growth factors: a class of biologically relevant proteins that interact with cells to induce downstream effects such as proliferation, migration, and differentiation.[280, 281] Therapeutic efficacy of vascular endothethial growth factor (VEGF) and fibroblast growth factor (FGF) were measured by the migration of HUVECs across a transwell membrane. Because of the degradation profile and its ability to precisely deposit, PEG-DTT/Laponite hydrogels would be an advanced hydrogel appropriate for wound healing applications. VEGF and FGF induce migration of proliferation of human umbilical vein endothethial cells (HUVECs) *via* the MAPK pathway. Laponite was co-loaded with both VEGF and FGF in similar fashion as albumin. Hydrogels were placed on the bottom of a well and HUVECs were seeded on the top of transwell inserts. Nuclei and action staining *via* DAPI and Phalloidin respectively, suggest that samples containing growth factors induced similar response to the positive control of exogenously delivered growth factor (Figure 4-6a & c). PEG-DTT/Laponite and exogenously delivery growth factor had no difference in total number of migrating cells. PEGDTT was significantly different from exogenous control ($p=0.0044$) and PEGDTT/Laponite ($p=0.0248$). Samples that did not contain growth factor showed little to no cell migration. PEG-DTT/Laponite control was significantly different from no administered growth factor negative control ($p=0.0010$). When the samples containing growth factor and not containing growth factor are examined together, it is possible the Laponite XLG potentially acts as an angiogenic agent. Overall, staining suggested that HUVECs migrated through the transwell towards the biological active chemo-tractive agent. As such, delivery of

angiogenic growth factors could be used within PEG-DTT scaffolds to promote migration of endothelial cells in wounds.

Further scanning electron microscopy (SEM) images of the transverse side (non-cell seeded side) of the transwell insert suggest extracellular matrix deposition caused by migratory HUVECs on the growth factor containing scaffolds (Figure 4-6b). Growth factor free samples, expect for PEGDTT/Laponite, contained no amounts of deposited extracellular matrix. Small amounts of deposition of PEG-DTT/Laponite samples did occur due to possible ion dissolution that could influence cell phenotype.[273] SEM images coupled with actin/nuclei staining suggested that conjugated VEGF and FGF to Laponite retained bioactivity once released. Promoting retained bioactivity of growth factors could reduce the amount of growth factors to be administered and reduce potentially negative side-effects of supra-physiological growth factor doses.

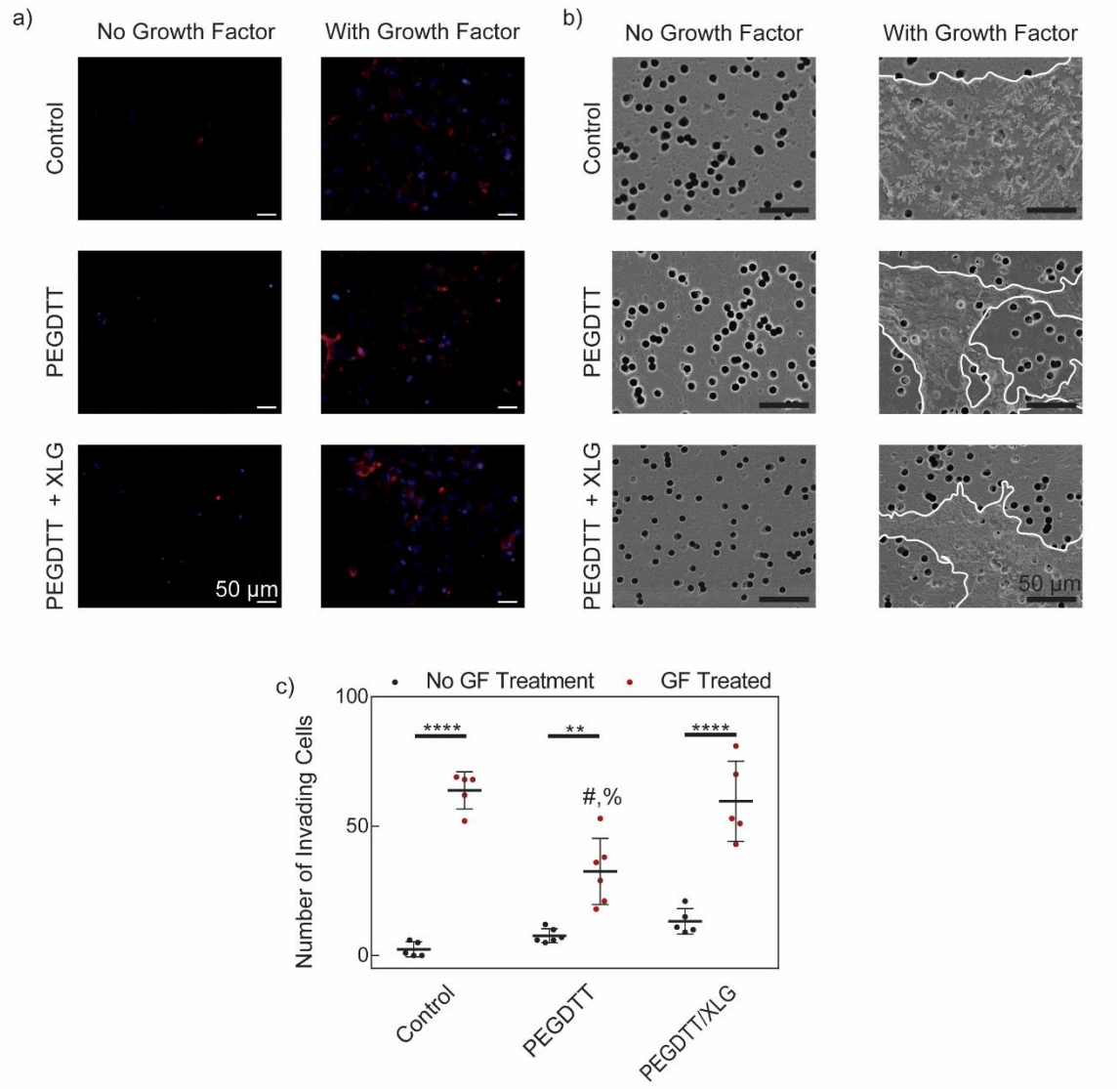

Figure 4-6. Cell response to release growth factors (a) Actin and nuclei staining of migrate HUVECs across transwell. Addition of growth factor influences cell migration. (b) SEM images of deposited extracellular matrix due to cell migration. (c) Invasion cell quantification.

Promotion of HUVEC migration *via* VEGF and FGF inclusion precludes the use of PEGDTT/Laponite as a possible arterial graft. A bifurcated vessel (3 cm height) was printed using the HYREL system (Figure 4-7a). Several needle gauges were tested and extrudate swell was calculated (Figure 4-7 b & c). 20-gauge needle extrudates swelled 3.49 ± 0.12% while 21-gauge

and 23-gauge needle extrudates swelled 24.55 ± 0.45% and 8.465 ± 0.26% respectfully. Volumetric flow rate and printing parameters were kept constant for all experiments. Extrudate swell along with rheological properties such as recovery time of sheared, un-crosslinked precursor solutions and the storage modulus of similar solutions dictate how well a material will print. Here, the print using 20-gauge needle did not collapse upon its own weight nor did it sag. The ability to print complex shapes warrants further investigation into HUVEC migration and direct interaction with PEG-DTT based scaffolds. Earlier studies have incorporated RGD binding sequences within PEG-DTT, which suggests that proteins cannot adhere to the surface due the hydrophilic nature of PEG and its relatively long backbone.[253] However, due to the large mesh size of PEGDTT, high viability of mesenchymal stem cells were observed. Further, incorporation of VEGF, FGF, or tethering of RGD hold potential for PEGDTT to become a fully functional tissue engineered scaffold.

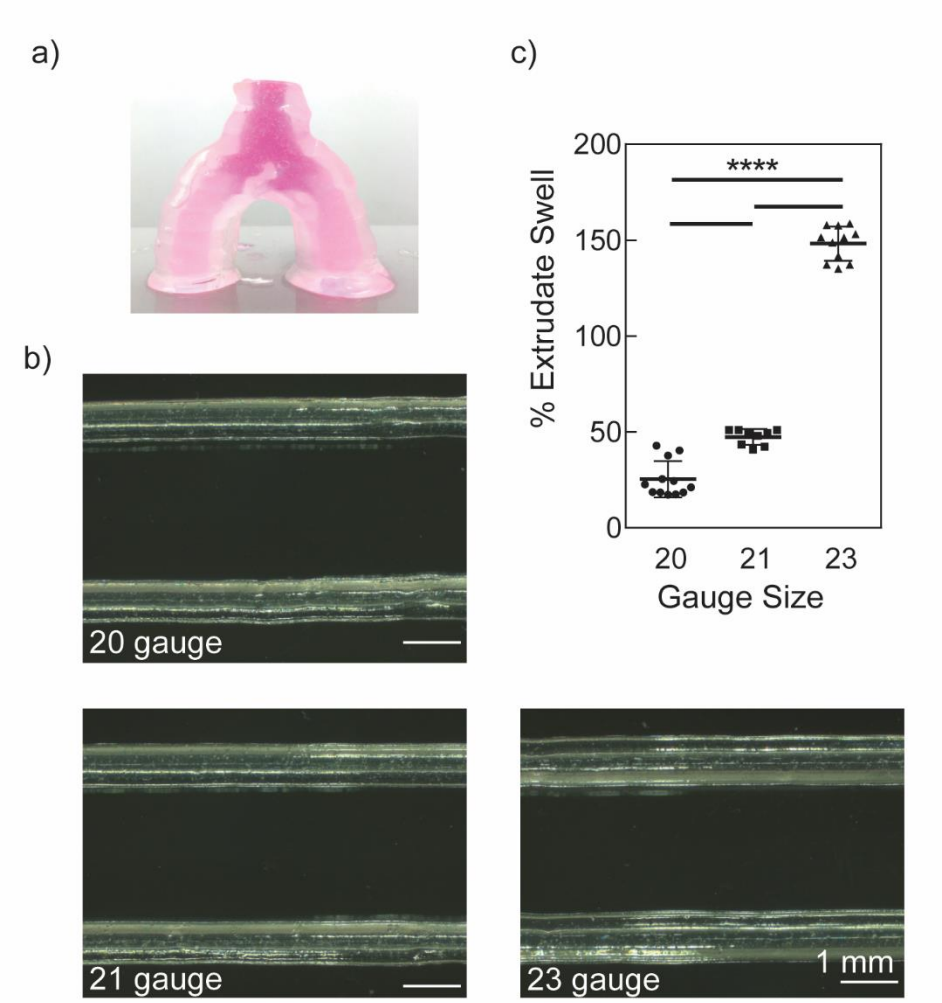

Figure 4-7. Printing PEGDTT/Laponite hydrogel. (a) Printed bifurcated vessel with rhodamine-B dyed PBS in the lumen. (b) Line prints using 20, 21, 23 gauge needle (c) Quantification of prints.

4.4 Conclusions

PEGDTT/Laponite XLG hydrogels have been examined for inclusion of and precision deposition of growth factor and modulation of degradation rate. Here, PEGDTT (initial molar ratios of 3:2::PEG:DTT) swelled and degraded within 21 days while the inclusion of Laponite decreased the degradation to ca. 7 days. Overall, modulating the degradation rate can be controlled via the

amount of PEG-DA included into the system. Furthermore, PEG molecular weight can influence swelling and degradation as demonstrated by earlier study.[253] The facile synthesis and modulation of degradation contributes to expansion of bioink compositions that undergo hydrolytic degradation. Using the cation exchange capacity of added Laponite, growth factors were able to be retained and released and also remained bioactive during this process. PEG-DTT/Laponite hydrogels hold promise for use as a hydrolytically degradable bioink that can be used in tissue engineering and in drug delivery applications.

5. TWO-DIMENSIONAL NANOSILICATES LOADED WITH PRO-ANGIOGENIC FACTORS STIMULATE ENDOTHELIA SPROUTING*

5.1 Introduction

Angiogenesis is a dynamic, multistep process that requires endothelial cells to undergo biochemical, morphological and biophysical changes such as basement membrane degradation, sprout initiation, proliferation, migration, lumen formation and stabilization.[282, 283] A range of rationally designed approaches are proposed to engineer angiogenic biomaterials.[284] However, therapeutic angiogenesis remains a major clinical challenge and only a few approaches have reached the market for wound-healing application.[284] Thus there is an unmet clinical need to develop new approaches to deliver pro-angiogenic therapeutics. Here, we introduce two-dimensional (2D) nanosilicates as a platform technology to sequester and deliver multiple pro-angiogenic growth factors to stimulate angiogenesis. These 2D nanosilicates are discotic charged nanoparticles that are 30-50 nm in diameter and 1-2 nm in thickness.[285, 286] Due to unique structural arrangements, the surface of nanosilicates are negatively charged and edge is positively charged. We propose to use the high surface area and charged characteristics of nanosilicates for sustained and prolonged delivery of pro-angiogenic molecules.

* D.W. Howell, C.W. Peak, K.J. Bayless, A.K. Gaharwar, Submitted to *Advanced Biosystems*, March 2018

Sequestering pro-angiogenic factors within biomaterials can be used to pattern and direct angiogenesis in tissue engineered scaffolds. Pro-angiogenic factors, such as VEGF, bFGF, and/or PDGF have been used to stimulate endothelial cells to form capillary networks in synthetic scaffolds.[287, 288] If these pro-angiogenic factors are randomly distributed in a tissue engineered scaffold, this could affect the normal growth and activities of non-vascular cells. The inability to accurately pattern angiogenic factors in a scaffold is a critical limiting step of engineering vascular tissues.[289, 290, 291] Although covalent crosslinking can solve this problem by appending functional proteins to the materials, crosslinking agents can also inactivate the tethered protein or remain embedded in the materials, rendering them toxic to cells.[292, 293]

A variety of polymeric, metallic and ceramic nanomaterials are being investigated to design angiogenic biomaterials.[294, 295, 296] However, most of these nanoengineered biomaterials are not able to sequester biomolecules for prolonged durations. Thus, there is a need to design and develop new nanocomposite biomaterials that deliver specific molecular cues and direct vascular cell adhesion, differentiation, migration, and extracellular matrix deposition.[297, 298] Extracellular responses to growth factors *in vitro* are dependent on exposure to adequate concentrations[299] while *in vivo*, overexpression of pro-angiogenic factors can result in aberrant angiogenesis[300] and enhanced angiogenic responses within tumors[301, 302]. Sustained and prolonged release of physiologically relevant dose of biomolecules can overcome these problems.

We propose to use 2D nanosilicates to delay the release of multiple growth factors, illustrating their utility in directing angiogenesis. Nanosilicate (Laponite, $Na^{+}_{0.7}[(Mg_{5.5}Li_{0.3})Si_8O_{20}\cdot(OH)_4]^{-}_{0.7}$) is a hydrous sodium lithium magnesium silicate and its ionic dissociation products of magnesium,

orthosilicic acid, and lithium can be readily absorbed *in vivo* and have been shown to be biocompatible.[77, 303] The complex phase diagram and presence of an electrical double layer permits therapeutic binding to the nanosilicates surface.[304, 305] Establishing nanosilicates as a platform technology for sequestering and delivery of pro-angiogenic factors will have significant impact on designing next-generation of bioactive scaffolds.

The bioactivity of sequestered pro-angiogenic molecules can be determined using three-dimensional (3D) invasion assays. Three-dimensional (3D) *in vitro* models of angiogenesis have emerged as reliable tools for studying different steps of angiogenesis[287, 306], along with a number of useful *in vivo* models.[307] These approaches have illuminated underlying mechanisms that control lumen formation[308, 309, 310] and endothelial cell sprouting.[287, 308, 311] Recently, we reported a straightforward and quantitative approach to investigate the bioactivity of pro-angiogenic factors using invasion assays,[312] which allow examination of the sprouting step of angiogenesis. Monolayers of endothelial cells penetrate three-dimensional collagen matrices and form sprouting structures orthogonal to the monolayer. The activity of biomolecules can be determined by quantifying invasion distance and frequency.

After establishing nanosilicates as a therapeutic delivery platform, we will develop a collagen based platform to promote angiogenesis. The presence of an electrical double layer permits therapeutic binding to and delayed release from nanosilicates.[304, 305] Utilizing the ion exchange capacity of nanosilicates, various growth factors are incorporated into collagen-based hydrogels that can be injected into a localized site and thermo-gelled. We hypothesize that the incorporation of nanosilicates will provide enhanced growth factor retention and prolonged release. The

interactions mediated by nanosilicates have the potential to be broadly used as a growth factor delivery and release mechanism while not interfering with mechanical properties of samples. The proposed collagen/ nanosilicates scaffolds further our understanding of this emerging class of biomaterials.

5.2 Materials and Methods

5.2.1 Cell Culture

Certified single-donor human umbilical vein endothelial cells (HUVECs; Lonza, Allendale, NJ) at passages 3–6 were cultured in 75 cm^2 flasks (Corning) coated with 1 mg/mL sterile gelatin. Growth medium was previously described in detail[313] and consisted of M199, supplemented with fetal bovine serum, bovine hypothalamic extract, heparin, antibiotics, and gentamycin.

5.2.2 Invasion Assay

3D invasion experiments were established using 2.5 mg/ml type I collagen matrices containing 1 μM S1P (Sigma, St Louis, MO). Confluent endothelial cell monolayers were seeded at 30,000 cells per well in M199 supplemented with 1× RSII and in controls, 40 ng/mL VEGF and bFGF. Where indicated, growth factors were incubated with multiple concentrations of Laponite (nanosilicates, nSi) for 1 hour on ice. Laponite was then mixed into collagen matrices prior to plating in 96-well plate. After 24 hour incubation at 37 °C with 5% CO2, invading cells were fixed with 3% glutaraldehyde in phosphate buffered saline and stained with 0.1% toluidine blue/30% methanol. Results from at least three independent experiments are shown.

5.2.3 Quantification of Invasion Responses

For invasion density measurements, a minimum of three fields were quantified manually with a Nikon Eclipse TE200-U microscope equipped with Metamorph software. For invasion distance, 150 or more structures from each treatment group were included in the analysis, where the distance migrated from the monolayer was recorded using side view images. Image-Pro PLUS (MediaCybernetics, MD) software was used to quantify invasion number and distance.

5.2.4 Dynamic Light Scattering and Zeta Potential Measurements

Dynamic light scattering (DLS) and zeta potential were measured on a Zetasizer Nano ZS (Malvern Instruments). One mL of nanosilicates or nanosilicates + fetal bovine serum (mixed for 1 hour) was diluted 1:100 with PBS and loaded into the instrument for both measurements. DLS samples were subsequently used for Zeta-potential samples and then discarded. Data was analyzed plotted and analyzed using Prism Graphpad 6.

5.2.5 Mechanical Analysis

A Discovery Hybrid Rheometer 2 (DHR-2) (TA Instruments, New Castle, Delaware, USA) with attached 40 mm parallel plate at gap height of 0.1 mm and Peltier plate accessory was used for all experiments. Pre-cursor solutions of collagen and collagen/0.05% nanosilicates (highest experimental concentration) were used for all experiments unless otherwise noted. Rotational shear rate sweeps were executed between 10^{-2}-10^{2} (s^{-1}) to determine shear-thinning behavior of solutions. Rotational temperature-time sweep combination were executed to determine curing characteristics. First a temperature ramp of 5°C/min was carried out from 25°C -37°C at 1% strain,

1 Hz. Subsequently a time sweep at 1% strain, 1 Hz was used to determine the amount of time for curing to occur. Oscillatory shear strain sweeps between 10^{-1}-10^{3} performed at 1 Hz and frequency sweeps between 10^{0}-10^{2} performed at 1% strain were conducted to monitor the linear visco-elastic region and determine yield strain.

5.2.6 Statistical Analysis

All statistical analyses were performed using Prism 6 (Graphpad Software, Inc.). For all experiments, at least three independent experiments were performed with n>3 replicate samples per experiment. No statistical method was used to predetermine sample size. Unpaired Student's t-test was performed on data comparing two groups, assuming similar variance. One-way or two-way analysis of variance with Holm-Sidak or Tukey's post hoc test for multiple comparisons and multiplicity-adjusted P-values are reported. In all studies, P-values <0.05 were considered significant.

5.3 Results and Discussion

5.3.1 Functionalization of Nanosilicates with Pre-angiogenic Growth Factor

Nanosilicates form stable colloidal networks in aqueous solution releasing counter ions from the surface.[314] The displacement of counter ions from nanosilicate surface enables conjugation of growth factors and drugs through ionic exchange. VEGF and FGF were mixed with increasing amounts of pre-exfoliated nanosilicates, mixed for 24 hrs, and centrifuged to separate nanosilicates/growth factor conjugate from media and unbound growth factor (Figure 5-1a). To confirm conjugation to nanosilicates, bovine serum albumin (40 ng/mL) was used as a model

protein. Dynamic light scattering and zeta potential measurements confirmed that nanosilicates/albumin conjugation occurred. Exfoliated nanosilicates are disc-shaped particles 1-2 nm thick and 20-30 nm in diameter.[303] Addition of growth factor *via* hydrogen bonding and van der Waals interactions results in an increase in hydrodynamic diameter of nanosilicates. Growth factor were ionically exchanged with the sodium ion to stabilize the solution but growth factors are much larger than sodium ions, resulting in a larger particle size. Similar work with dexamethasone and doxorubicin showed similarly that the spacing between particles is increased.[277, 315, 316] Bone morphogenic protein-2 (BMP2) and vascular endothelial growth factor (VEGF) have been delivered using clay based gels.[286, 317]

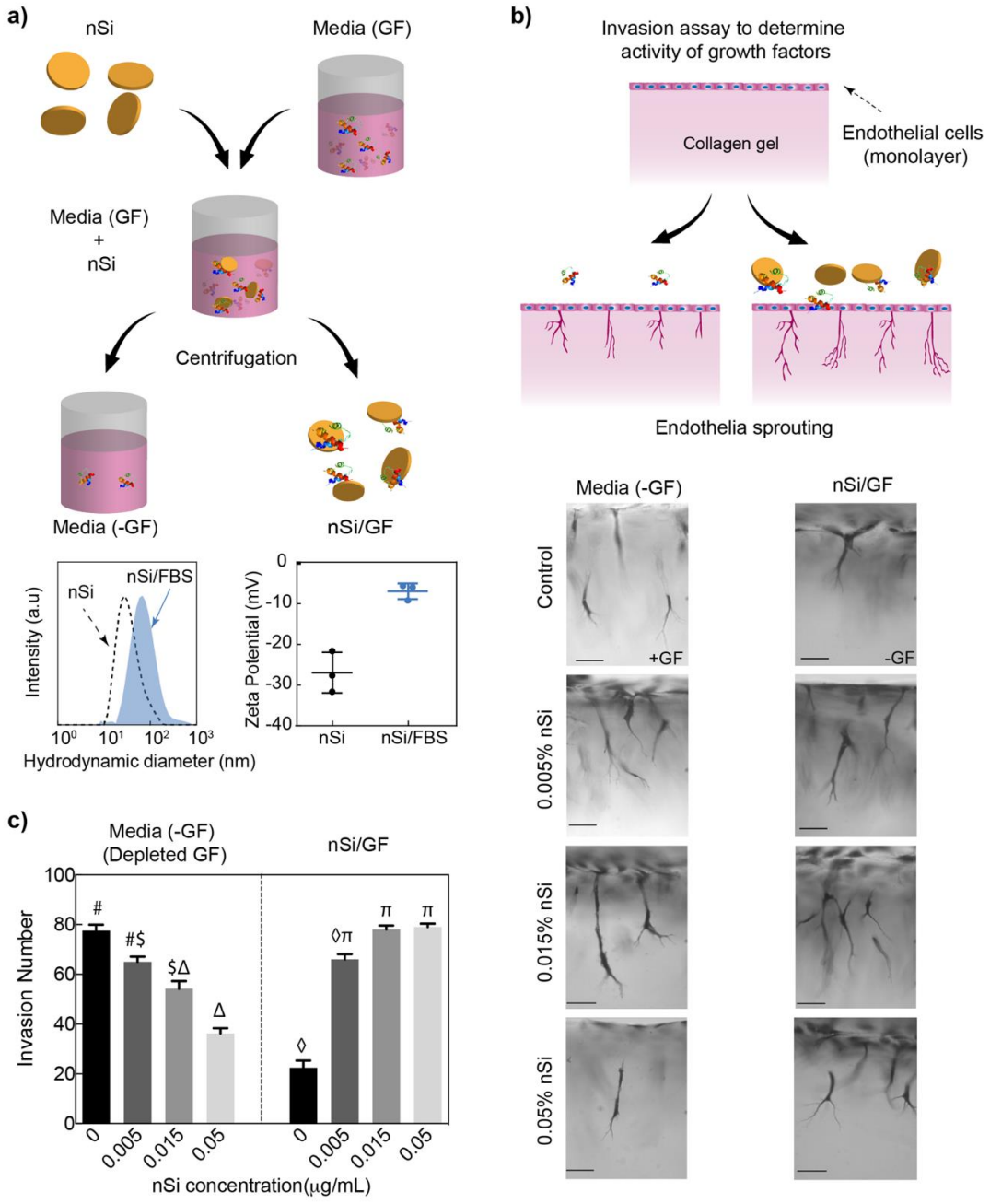

Figure 5-1. Nanosilicates sequester pro-angiogenic factors. **(a)** Sequestration of growth factor. Growth factors (VEGF and bFGF) were incubated with 0, 0.005%, 0.015%, and 0.05% nanosilicate before mixtures were centrifuged to pellet the nanosilicate and the media (unbound GF) is added in endothelial invasion assays. The pelleted nanosilicate is resuspended and tested separately (GF loaded nanosilicates). Sequestering of protein on nanosilicates results in increase in hydrodynamic diameter and zeta potential. (**b)** Schematic showing *in vitro* assay to determine the ability of nanosilicate (nSi) to sequester growth factors. Images of each invasion condition show the response to GFs incubated with increasing amounts of NS. **(c)** The number of invading structures that form in response to depleted GF and GF loaded nanosilicate media.

Additionally, the zeta potential is increased suggesting that the growth factor can readily adsorb and desorb compared to blank nanosilicates and exogenously delivered growth factor. To further understand these interactions and the ability of nanosilicates to control growth factor release, we designed invasion assays to test for an ability of nanosilicates to interact with growth factor and affect cell behavior.

In this study, we use an established three-dimensional invasion assay (Figure 5-1b) to examine the sprouting step of angiogenesis.[287, 313, 318] As a control, collagen gel containing sphingosine 1-phosphate (S1P)[319, 320] and growth factors (VEGF and bFGF) to stimulate the invasion of a monolayer of endothelia cells (ECs) into a basal 3D collagen matrix (Figure C-1a)[321, 322]. Endothelial cells subsequently penetrate the collagen matrices overnight and form sprouting structures orthogonal to the monolayer and exhibit a uniform response. Quantification of sprouting indicates that growth factors and S1P both promote invasion independently, but are most effective in combination **(**Figure C-1b). Similarly, the nanosilicates/growth factor conjugate and the excess media with growth factors were tested. A range of nanosilicates (0.005%, 0.015% and 0.05% wt/vol) were used to determine the minimum concentration of nanosilicates necessary to induce comparable invasion to exogenously delivered growth factor. After 24 hours, the invasion distance and frequency was quantified (Figure 5-1b). Interestingly, both media-depleted with growth factor and nanosilicates/growth factor conjugates showed invasion. However, upon quantification of cell invasion number two trends emerge: the ability of depleted media to induce invasion decreases with increasing nanosilicates concentration, and the number of invading cells increases with higher

nanosilicates/growth factor conjugates (Figure 5-1c; similar symbols denote significance, $p<0.01$). Further, the data suggests a minimum concentration of 0.015% nanosilicates is required to match the exogenously administered growth factor. There is a strong correlation between the invasion number and the concentration of nanosilicates. As nanosilicate concentration increases, the ability to adsorb growth factors when placed in media increases, suggesting that there is a minimum ratio between nanosilicates and growth factor. An increase in invasion with samples containing nanosilicates compared to exogenously delivered growth factors is hypothesized to occur since the growth factor can be released overtime. From these data alone, a minimum of 0.015% wt/vol nanosilicate has potential to deliver the physiological relevant concentration of growth factors. As such, nanosilicates/growth factor hold promise as an exogenous delivery vehicle.

5.3.2 Synthesis of Collagen/Nanosilicates Hydrogels

Bolus delivery of nanoparticles loaded with pro-angiogenic growth factors is not effective to direct angiogenesis. However, sequestering pro-angiogenic factors within collagen hydrogels can direct cell migration and angiogenesis. Here, we will evaluate the effect of nanosilicates on gelation kinetics and mechanical stability of collagen gels. Collagen matrices are formed *via* polymerization between three collagen fibrils at a neutral pH and at 37°C. Prior to matrix formation the collagen solutions have fluid-like consistency. Shear rate dependence of viscosity for collagen and collagen/nanosilicates matrices were investigated using continuous shear flow measurements. Shear-thinning behavior of gels is observed as demonstrated with a decrease in viscosity over increasing shear rate (Figure 5-2a). Shear-thinning behavior is important for localization of the matrices after injection within the body. Both collagen and collagen/nanosilicates exhibit shear-

thinning behavior and the inclusion of nanosilicates (0.015%) did not influence the shear-thinning ability of collagen gels. Temperature was precisely controlled at 37°C using a Peltier plate during shear-thinning experiments suggesting collagen has not fully crosslinked and can be extruded through a needle to be delivered in precise locations while undergoing bundle formation. Subsequent temperature ramp followed by a time sweep corroborates these conclusions (Figure 5-2b). Initially the storage modulus (G') is equal to or less than the loss modulus (G"). With an increase in temperature from 25°C to 37°C a rapid increase in both G' and G" occurs with G' overtaking G". Upon reaching physiological temperature (37°C), G' is approximately 100 Pa for both samples. This suggests that during matrix formation and curing that nanosilicates do not interfere with collagen fibril formation and that there is no difference in mechanical stability of the samples. Strain sweep suggest that samples containing nanosilicates have a storage modulus equal to those that do not contain nanosilicates. Further, nanosilicates samples could can withstand as much strain as those without (Figure 5-2c). These data suggest that collagen and collagen/nanosilicates matrices mechanically behave similarly. Additionally, there is no frequency dependence in modulus (Figure 5-2d). Overall, these data suggest that nanosilicates addition at such low concentration (0.015%) does not increase the mechanical properties of collagen matrices.

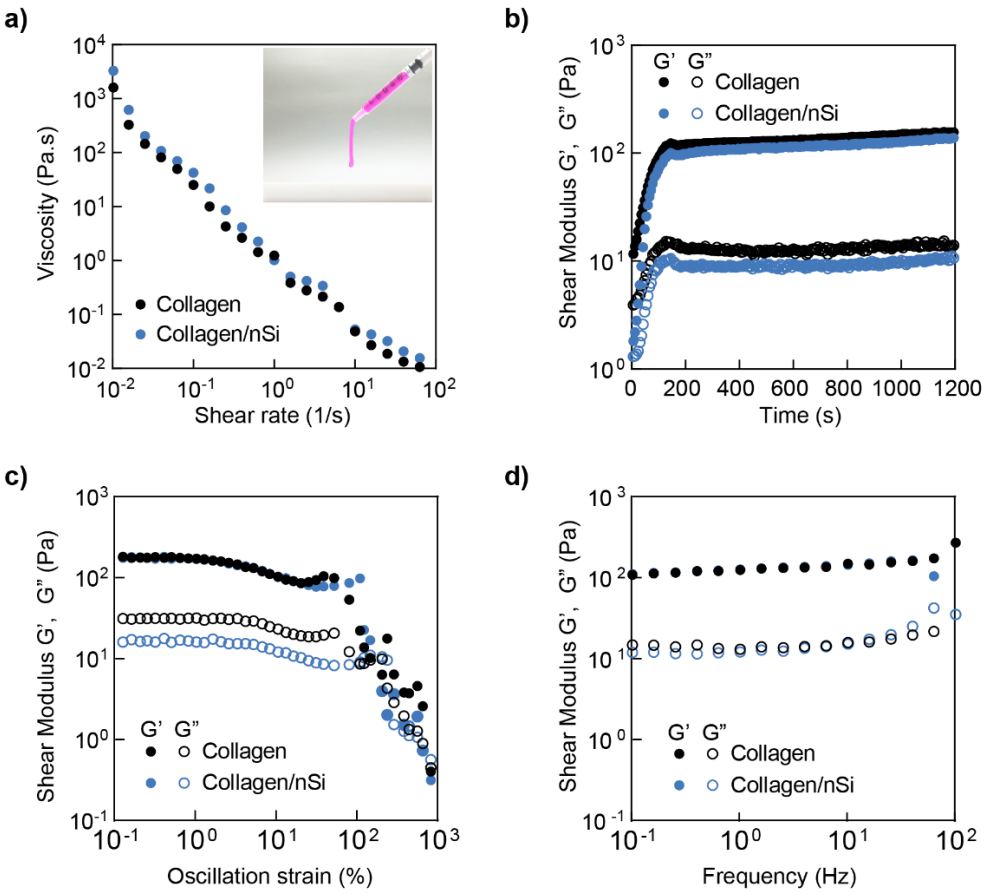

Figure 5-2. Rheological analysis for collagen and collagen/nanosilicates (nSi) hydrogels. (a) Shear-rate sweeps indicating shear-thinning behavior, (b) temperature/time sweep indicating the curing of collagen hydrogels, (c) amplitude sweep, and (d) frequency sweep. All tests indicate that addition of nSi (0.015%) do not alter mechanical properties of collagen matrices.

5.3.3 Sequestering Pro-angiogenic Growth Factor within Collagen/Nanosilicates Hydrogels

Nanosilicates can maintain growth factor bioavailability compared to exogenously delivered factors. Previously, we showed that growth factor loaded nanosilicate is capable of inducing an appropriate angiogenic response (Figure 5-1). However, nanosilicates must be incorporated into a stable matrix to prevent diffusion. Therefore, growth factors loaded onto nanosilicates to induce angiogenesis must be incorporated into a scaffold such as a collagen matrix. To fully develop a

nanocomposite material, two main concerns surround nanoparticle use: cytocompatibility and matrix mechanics. Our earlier study showed that the IC_{50} value of nanosilicates to be above 10^3 μg/mL.[323] Rheological analysis (Figure 5-2) shows that nanosilicates do not alter mechanical behavior of collagen matrices. Together, there is strong potential for nanosilicates to be used in collagen matrices solely as a growth factor delivery vehicle. To examine possible effects of nanosilicates in our 3D collagen invasion system, we used four different conditions in the 3D invasion system (Figure 5-3a): 1) collagen matrix with growth factors in the media (control); 2) collagen matrix with growth factors embedded in the matrix; 3) blank nanosilicate embedded in the collagen matrix with growth factors in the media; and 4) growth factor loaded nanosilicate embedded in the collagen matrix. Both the number and distance of invading structures are critical components of assessing an angiogenic response and are dependent on mechanical stiffness of the matrix[324], fluid shear stress[318], and delivery of appropriate concentrations of angiogenic factors (Figure C-1).[287]

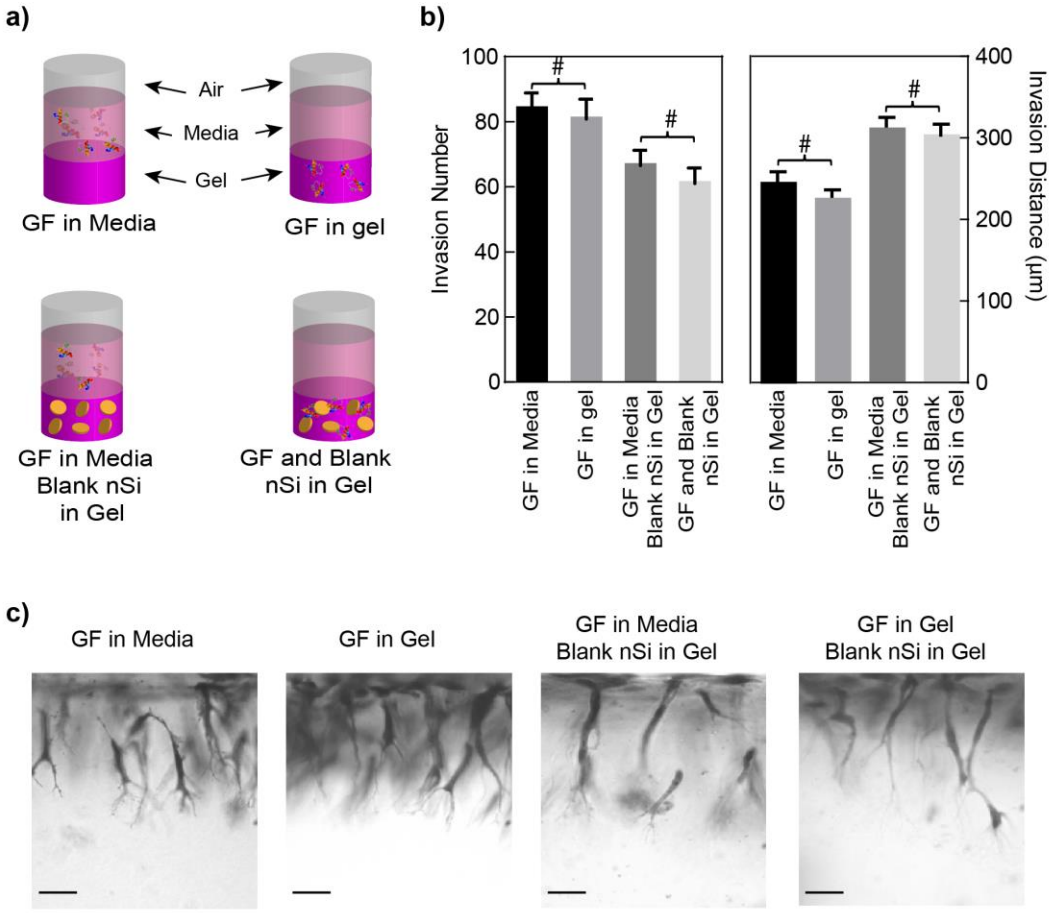

Figure 5-3. Nanosilicates incorporated into collagen matrices reduce invasion density but increase invasion distance. (a) Schematic illustrating the presence of growth factor (GF) and blank nanosilicate (nSi) in media and collagen matrix. (b) Quantification of invading structures and invasion distance. (c) Photographs of invading structures (Scale bar= 50 μm).

The results (Figure 5-1 and 5-3) support that nanosilicates increased the number of invading cells by sequestering growth factors. Growth factors exogenously delivered in media supports a large amount of invading cells but low invasion distance while inclusion of nanosilicates supports less invasion but longer distance (Figure 5-3b; # denotes significant difference, $p<0.001$). While this is confounding, the localization and sequestration of growth factors on the nanosilicates is responsible for these results. With exogenously delivered growth factor, denaturation can occur

and/or cells may immediately uptake leading to increased number of invading structures. However, since the growth factor is administered in bolus the cells have no factors to induce depth of invasion. Growth factor adsorbed onto nanosilicates appears to remain bioactive and homogenously localized throughout the collagen matrix compared to growth factor that can freely diffuse through the matrix. Interestingly, blank nanosilicates loaded with collagen matrices behave very similarly to pre-growth factor loaded nanosilicates suggesting that when growth factor is administered exogenously and not immediately used sequestration may occur. Morphology of invading cells appears consistent throughout all samples (Figure 5-3c) suggesting that collagen matrix is predominate in morphology formation while nanosilicates/growth factors are responsible for cell invasion.

5.3.4 Nanocomposites with Gradient of Pro-angiogenic Factors

Developing nanocomposite hydrogels with tailored functionality has opened up new possibilities in engineering advanced biomaterials for various biomedical and biotechnological applications.[325, 326] Unfortunately, very few nanoparticles have been developed to influence cell migration and angiogenesis. Previously, a range of appropriate biological clues, such as VEGF, FGF, and PDGF have been incorporated within hydrogels to direct cell migration.[327, 328] While effective, this incorporation strategy limits the time that growth factors are available since they may freely diffuse through the matrix or solution therefore causing sprouting to occur at random locations. To limit diffusion, methods such as encapsulation, tethering, or isolation have been utilized. Adsorption of growth factor milieu to nanosilicates has previously been established (Figure 5-1). To further establish that individual growth factors adsorb to nanosilicates surface and that there is a

synergistic effect, similar invasion assay is carried out with each growth factor individually and in combination. In all cases nanosilicates loaded with growth factors and embedded in three-dimensional collagen matrices induced endothelial invasion (Figure 5-4a). Single growth factors produced a mild response with a relatively low number (<50) and low distance (<250 μm). While PDGF has been well studied as an important growth factor during wound healing by promoting angiogenesis, the combination with nanosilicates did not produce as strong of a response as expected. There is a statistically significant ($p<0.001$) difference of combining PDGF with VEGF or FGF compared to PDGF by itself (Figure 5-4b). FGF and VEGF combinations resulted in little to no change when compared to combinations, except for the combination of all three growth factors. Results could be due to the short half-life of PDGF compared to FGF and VEGF or PDGF inability to bind to nanosilicates. Overall, these results are consistent with the behavior of these growth factors in the literature[287, 313, 329, 330] and confirm the ability of nanosilicates to deliver angiogenic factors in specific combinations and efficiencies to direct cellular invasion.

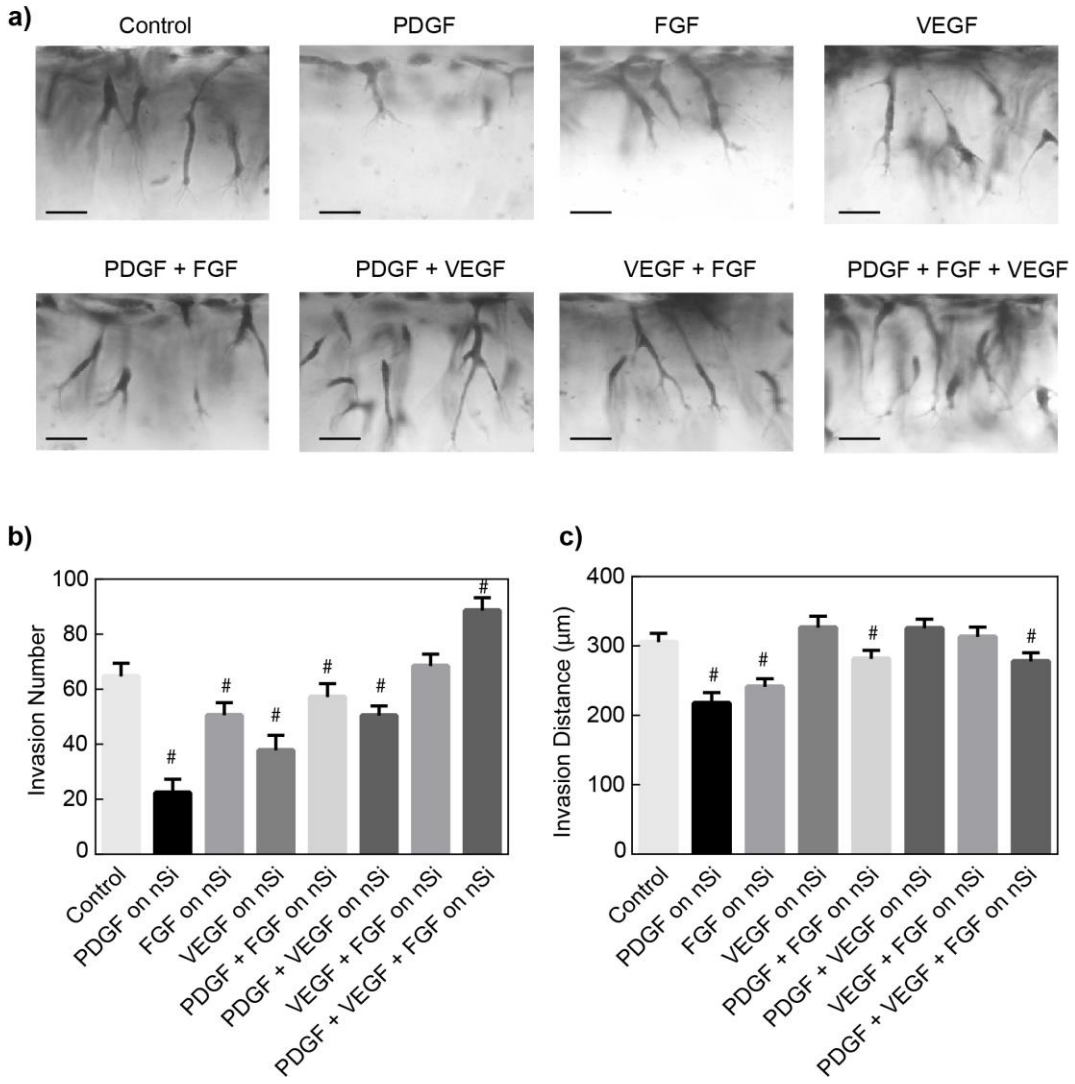

Figure 5-4. Nanosilicates deliver multiple GFs to enhance angiogenic responses. Nanosicliates (nSi) are loaded with PDGF, bFGF, VEGF alone and in combination prior to embedding in collagen matrices. Control is growth factors in media with blank nanosilicates in the gel (see Figure 3, condition 3) (a) Photographs of invasion responses (Scale bar= 50 μm), and quantification of (b) invading structures and (c) invasion distance.

5.3.5 Patterning Nanosilicate Delivery of Growth Factor

Tissues and interfaces within the human body display complex cellular and mechanical characteristics. Current approaches rely on discrete material steps with individual properties rather

than continuous gradient designs.[331] Commonly, layered or stratified scaffolds often incorporate multiple materials and cell types to mimic the distinct tissue regions.[332] Alternatively, gradient scaffold designs can mimic the gradual change in the physical and mechanical properties that are present at the native tissue interface and therefore offer a seamless transition between tissue regions without being susceptible to delamination.[333, 334] Previous development of a facile approach to fabricate a nanocomposite gradient hydrogel using the material's flow properties has occurred.[333] As a culmination, we aim to fabricate injectable collagen based scaffolds that can be patterned by the inclusion of specific growth factors. A 2 mm deep, 1 cm long well was created on Teflon in which to inject various solutions. Collagen/nanosilicates matrices were injected into the well and allowed to flow through the channel (Figure 5). Nanosilicate addition to the collagen matrics does not change its flow properties (Figure 5-2a) and the flow is dependent on the time it takes the solution to crosslink. During the crosslinking phase, there was sufficient time for two separate solutions to flow to the middle and form a complete matrix. The concentration of nanosilicates is constant throughout but in one solution the nanosilicates were previously loaded with growth factor (FGF and VEGF), while the second contained pure collagen with no growth factor. Invasion of seeded endothelial cells were observed on the end containing growth factors and not on the pure collagen/nanosilicates matrix. Of note, there appears to be an increasing number of invading cells as the gradient progresses toward the end where growth factor loaded nanosilicates were placed. This suggests that the two similar materials (difference being the inclusion of growth factor) mixed through simple diffusion and flow through the channel. This facile approach demonstrates a method to pattern endothelial cell ingrowth while maintaining mechanical properties. Potential applications are in tendon or ligament repair where there is a gradient of cells but no difference in matrix material properties. A simple unidirectional channel and nanosilicates/growth factor

(combination) suggests that this concept can be furthered for precision localization of growth factor and for more complex structures.

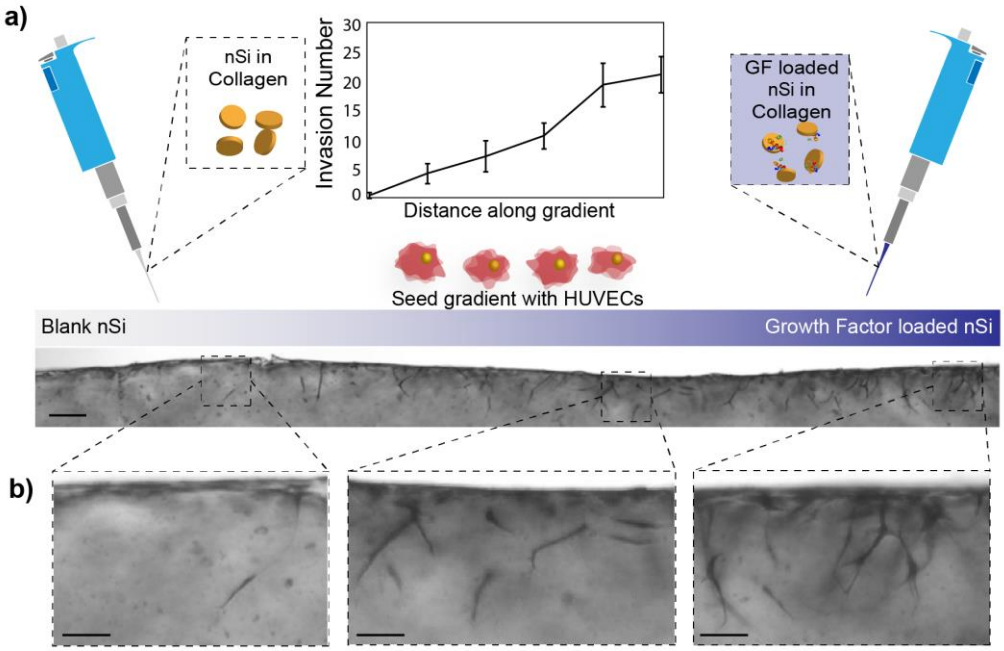

Figure 5-5. Nanosilicates offer the unique ability to pattern the delivery of growth factors. (a) In this assay, nanosilicates(nSi) is incorporated into 3D collagen matrices as a gradient. The number of invading structures was quantified and averaged from 3 independent experiments. Data shown are average numbers of invading cells (+/- st.dev). (b) Photograph of entire 8mm gradient formed with blank nanosilicates and growth factor loaded nanosilicates. Insets show enlarged view of indicated structures (lower panels).

5.4 Conclusions

In summary, our results demonstrate the stability of nanosilicates/growth factor conjugates and their ability to deliver growth factors to induce an angiogenic response. The sequestration of growth factor permits greater depth penetration of invading cells, creating more fully formed lumen of potential blood vessels. We observe robust response of cell penetration into collagen

matrices loaded with nanosilicates. The resulting invasions are controlled predominately by the type of growth factors conjugated to the nanosilicates. This work illustrates the importance of nanoparticle-therapeutic conjugation for angiogenic potential with important ramifications in the selection of growth factors and ability to investigate new therapeutics through use of a 3D cellular invasion assay.

6. FUTURE RECOMMENDATIONS

Engineering complex tissues that can mimic, augment or replace native tissue functions hold enormous promise in treating organ failures resulting from injuries, aging, and diseases. [228, 335, 336, 337, 338, 339] The current tissue engineering paradigm consisting of cells, signals, and scaffolds hold promise; however, the inability to mimic complex tissue architectures and provide the essential cellular microenvironment is a challenge that needs to be addressed to control the formation of functional tissues.[291, 340, 341] Poly(ethylene glycol) hydrogels have been proven to be useful for studying fundamental interactions between polymer and nanoparticles along with changes in stiffness, adhesion ligand addition, and other factors.[279, 342, 343] In the afore studies, rotational rheometry was used to understand underlaying mechanics of injectable and printable hydrogel precursors. Modifications to the hydrogel composition enhanced cell proliferation and aided hydrolytic degradation as well. Consideration of polymer molecular weight was governed by the kidney clearance[270] without considerations into anatomical pore size, limiting the use of the designed hydrogels in application.

One challenge in design of injectable, recoverable hydrogel precursors is mesh size optimization and oxygen diffusivity. Short chain (<10 kDa molecular weight) non-ionic polymer quickly adsorbs and desorbs from Laponite XLG surface permitting Laponite-Laponite interactions. However in pure poly(ethylene glycol) hydrogels, short chains cause small mesh size. While we examined mesh size via SEM, application of Flory-Rehner equations is more appropriate. Calculating mesh size via Flory-Rehner across multiple PEG molecular weights validates release

rate of various therapeutics.[344] Validating mesh size for is vital for nutrient diffusion and cell micro-mechanics. However, balance between pore size via long chain polymer and flow properties is crucial for potential bioinks. With increased molecular weight polymer, Laponite-Laponite electro-static interactions may be impeded by polymer chains wrapping around the particles resulting in flocculations.[345] The resulting solution viscosity will be determined by the amount of free-chain polymer in solution which tend to have low viscosity. Variation of polymer molecular weight will further influence oxygen diffusion which is of importance for cell integration.

A challenge with constructing nanocomposite hydrogels is determining the physical interactions between polymer and nanoparticles. Rheology summates the interactions between all components; however, Laponite-Laponite and Laponite-PEG can be expanded via use of the Hamaker equation and Huckel-Debye equations. Previous work by Nelson et al.[164, 166, 174] investigated the Debye screening length via small-angle neutron scattering and dynamic light scattering. Calculating the screening lengths of Laponite-Laponite interactions can inform the maximum distance for "house-of cards" formation. Approximating appropriate non-ionic polymer chain lengths can occur through further determining interactions between polymer and Laponite. Through physical characterization of these interactions, nanocomposite design can progress in theory rather than using experimentally.

The developed hydrogel precursors exhibit necessary yield stress, shear-thinning indexes, and recovery times to be used as printable cell-supportive matrices. Upon the establishment of rheological considerations, further biological characterization can be completed. While literature supports two-dimensional cell proliferation with PEG/Laponite hydrogels, there is little

information concerning three-dimensional culture. Examination of GAG and collagen deposition for encapsulated cells will be integral for future assessments of 3D printed constructs.[346, 347] Increasing physiological complexity will also accelerate adoption of printable hydrogels. Currently, most studies incorporate one cell and material type. In Study 2 we incorporated mc3T3 and MOSJ cells in a co-culture model and it exhibits flow properties complementary to direct write extrusion bioprinting. Future work can further physiological systems that can be mimicked. For example, a hollow tube reminiscent of blood vessels with encapsulated smooth muscle cells and seeded endothelial cells could printed and is an appropriate physiological model.

Increasing physiological complexity encourages expansion of printable polymers. Current systems, such as alginate, have been widely used but poorly studied in terms of their various rheological profiles. Future endeavors should examine the recovery time of "classical" 3D printable polymers such as alginate and gelatin. A library can be constructed to aid biomedical engineers in selection of printable hydrogels.

7. CONCLUSIONS

Throughout these works, we have designed a family of shear-thinning hydrogel bioinks. Understanding the interactions between polymer and nanoparticles, flow behavior of hydrogels can be controlled. We have found that recovery of hydrogel precursors as determined by peak-hold rheological characterization is a better predictor of printability.

In Study 1, "*Nanoengineering Colloidal Inks for 3D Bioprinting*," fundamental interactions between poly(ethylene glycol) (PEG) and Laponite XLG were investigated through rheological characterization. Laponite XLG was predominately responsible for inducing shear-thinning characteristics and increasing solution viscosity. From these experiments, flow behavior index, n, should be < 0.3 and flow consistency index, K, should be ~ 1000 Pa·s for use as a bioink. Additionally, for solutions having zero-shear viscosities > 1000 Pa·s, 80% recovery time post high shear rates (>1000s^{-1}) should be < 30 s. These parameters ensure prints that do not have large post-printing swelling, sagging, or collapse of structure.

In Study 2, "*Elastomeric Cell-laden Nanocomposite Microfibers for Engineering Complex Tissues*," the addition of gelatin methacrylate facilitated pre-osteoblast adhesion and spreading as compared to pure poly(ethylene glycol)/Laponite hydrogel precursor solutions. We were able to provide spatiotemporal control over multiple cell types *via* encapsulation and 2D seeding. Overall,

validation of gelatin inclusion *via* cell spreading measurement while maintaining the proper flow properties was used to design microfibers that can be formulated for 3D printing. Degradation of the matrix was able to occur due to gelatin presence.

Alternatively, in Study 3, "*Therapeutic Delivery via 3D Printing Viscous Bioink*," hydrolytic degradation of the hydrogel occurred. Modification of the poly(ethylene glycol) backbone *via* Michael-like addition with dithiothreitol causes the susceptibility of the ester to accelerated degradation. Further, pH changes due to Laponite XLG facilitate modulation of the degradation while providing a means of growth factor conjugation. Through ion exchange growth factors were conjugated and released from PEG-DTT/Laponite hydrogels that exhibited the flow parameters elucidated from Study 1. Inclusion of Laponite XLG permitted the solutions to be printable into complex (bifurcated vessel) shapes. Migration of HUVECs across a transwell spurred further investigation of Laponite and a therapeutic delivery vehicle.

Using Laponite XLG/nanosilicates as a delivery vehicle was investigated in Study 4, "*Two-dimensional Nanosilicates Loaded with Pro-angiogneic Factors Stimulate Endothelia Sprouting*." VEGF, FGF, and PDGF were used as pro-angiogenic factors while conjugated and released from Laponite within 3D collagen gels. Sprouting number and frequency increased when the factors were administered with Laponite as compared to individually. Specifically, we were able to pattern specific areas of the collagen gel with nanosilicate conjugated growth factor as compared to current standards that have a homogenous distribution of growth factor. This technique is advantageous

since selective patterning of ex vivo constructs can occur. Vascularization of tissue engineered constructs remains a major hurdle within the field and these experiments provide an alternative method for sustained delivery of growth factors.

These works present significant advances in understanding the rheological characterization of hydrogel precursor solutions that are to be used as bioinks. In particular examination of recovery through peak-hold experiments are essential to accurately mimic the flow process of hydrogel precursors during the extrusion process. Application of precise shear rates experiences as determined using the flow behavior index best predicts a solutions ability to print without spreading. Careful control of the amount of interactions between polymer and Laponite nanoparticles govern the flow consistence and flow index values. High molecular weight polymers without electrical charge or high concentration of polymer have potential to block Laponite-Laponite interactions which interferes with internal "house-of-cards" structure formation leading to a decrease in polymer. Alternatively, low molecular weight or concentration of polymer aids in formation of internal structure as Laponite-Laponite interactions are dominate. Formation of the internal hydrogel precursor structure elicits characteristics such as yield stress, storage modulus, and viscosity.

For biomedical applications, control of hydrogel precursor rheological properties directs ease of cell incorporation, shear stress experienced by cells, and overall anatomical shape formation. Higher yield stresses cause inhomogeneous cell incorporation (study 1). In modulating the concentrations of polymer and Laponite, yield stress can be carefully controlled for homogeneous

cell incorporation. For biological applications, homogeneous cell incorporation permits for consistent cell response, growth, proliferation, and long term functionality. Shear-thinning hydrogels lower the shear-stress cell experience, increasing cell viability. When printing cell-laden hydrogel precursors, anatomical structures will be necessary long-term. Quickly recovering hydrogel precursor solutions when coupled with solutions viscosities above 1000 Pa·s permit for complex structure formation.

Rheological characterization of hydrogel precursor bioinks is an integral step in determination of hydrogel viability for printing purposes. Combined, these work elucidate fundamental flow properties while demonstrating modulation in cell adhesion and degradation of the hydrogel.

REFERENCES

1. Gibson, I.; Rosen, D. W.; Stucker, B. *Additive Manufacturing Technologies: Rapid Prototyping to Direct Digital Manufacturing* 2010. p 1-459.

2. Marx, V. Tissue engineering: Organs from the lab. *Nature* **2015,** *522* (7556), 373-377.

3. Hern, D. L.; Hubbell, J. A. Incorporation of adhesion peptides into nonadhesive hydrogels useful for tissue resurfacing. *J. Biomed. Mater. Res.* **1998,** *39* (2), 266-276.

4. Zhou, M.; Smith, A. M.; Das, A. K.; Hodson, N. W.; Collins, R. F.; Ulijn, R. V.; Gough, J. E. Self-assembled peptide-based hydrogels as scaffolds for anchorage-dependent cells. *Biomaterials* **2009,** *30* (13), 2523-2530.

5. Brandl, F.; Sommer, F.; Goepferich, A. Rational design of hydrogels for tissue engineering: Impact of physical factors on cell behavior. *Biomaterials* **2007,** *28* (2), 134-146.

6. Ventre, M.; Causa, F.; Netti, P. A. Determinants of cell–material crosstalk at the interface: towards engineering of cell instructive materials. *Journal of The Royal Society Interface* **2012,** doi: 10.1098/rsif.2012.0308.

7. Kisiday, J.; Jin, M.; Kurz, B.; Hung, H.; Semino, C.; Zhang, S.; Grodzinsky, A. J. Self-assembling peptide hydrogel fosters chondrocyte extracellular matrix production and cell division: Implications for cartilage tissue repair. *Proceedings of the National Academy of Sciences* **2002,** *99* (15), 9996-10001.

8. Mann, B. K.; Schmedlen, R. H.; West, J. L. Tethered-TGF-β increases extracellular matrix production of vascular smooth muscle cells. *Biomaterials* **2001,** *22* (5), 439-444.

9. Zeltinger, J.; Sherwood, J. K.; Graham, D. A.; Mueller, R.; Griffith, L. G. Effect of pore size and void fraction on cellular adhesion, proliferation, and matrix deposition. *Tissue Eng.* **2001,** *7* (5), 557-572.

10. Slaughter, B. V.; Khurshid, S. S.; Fisher, O. Z.; Khademhosseini, A.; Peppas, N. A. Hydrogels in regenerative medicine. *Adv. Mater.* **2009,** *21* (32-33), 3307-3329.

11. Drury, J. L.; Mooney, D. J. Hydrogels for tissue engineering: scaffold design variables and applications. *Biomaterials* **2003,** *24* (24), 4337-4351.

12. Billiet, T.; Vandenhaute, M.; Schelfhout, J.; Van Vlierberghe, S.; Dubruel, P. A review of trends and limitations in hydrogel-rapid prototyping for tissue engineering. *Biomaterials* **2012,** *33* (26), 6020-6041.

13. Mohammadi, A. Transport in droplet-hydrogel composites: response to external stimuli. *Colloid Polym. Sci.* **2015,** *293* (3), 941-962.

14. Aktas, S.; Kalyon, D. M.; Marin-Santibanez, B. M.; Perez-Gonzalez, J. Shear viscosity and wall slip behavior of a viscoplastic hydrogel. *J Rheol* **2014,** *58* (2), 513-535.

15. Unger, C.; Gruene, M.; Koch, L.; Koch, J.; Chichkov, B. N. Time-resolved imaging of hydrogel printing via laser-induced forward transfer. *Appl Phys a-Mater* **2011,** *103* (2), 271-277.

16. Roth, E. A.; Xu, T.; Das, M.; Gregory, C.; Hickman, J. J.; Boland, T. Inkjet printing for high-throughput cell patterning. *Biomaterials* **2004,** *25* (17), 3707-3715.

17. Elisseeff, J.; Anseth, K.; Sims, D.; McIntosh, W.; Randolph, M.; Yaremchuk, M.; Langer, R. Transdermal photopolymerization of poly (ethylene oxide)-based injectable hydrogels for tissue-engineered cartilage. *Plastic and Reconstructive Surgery* **1999,** *104* (4), 1014-1022.

18. Tan, H.; Marra, K. G. Injectable, Biodegradable hydrogels for tissue engineering applications. *Materials* **2010,** *3* (3), 1746.

19. Tharp, K. M.; Jha, A. K.; Kraiczy, J.; Yesian, A.; Karateev, G.; Sinisi, R.; Dubikovskaya, E. A.; Healy, K. E.; Stahl, A. Matrix-assisted transplantation of functional beige adipose tissue. *Diabetes* **2015,** *64* (11), 3713-3724.

20. Choi, S.-W.; Zhang, Y.; Xia, Y. Three-dimensional scaffolds for tissue engineering: the importance of uniformity in pore size and structure. *Langmuir* **2010,** *26* (24), 19001-19006.

21. Lu, W. N.; Lu, S. H.; Wang, H. B.; Li, D. X.; Duan, C. M.; Liu, Z. Q.; Hao, T.; He, W. J.; Xu, B.; Fu, Q.; Song, Y. C.; Xie, X. H.; Wang, C. Y. Functional improvement of infarcted heart by co-injection of embryonic stem cells with temperature-responsive chitosan hydrogel. *Tissue Eng. Part A* **2009,** *15* (6), 1437-1447.

22. Plotkin, M.; Vaibavi, S. R.; Rufaihah, A. J.; Nithya, V.; Wang, J.; Shachaf, Y.; Kofidis, T.; Seliktar, D. The effect of matrix stiffness of injectable hydrogels on the preservation of cardiac function after a heart attack. *Biomaterials* **2014,** *35* (5), 1429-1438.

23. Yoon, S. J.; Fang, Y. H.; Lim, C. H.; Kim, B. S.; Son, H. S.; Park, Y.; Sun, K. Regeneration of ischemic heart using hyaluronic acid-based injectable hydrogel. *Journal of Biomedical Materials Research Part B: Applied Biomaterials* **2009,** *91B* (1), 163-171.

24. Park, H.; Choi, B.; Hu, J.; Lee, M. Injectable chitosan hyaluronic acid hydrogels for cartilage tissue engineering. *Acta Biomater.* **2013,** *9* (1), 4779-4786.

25. Temenoff, J. S.; Athanasiou, K. A.; Lebaron, R. G.; Mikos, A. G. Effect of poly(ethylene glycol) molecular weight on tensile and swelling properties of oligo(poly(ethylene glycol) fumarate) hydrogels for cartilage tissue engineering. *J. Biomed. Mater. Res.* **2002,** *59* (3), 429-437.

26. Elisseeff, J. Injectable cartilage tissue engineering. *Expert Opinion on Biological Therapy* **2004,** *4* (12), 1849-1859.

27. Lee, W.; Debasitis, J. C.; Lee, V. K.; Lee, J.-H.; Fischer, K.; Edminster, K.; Park, J.-K.; Yoo, S.-S. Multi-layered culture of human skin fibroblasts and keratinocytes through three-dimensional freeform fabrication. *Biomaterials* **2009,** *30* (8), 1587-1595.

28. Murphy, S. V.; Skardal, A.; Atala, A. Evaluation of hydrogels for bio-printing applications. *J. Biomed. Mater. Res. Part A* **2013,** *101* (1), 272-284.

29. Das, S.; Bourell, D. L.; Babu, S. S. Metallic materials for 3D printing. *Mrs Bulletin* **2016,** *41* (10), 729-741.

30. Hwa, L. C.; Rajoo, S.; Noor, A. M.; Ahmad, N.; Uday, M. B. Recent advances in 3D printing of porous ceramics: a review. *Current Opinion in Solid State and Materials Science* **2017**.

31. Ligon, S. C.; Liska, R.; Stampfl, J.; Gurr, M.; Mülhaupt, R. Polymers for 3D printing and customized additive manufacturing. *Chem Rev* **2017,** *117* (15), 10212-10290.

32. Peak, C. W.; Wilker, J. J.; Schmidt, G. A review on tough and sticky hydrogels. *Colloid Polym. Sci.* **2013,** *291* (9), 2031-2047.

33. Malda, J.; Visser, J.; Melchels, F. P.; Jungst, T.; Hennink, W. E.; Dhert, W. J. A.; Groll, J.; Hutmacher, D. W. 25th Anniversary Article: Engineering hydrogels for biofabrication. *Adv. Mater.* **2013,** *25* (36), 5011-5028.

34. Chimene, D.; Lennox, K. K.; Kaunas, R. R.; Gaharwar, A. K. Advanced bioinks for 3D printing: a materials science perspective. *Annals of Biomedical Engineering* **2016,** *44* (6), 2090-2102.

35. Raphael, B.; Khalil, T.; Workman, V. L.; Smith, A.; Brown, C. P.; Streuli, C.; Saiani, A.; Domingos, M. 3D cell bioprinting of self-assembling peptide-based hydrogels. *Mater. Lett.* **2017,** *190* (Supplement C), 103-106.

36. Compton, B. G.; Lewis, J. A. 3D-printing of lightweight cellular composites. *Adv. Mater.* **2014,** *26* (34), 5930-5935.

37. Bertassoni, L. E.; Cardoso, J. C.; Manoharan, V.; Cristino, A. L.; Bhise, N. S.; Araujo, W. A.; Zorlutuna, P.; Vrana, N. E.; Ghaemmaghami, A. M.; Dokmeci, M. R.; Khademhosseini, A. Direct-write bioprinting of cell-laden methacrylated gelatin hydrogels. *Biofabrication* **2014,** *6* (2).

38. Du, M. C.; Chen, B.; Meng, Q. Y.; Liu, S. M.; Zheng, X. F.; Zhang, C.; Wang, H. R.; Li, H. Y.; Wang, N.; Dai, J. W. 3D bioprinting of BMSC-laden methacrylamide gelatin scaffolds with CBD-BMP2-collagen microfibers. *Biofabrication* **2015,** *7* (4).

39. Khalil, S.; Sun, W. Bioprinting endothelial cells with alginate for 3D tissue constructs. *Journal of Biomechanical Engineering* **2009,** *131* (11), 111002-111002-8.

40. Jia, J.; Richards, D. J.; Pollard, S.; Tan, Y.; Rodriguez, J.; Visconti, R. P.; Trusk, T. C.; Yost, M. J.; Yao, H.; Markwald, R. R.; Mei, Y. Engineering alginate as bioink for bioprinting. *Acta Biomater.* **2014,** *10* (10), 4323-4331.

41. Wang, X. H.; Ao, Q.; Tian, X. H.; Fan, J.; Tong, H.; Hou, W. J.; Bai, S. L. Gelatin-based hydrogels for organ 3D bioprinting. *Polymers* **2017,** *9* (9).

42. Blaeser, A.; Campos, D. F. D.; Puster, U.; Richtering, W.; Stevens, M. M.; Fischer, H. Controlling shear stress in 3D bioprinting is a key factor to balance printing resolution and stem cell integrity. *Advanced Healthcare Materials* **2016,** *5* (3), 326-333.

43. Yang, J. Z.; Zhang, Y. S.; Yue, K.; Khademhosseini, A. Cell-laden hydrogels for osteochondral and cartilage tissue engineering. *Acta Biomater.* **2017,** *57*, 1-25.

44. Gao, G. F.; Schilling, A. F.; Hubbell, K.; Yonezawa, T.; Truong, D.; Hong, Y.; Dai, G. H.; Cui, X. F. Improved properties of bone and cartilage tissue from 3D inkjet-bioprinted human

mesenchymal stem cells by simultaneous deposition and photocrosslinking in PEG-GelMA. *Biotechnology Letters* **2015,** *37* (11), 2349-2355.

45. Sawkins, M. J.; Mistry, P.; Brown, B. N.; Shakesheff, K. M.; Bonassar, L. J.; Yang, J. Cell and protein compatible 3D bioprinting of mechanically strong constructs for bone repair. *Biofabrication* **2015,** *7* (3).

46. Huang, J.; Fu, H.; Wang, Z. Y.; Meng, Q. Y.; Liu, S. M.; Wang, H. R.; Zheng, X. F.; Dai, J. W.; Zhang, Z. J. BMSCs-laden gelatin/sodium alginate/carboxymethyl chitosan hydrogel for 3D bioprinting. *RSC Adv.* **2016,** *6* (110), 108423-108430.

47. Saha, K.; Keung, A. J.; Irwin, E. F.; Li, Y.; Little, L.; Schaffer, D. V.; Healy, K. E. Substrate modulus directs neural stem cell behavior. *Biophys. J.* **2008,** *95* (9), 4426-4438.

48. Tse, J. R.; Engler, A. J. Stiffness gradients mimicking in vivo tissue variation regulate mesenchymal stem cell fate. *Plos One* **2011,** *6* (1).

49. Pek, Y. S.; Wan, A. C. A.; Ying, J. Y. The effect of matrix stiffness on mesenchymal stem cell differentiation in a 3D thixotropic gel. *Biomaterials* **2010,** *31* (3), 385-391.

50. Cruise, G. M.; Scharp, D. S.; Hubbell, J. A. Characterization of permeability and network structure of interfacially photopolymerized poly(ethylene glycol) diacrylate hydrogels. *Biomaterials* **1998,** *19* (14), 1287-1294.

51. Dikovsky, D.; Bianco-Peled, H.; Seliktar, D. The effect of structural alterations of PEG-fibrinogen hydrogel scaffolds on 3-D cellular morphology and cellular migration. *Biomaterials* **2006,** *27* (8), 1496-1506.

52. Husseman, M.; Malmstrom, E. E.; McNamara, M.; Mate, M.; Mecerreyes, D.; Benoit, D. G.; Hedrick, J. L.; Mansky, P.; Huang, E.; Russell, T. P.; Hawker, C. J. Controlled synthesis of

polymer brushes by "living" free radical polymerization techniques. *Macromolecules* **1999,** *32* (5), 1424-1431.

53. Tayal, A.; Kelly, R. M.; Khan, S. A. Rheology and molecular weight changes during enzymatic degradation of a water-soluble polymer. *Macromolecules* **1999,** *32* (2), 294-300.

54. Bryant, S. J.; Anseth, K. S. Controlling the spatial distribution of ECM components in degradable PEG hydrogels for tissue engineering cartilage. *J. Biomed. Mater. Res. Part A* **2003,** *64A* (1), 70-79.

55. Zhu, J. M. Bioactive modification of poly(ethylene glycol) hydrogels for tissue engineering. *Biomaterials* **2010,** *31* (17), 4639-4656.

56. Wehrli, F. W. From NMR diffraction and zeugmatography to modern imaging and beyond. *Progress in Nuclear Magnetic Resonance Spectroscopy* **1995,** *28* (1), 87-135.

57. Geva, T. Magnetic resonance imaging: historical perspective. *Journal of Cardiovascular Magnetic Resonance* **2006,** *8* (4), 573-580.

58. Litvinov, V. M.; Dias, A. A. Analysis of network structure of UV-cured acrylates by 1H NMR relaxation, 13C NMR spectroscopy, and dynamic mechanical experiments. *Macromolecules* **2001,** *34* (12), 4051-4060.

59. Espartero, J. L.; Rashkov, I.; Li, S. M.; Manolova, N.; Vert, M. NMR analysis of low molecular weight poly(lactic acid)s. *Macromolecules* **1996,** *29* (10), 3535-3539.

60. Bachus, R.; Kimmich, R. Molecular weight and temperature dependence of self-diffusion coefficients in polyethylene and polystyrene melts investigated using a modified n.m.r. field-gradient technique. *Polymer* **1983,** *24* (8), 964-970.

61. Liu, K.-J. NMR studies of polymer solutions. VI. Molecular weight determination of poly(ethylene glycol) by NMR analysis of near-end groups. *Die Makromolekulare Chemie* **1968,** *116* (1), 146-151.

62. Scherzer, T.; Decker, U. Real-time FTIR–ATR spectroscopy to study the kinetics of ultrafast photopolymerization reactions induced by monochromatic UV light. *Vibrational Spectroscopy* **1999,** *19* (2), 385-398.

63. Guttman, C. M.; Dimarzio, E. A. Polymer separation by flow and its relation to GPC. *Bulletin of the American Physical Society* **1969,** *14* (3), 424-&.

64. Balke, S. T.; Hamielec, A. E. Polymer reactors and molecular weight distribution. 8. A method of interpreting skewed GPC chromatograms. *J. Appl. Polym. Sci.* **1969,** *13* (7), 1381.

65. He, Y.; Yang, F.; Zhao, H.; Gao, Q.; Xia, B.; Fu, J. Research on the printability of hydrogels in 3D bioprinting. *Scientific Reports* **2016,** *6*, 29977.

66. Glassman, M. J.; Olsen, B. D. Structure and mechanical response of protein hydrogels reinforced by block copolymer self-assembly. *Soft Matter* **2013,** *9* (29), 6814-6823.

67. Glassman, M. J.; Chan, J.; Olsen, B. D. Reinforcement of shear thinning protein hydrogels by responsive block copolymer self-assembly. *Adv. Funct. Mater.* **2013,** *23* (9), 1182-1193.

68. Senff, H.; Richtering, W. Temperature sensitive microgel suspensions: colloidal phase behavior and rheology of soft spheres. *Journal of Chemical Physics* **1999,** *111* (4), 1705-1711.

69. Beck, E. C.; Barragan, M.; Tadros, M. H.; Kiyotake, E. A.; Acosta, F. M.; Kieweg, S. L.; Detamore, M. S. Chondroinductive hydrogel pastes composed of naturally derived devitalized cartilage. *Annals of Biomedical Engineering* **2016,** *44* (6), 1863-1880.

70. Duan, B.; Kapetanovic, E.; Hockaday, L. A.; Butcher, J. T. Three-dimensional printed trileaflet valve conduits using biological hydrogels and human valve interstitial cells. *Acta Biomater.* **2014,** *10* (5), 1836-1846.

71. Peak, C. W.; Stein, J.; Gold, K. A.; Gaharwar, A. K. Nanoengineered colloidal inks for 3D bioprinting. *Langmuir* **2017**.

72. Rezende, R. A.; Bartolo, P. J.; Mendes, A.; Maciel, R. Rheological behavior of alginate solutions for biomanufacturing. *J. Appl. Polym. Sci.* **2009,** *113* (6), 3866-3871.

73. Liu, W.; Heinrich, M. A.; Zhou, Y.; Akpek, A.; Hu, N.; Liu, X.; Guan, X.; Zhong, Z.; Jin, X.; Khademhosseini, A.; Zhang, Y. S. Extrusion bioprinting of shear-thinning gelatin methacryloyl bioinks. *Advanced Healthcare Materials* **2017,** *6* (12), n/a-n/a.

74. Skardal, A.; Zhang, J.; Prestwich, G. D. Bioprinting vessel-like constructs using hyaluronan hydrogels crosslinked with tetrahedral polyethylene glycol tetracrylates. *Biomaterials* **2010,** *31* (24), 6173-6181.

75. Aguado, B. A.; Mulyasasmita, W.; Su, J.; Lampe, K. J.; Heilshorn, S. C. Improving viability of stem cells during syringe needle flow through the design of hydrogel cell carriers. *Tissue Eng. Part A* **2012,** *18* (7-8), 806-815.

76. Schuurman, W.; Levett, P. A.; Pot, M. W.; van Weeren, P. R.; Dhert, W. J. A.; Hutmacher, D. W.; Melchels, F. P. W.; Klein, T. J.; Malda, J. Gelatin-methacrylamide hydrogels as potential biomaterials for fabrication of tissue-engineered cartilage constructs. *Macromol. Biosci.* **2013,** *13* (5), 551-561.

77. Xavier, J. R.; Thakur, T.; Desai, P.; Jaiswal, M. K.; Sears, N.; Cosgriff-Hernandez, E.; Kaunas, R.; Gaharwar, A. K. Bioactive nanoengineered hydrogels for bone tissue engineering: a growth-factor-free approach. *ACS Nano* **2015,** *9* (3), 3109-3118.

78. Li, H. J.; Liu, S. J.; Li, L. Rheological study on 3D printability of alginate hydrogel and effect of graphene oxide. *International Journal of Bioprinting* **2016,** *2* (2), 54-66.

79. Smith, R. L.; Carter, D. R.; Schurman, D. J. Pressure and shear differentially alter human articular chondrocyte metabolism - a review. *Clinical Orthopaedics and Related Research* **2004,** (427), S89-S95.

80. Zhao, F.; Chella, R.; Ma, T. Effects of shear stress on 3-D human mesenchymal stem cell construct development in a perfusion bioreactor system: experiments and hydrodynamic modeling. *Biotechnol. Bioeng.* **2007,** *96* (3), 584-595.

81. Billiet, T.; Gevaert, E.; De Schryver, T.; Cornelissen, M.; Dubruel, P. The 3D printing of gelatin methacrylamide cell-laden tissue-engineered constructs with high cell viability. *Biomaterials* **2014,** *35* (1), 49-62.

82. Kolesky, D. B.; Truby, R. L.; Gladman, A. S.; Busbee, T. A.; Homan, K. A.; Lewis, J. A. 3D bioprinting of vascularized, heterogeneous cell-laden tissue constructs. *Adv. Mater.* **2014,** *26* (19), 3124-3130.

83. Raphael, B.; Khalil, T.; Workman, V. L.; Smith, A.; Brown, C. P.; Streuli, C.; Saiani, A.; Domingos, M. 3D cell bioprinting of self-assembling peptide-based hydrogels. *Mater. Lett.* **2017,** *190*, 103-106.

84. Loo, Y. H.; Hauser, C. A. E. Bioprinting synthetic self-assembling peptide hydrogels for biomedical applications. *Biomed. Mater.* **2016,** *11* (1).

85. Loo, Y. H.; Lakshmanan, A.; Ni, M.; Toh, L. L.; Wang, S.; Hauser, C. A. E. Peptide bioink: self-assembling nanofibrous scaffolds for three-dimensional organotypic cultures. *Nano Letters* **2015,** *15* (10), 6919-6925.

86. Kundu, J.; Shim, J. H.; Jang, J.; Kim, S. W.; Cho, D. W. An additive manufacturing-based PCL-alginate-chondrocyte bioprinted scaffold for cartilage tissue engineering. *Journal of Tissue Engineering and Regenerative Medicine* **2015,** *9* (11), 1286-1297.

87. Kim, B. S.; Jang, J.; Chae, S.; Gao, G.; Kong, J. S.; Ahn, M.; Cho, D. W. Three-dimensional bioprinting of cell-laden constructs with polycaprolactone protective layers for using various thermoplastic polymers. *Biofabrication* **2016,** *8* (3).

88. Zhang, K. L.; Fu, Q.; Yoo, J.; Chen, X. X.; Chandra, P.; Mo, X. M.; Song, L. J.; Atala, A.; Zhao, W. X. 3D bioprinting of urethra with PCL/PLCL blend and dual autologous cells in fibrin hydrogel: an in vitro evaluation of biomimetic mechanical property and cell growth environment. *Acta Biomater.* **2017,** *50*, 154-164.

89. Thakur, A.; Jaiswal, M. K.; Peak, C. W.; Carrow, J. K.; Gentry, J.; Dolatshahi-Pirouz, A.; Gaharwar, A. K. Injectable shear-thinning nanoengineered hydrogels for stem cell delivery. *Nanoscale* **2016,** *8* (24), 12362-12372.

90. Bakarich, S. E.; Balding, P.; Gorkin, R.; Spinks, G. M.; Panhuis, M. I. H. Printed ionic-covalent entanglement hydrogels from carrageenan and an epoxy amine. *RSC Adv.* **2014,** *4* (72), 38088-38092.

91. Wang, B. C.; Benitez, A. J.; Lossada, F.; Merindol, R.; Walther, A. Bioinspired mechanical gradients in cellulose nanofibril/polymer nanopapers. *Angew Chem Int Edit* **2016,** *55* (20), 5966-5970.

92. Birkholz, M. N.; Agrawal, G.; Bergmann, C.; Schroder, R.; Lechner, S. J.; Pich, A.; Fischer, H. Calcium phosphate/microgel composites for 3D powderbed printing of ceramic materials. *Biomedical Engineering-Biomedizinische Technik* **2016,** *61* (3), 267-279.

93. Hinton, T. J.; Hudson, A.; Pusch, K.; Lee, A.; Feinberg, A. W. 3D printing PDMS elastomer in a hydrophilic support bath via freeform reversible embedding. *Acs Biomater Sci Eng* **2016,** *2* (10), 1781-1786.

94. Lee, K. Y.; Mooney, D. J. Alginate: properties and biomedical applications. *Prog. Polym. Sci.* **2012,** *37* (1), 106-126.

95. Halstenberg, S.; Panitch, A.; Rizzi, S.; Hall, H.; Hubbell, J. A. Biologically engineered protein-graft-poly(ethylene glycol) hydrogels: a cell adhesive and plasm in-degradable biosynthetic material for tissue repair. *Biomacromolecules* **2002,** *3* (4), 710-723.

96. Discher, D. E.; Janmey, P.; Wang, Y. L. Tissue cells feel and respond to the stiffness of their substrate. *Science* **2005,** *310* (5751), 1139-1143.

97. Ahmad Khalili, A.; Ahmad, M. R. A review of cell adhesion studies for biomedical and biological applications. *International Journal of Molecular Sciences* **2015,** *16* (8), 18149-18184.

98. Aigner, T.; Neureiter, D.; Muller, S.; Kuspert, G.; Belke, J.; Kirchner, T. Extracellular matrix composition and gene expression in collagenous colitis. *Gastroenterology* **1997,** *113* (1), 136-143.

99. Kass, L.; Erler, J. T.; Dembo, M.; Weaver, V. M. Mammary epithelial cell: influence of extracellular matrix composition and organization during development and tumorigenesis. *The International Journal of Biochemistry & Cell Biology* **2007,** *39* (11), 1987-1994.

100. Sulzer, M. A.; Leers, M. P.; van Noord, J. A.; Bollen, E. C.; Theunissen, P. H. Reduced E-cadherin expression is associated with increased lymph node metastasis and unfavorable prognosis in non-small cell lung cancer. *American journal of respiratory and critical care medicine* **1998,** *157* (4), 1319-1323.

101. van Gurp, R. J.; Oosterhuis, J. W.; Kalscheuer, V.; Mariman, E. C.; Looijenga, L. H. Biallelic expression of the H19 and IGF2 genes in human testicular germ cell tumors. *JNCI: Journal of the National Cancer Institute* **1994,** *86* (14), 1070-1075.

102. Huang, S.; Ingber, D. E. The structural and mechanical complexity of cell-growth control. *Nature cell biology* **1999,** *1* (5).

103. Liu, W.; Heinrich, M. A.; Zhou, Y.; Akpek, A.; Hu, N.; Liu, X.; Guan, X.; Zhong, Z.; Jin, X.; Khademhosseini, A.; Zhang, Y. S. Extrusion bioprinting of shear-thinning gelatin methacryloyl bioinks. *Advanced Healthcare Materials* **2017**, 1601451-n/a.

104. Gaharwar, A. K.; Avery, R. K.; Assmann, A.; Paul, A.; McKinley, G. H.; Khademhosseini, A.; Olsen, B. D. Shear-thinning nanocomposite hydrogels for the treatment of hemorrhage. *Acs Nano* **2014,** *8* (10), 9833-9842.

105. He, Y.; Yang, F. F.; Zhao, H. M.; Gao, Q.; Xia, B.; Fu, J. Z. Research on the printability of hydrogels in 3D bioprinting. *Scientific Reports* **2016,** *6*, 13.

106. Obara, K.; Ishihara, M.; Ishizuka, T.; Fujita, M.; Ozeki, Y.; Maehara, T.; Saito, Y.; Yura, H.; Matsui, T.; Hattori, H. Photocrosslinkable chitosan hydrogel containing fibroblast growth factor-2 stimulates wound healing in healing-impaired db/db mice. *Biomaterials* **2003,** *24* (20), 3437-3444.

107. Khattak, S. F.; Spatara, M.; Roberts, L.; Roberts, S. C. Application of colorimetric assays to assess viability, growth and metabolism of hydrogel-encapsulated cells. *Biotechnology letters* **2006,** *28* (17), 1361-1370.

108. Cheng, Y.-H.; Yang, S.-H.; Su, W.-Y.; Chen, Y.-C.; Yang, K.-C.; Cheng, W. T.-K.; Wu, S.-C.; Lin, F.-H. Thermosensitive chitosan–gelatin–glycerol phosphate hydrogels as a cell carrier

for nucleus pulposus regeneration: an in vitro study. *Tissue Engineering Part A* **2009,** *16* (2), 695-703.

109. Ribeiro, M.; Morgado, P.; Miguel, S.; Coutinho, P.; Correia, I. Dextran-based hydrogel containing chitosan microparticles loaded with growth factors to be used in wound healing. *Materials Science and Engineering: C* **2013,** *33* (5), 2958-2966.

110. Balestrin, L.; Bidone, J.; Bortolin, R.; Moresco, K.; Moreira, J.; Teixeira, H. Protective effect of a hydrogel containing Achyrocline satureioides extract-loaded nanoemulsion against UV-induced skin damage. *Journal of Photochemistry and Photobiology B: Biology* **2016,** *163,* 269-276.

111. e Silva, S. A. M.; Calixto, G. M. F.; Cajado, J.; de Carvalho, P. C. A.; Rodero, C. F.; Chorilli, M.; Leonardi, G. R. Gallic acid-loaded gel formulation combats skin oxidative stress: development, characterization and ex vivo biological assays.

112. Mahoney, M. J.; Anseth, K. S. Three-dimensional growth and function of neural tissue in degradable polyethylene glycol hydrogels. *Biomaterials* **2006,** *27* (10), 2265-2274.

113. Galateanu, B.; Dimonie, D.; Vasile, E.; Nae, S.; Cimpean, A.; Costache, M. Layer-shaped alginate hydrogels enhance the biological performance of human adipose-derived stem cells. *BMC biotechnology* **2012,** *12* (1), 35.

114. Lu, J.; He, Y. S.; Cheng, C.; Wang, Y.; Qiu, L.; Li, D.; Zou, D. Self-supporting graphene hydrogel film as an experimental platform to evaluate the potential of graphene for bone regeneration. *Advanced Functional Materials* **2013,** *23* (28), 3494-3502.

115. Saladino, S.; Di Leonardo, E.; Salamone, M.; Mercuri, D.; Segatti, F.; Ghersi, G. Formulation of different chitosan hydrogels for cartilage tissue repair. *Chemical Engineering Transactions* **2014,** *38,* 505-510.

116. Devine, D. M.; Devery, S. M.; Lyons, J. G.; Geever, L. M.; Kennedy, J. E.; Higginbotham, C. L. Multifunctional polyvinylpyrrolidinone-polyacrylic acid copolymer hydrogels for biomedical applications. *International journal of pharmaceutics* **2006,** *326* (1), 50-59.

117. Yin, L.; Zhao, X.; Cui, L.; Ding, J.; He, M.; Tang, C.; Yin, C. Cytotoxicity and genotoxicity of superporous hydrogel containing interpenetrating polymer networks. *Food and Chemical Toxicology* **2009,** *47* (6), 1139-1145.

118. Suri, S.; Schmidt, C. E. Cell-laden hydrogel constructs of hyaluronic acid, collagen, and laminin for neural tissue engineering. *Tissue Engineering Part A* **2010,** *16* (5), 1703-1716.

119. Pawlaczyk, M.; Lelonkiewicz, M.; Wieczorowski, M. Age-dependent biomechanical properties of the skin. *Advances in Dermatology and Allergology/Postępy Dermatologii i Alergologii* **2013,** *30* (5), 302-306.

120. Rho, J. Y.; Ashman, R. B.; Turner, C. H. Young's modulus of trabecular and cortical bone material: ultrasonic and microtensile measurements. *Journal of Biomechanics* **1993,** *26* (2), 111-119.

121. Muiznieks, L. D.; Keeley, F. W. Molecular assembly and mechanical properties of the extracellular matrix: a fibrous protein perspective. *Biochimica et Biophysica Acta (BBA) - Molecular Basis of Disease* **2013,** *1832* (7), 866-875.

122. Roohani-Esfahani, S.-I.; Newman, P.; Zreiqat, H. Design and fabrication of 3D printed scaffolds with a mechanical strength comparable to cortical bone to repair large bone defects. *Scientific Reports* **2016,** *6*, 19468.

123. El-Hajje, A.; Kolos, E. C.; Wang, J. K.; Maleksaeedi, S.; He, Z.; Wiria, F. E.; Choong, C.; Ruys, A. J. Physical and mechanical characterisation of 3D-printed porous titanium for

biomedical applications. *Journal of Materials Science: Materials in Medicine* **2014,** *25* (11), 2471-2480.

124. Johnson, B. D.; Beebe, D. J.; Crone, W. C. Effects of swelling on the mechanical properties of a pH-sensitive hydrogel for use in microfluidic devices. *Materials Science and Engineering: C* **2004,** *24* (4), 575-581.

125. Caló, E.; Khutoryanskiy, V. V. Biomedical applications of hydrogels: a review of patents and commercial products. *European Polymer Journal* **2015,** *65* (Supplement C), 252-267.

126. Peak, C. W.; Carrow, J. K.; Thakur, A.; Singh, A.; Gaharwar, A. K. Elastomeric cell-laden nanocomposite microfibers for engineering complex tissues. *Cel. Mol. Bioeng.* **2015,** *8* (3), 404-415.

127. Anderson, J. M.; Shive, M. S. Biodegradation and biocompatibility of PLA and PLGA microspheres. *Adv. Drug Deliv. Rev.* **1997,** *28* (1), 5-24.

128. Danhier, F.; Ansorena, E.; Silva, J. M.; Coco, R.; Le Breton, A.; Preat, V. PLGA-based nanoparticles: an overview of biomedical applications. *Journal of Controlled Release* **2012,** *161* (2), 505-522.

129. Freiberg, S.; Zhu, X. Polymer microspheres for controlled drug release. *Int. J. Pharm.* **2004,** *282* (1-2), 1-18.

130. Makadia, H. K.; Siegel, S. J. Poly lactic-co-Glycolic Acid (PLGA) as biodegradable controlled drug delivery carrier. *Polymers* **2011,** *3* (3), 1377-1397.

131. Peak, C. W.; Nagar, S.; Watts, R. D.; Schmidt, G. Robust and degradable hydrogels from poly(ethylene glycol) and semi-interpenetrating collagen. *Macromolecules* **2014,** *47* (18), 6408-6417.

132. Dai, X. S.; Chen, X.; Yang, L.; Foster, S.; Coury, A. J.; Jozefiak, T. H. Free radical polymerization of poly(ethylene glycol) diacrylate macromers: impact of macromer hydrophobicity and initiator chemistry on polymerization efficiency. *Acta Biomater.* **2011,** *7* (5), 1965-1972.

133. Guarino, V.; Gloria, A.; De Santis, R.; Ambrosio, L. *Composite Hydrogels for Scaffold Design, Tissue Engineering, and Prostheses* 2010. p 227-245.

134. Cushing, M. C.; Anseth, K. S. Hydrogel cell cultures. *Science* **2007,** *316* (5828), 1133-1134.

135. Hockaday, L. A.; Kang, K. H.; Colangelo, N. W.; Cheung, P. Y. C.; Duan, B.; Malone, E.; Wu, J.; Girardi, L. N.; Bonassar, L. J.; Lipson, H.; Chu, C. C.; Butcher, J. T. Rapid 3D printing of anatomically accurate and mechanically heterogeneous aortic valve hydrogel scaffolds. *Biofabrication* **2012,** *4* (3).

136. Ouyang, L. L.; Yao, R.; Zhao, Y.; Sun, W. Effect of bioink properties on printability and cell viability for 3D bioplotting of embryonic stem cells. *Biofabrication* **2016,** *8* (3).

137. Nikolaev, N. I.; Müller, T.; Williams, D. J.; Liu, Y. Changes in the stiffness of human mesenchymal stem cells with the progress of cell death as measured by atomic force microscopy. *Journal of Biomechanics* **2014,** *47* (3), 625-630.

138. Park, J. S.; Chu, J. S.; Tsou, A. D.; Diop, R.; Tang, Z.; Wang, A.; Li, S. The effect of matrix stiffness on the differentiation of mesenchymal stem cells in response to TGF-β. *Biomaterials* **2011,** *32* (16), 3921-3930.

139. Trappmann, B.; Chen, C. S. How cells sense extracellular matrix stiffness: a material's perspective. *Curr. Opin. Biotechnol.* **2013,** *24* (5), 948-953.

140. Dembo, M.; Wang, Y.-L. Stresses at the cell-to-substrate interface during locomotion of fibroblasts. *Biophysical Journal 76* (4), 2307-2316.

141. Kraning-Rush, C. M.; Califano, J. P.; Reinhart-King, C. A. Cellular traction stresses increase with increasing metastatic potential. *PloS one* **2012,** *7* (2), e32572.

142. Gupta, V.; Sraj, I. A.; Konstantopoulos, K.; Eggleton, C. D. Multi-scale simulation of L-selectin–PSGL-1-dependent homotypic leukocyte binding and rupture. *Biomechanics and modeling in mechanobiology* **2010,** *9* (5), 613-627.

143. Rupprecht, P.; Golé, L.; Rieu, J.-P.; Vézy, C.; Ferrigno, R.; Mertani, H. C.; Rivière, C. A tapered channel microfluidic device for comprehensive cell adhesion analysis, using measurements of detachment kinetics and shear stress-dependent motion. *Biomicrofluidics* **2012,** *6* (1), 014107-014107-12.

144. Alapan, Y.; Little, J. A.; Gurkan, U. A. Heterogeneous red blood cell adhesion and deformability in sickle cell disease. *Scientific reports* **2014,** *4*.

145. Thomas, G.; Burnham, N. A.; Camesano, T. A.; Wen, Q. Measuring the mechanical properties of living cells using atomic force microscopy. *Journal of visualized experiments : JoVE* **2013,** (76), 50497.

146. Fraley, S. I.; Feng, Y.; Krishnamurthy, R.; Kim, D.-H.; Celedon, A.; Longmore, G. D.; Wirtz, D. A distinctive role for focal adhesion proteins in three-dimensional cell motility. *Nature cell biology* **2010,** *12* (6), 598-604.

147. Woessner, J. F. The determination of hydroxyproline in tissue and protein samples containing small proportions of this imino acid. *Archives of Biochemistry and Biophysics* **1961,** *93* (2), 440-447.

148. Walsh, B. J.; Thornton, S. C.; Penny, R.; Breit, S. N. Microplate reader-based quantitation of collagens. *Analytical Biochemistry* **1992,** *203* (2), 187-190.

149. Bitter, T.; Muir, H. M. A modified uronic acid carbazole reaction. *Analytical Biochemistry* **1962,** *4* (4), 330-334.

150. Frazier, S. B.; Roodhouse, K. A.; Hourcade, D. E.; Zhang, L. The quantification of glycosaminoglycans: a comparison of HPLC, carbazole, and alcian blue methods. *Open glycoscience* **2008,** *1*, 31-39.

151. Barbosa, I.; Garcia, S.; Barbier-Chassefière, V.; Caruelle, J.-P.; Martelly, I.; Papy-García, D. Improved and simple micro assay for sulfated glycosaminoglycans quantification in biological extracts and its use in skin and muscle tissue studies. *Glycobiology* **2003,** *13* (9), 647-653.

152. Guillotin, B.; Guillemot, F. Cell patterning technologies for organotypic tissue fabrication. *Trends in Biotechnology* **2011,** *29* (4), 183-190.

153. Forgacs, G. Tissue engineering perfusable vascular networks. *Nat. Mater.* **2012,** *11* (9), 746-747.

154. Schexnailder, P.; Loizou, E.; Porcar, L.; Butler, P.; Schmidt, G. Heterogeneity in nanocomposite hydrogels from poly(ethylene oxide) cross-linked with silicate nanoparticles. *Physical Chemistry Chemical Physics* **2009,** *11* (15), 2760-2766.

155. Chimene, D.; Alge, D. L.; Gaharwar, A. K. Two-dimensional nanomaterials for biomedical applications: emerging trends and future prospects. *Advanced Materials* **2015,** *27* (45), 7261–7284.

156. Gaharwar, A. K.; Peppas, N. A.; Khademhosseini, A. Nanocomposite hydrogels for biomedical applications. *Biotechnology and Bioengineering* **2014,** *111* (3), 441-453.

157. Paineau, E.; Bihannic, I.; Baravian, C.; Philippe, A.-M.; Davidson, P.; Levitz, P.; Funari, S. S.; Rochas, C.; Michot, L. J. Aqueous suspensions of natural swelling clay minerals. 1. Structure and electrostatic interactions. *Langmuir* **2011,** *27* (9), 5562-5573.

158. Ruzicka, B.; Zaccarelli, E. A fresh look at the Laponite phase diagram. *Soft Matter* **2011,** *7* (4), 1268-1286.

159. Mourchid, A.; Delville, A.; Lambard, J.; Lecolier, E.; Levitz, P. Phase diagram of colloidal dispersions of anisotropic charged-particles - equilibrium properties, structure, and rheology of Laponite suspensions. *Langmuir* **1995,** *11* (6), 1942-1950.

160. Levitz, P.; Lecolier, E.; Mourchid, A.; Delville, A.; Lyonnard, S. Liquid-solid transition of Laponite suspensions at very low ionic strength: long-range electrostatic stabilisation of anisotropic colloids. *Europhysics Letters* **2000,** *49* (5), 672-677.

161. Avery, R. G.; Ramsay, J. D. F. Colloidal properties of synthetic hectorite clay dispersions 2: Light and small-angle neutron-scattering. *J. Colloid Interface Sci.* **1986,** *109* (2), 448-454.

162. Rosta, L.; Vongunten, H. R. Light-Scattering characterization of Laponite sols. *J. Colloid Interface Sci.* **1990,** *134* (2), 397-406.

163. Mori, Y.; Togashi, K.; Nakamura, K. Colloidal properties of synthetic hectorite clay dispersion measured by dynamic light scattering and small angle X-ray scattering. *Advanced Powder Technology* **2001,** *12* (1), 45-59.

164. Nelson, A.; Cosgrove, T. Dynamic light scattering studies of poly(ethylene oxide) adsorbed on laponite: layer conformation and its effect on particle stability. *Langmuir* **2004,** *20* (24), 10382-10388.

165. Pawar, N.; Bohidar, H. B. Surface selective binding of nanoclay particles to polyampholyte protein chains. *Journal of Chemical Physics* **2009,** *131* (4).

166. Nelson, A.; Cosgrove, T. Small-angle neutron scattering study of adsorbed pluronic tri-block copolymers on laponite. *Langmuir* **2005,** *21* (20), 9176-9182.

167. Wu, C. J.; Gaharwar, A. K.; Chan, B. K.; Schmidt, G. Mechanically tough Pluronic F127/Laponite nanocomposite hydrogels from covalently and physically cross-linked networks. *Macromolecules* **2011,** *44* (20), 8215-8224.

168. Boucenna, I.; Royon, L.; Colinart, P.; Guedeau-Boudeville, M. A.; Mourchid, A. Structure and thermorheology of concentrated pluronic copolymer micelles in the presence of Laponite particles. *Langmuir* **2010,** *26* (18), 14430-14436.

169. Haraguchi, K.; Xu, Y. J. Thermal analyses of poly(N-isopropylacrylamide) in aqueous solutions and in nanocomposite gels. *Colloid Polym. Sci.* **2012,** *290* (16), 1627-1636.

170. Haraguchi, K.; Xu, Y. J.; Li, G. Molecular characteristics of poly(N-isopropylacrylamide) separated from nanocomposite gels by removal of clay from the polymer/clay network. *Macromolecular Rapid Communications* **2010,** *31* (8), 718-723.

171. Haraguchi, K.; Li, H. J.; Okumura, N. Hydrogels with hydrophobic surfaces: abnormally high contact angles for water on PNIPA nanocomposite hydrogels. *Macromolecules* **2007,** *40*(7), 2299-2302.

172. Schmidt, G.; Nakatani, A. I.; Han, C. C. Rheology and flow-birefringence from viscoelastic polymer-clay solutions. *Rheologica Acta* **2002,** *41* (1-2), 45-54.

173. Schmidt, G.; Nakatani, A. I.; Butler, P. D.; Han, C. C. Small-angle neutron scattering from viscoelastic polymer-clay solutions. *Macromolecules* **2002,** *35* (12), 4725-4732.

174. Nelson, A.; Cosgrove, T. A small-angle neutron scattering study of adsorbed poly(ethylene oxide) on Laponite. *Langmuir* **2004,** *20* (6), 2298-2304.

175. Gaharwar, A. K.; Schexnailder, P. J.; Dundigalla, A.; White, J. D.; Matos-Perez, C. R.; Cloud, J. L.; Seifert, S.; Wilker, J. J.; Schmidt, G. Highly extensible bio-nanocomposite fibers. *Macromolecular Rapid Communications* **2011,** *32* (1), 50-57.

176. Ruzicka, B.; Zaccarelli, E.; Zulian, L.; Angelini, R.; Sztucki, M.; Moussaïd, A.; Narayanan, T.; Sciortino, F. Observation of empty liquids and equilibrium gels in a colloidal clay. *Nat. Mater.* **2011,** *10* (1), 56-60.

177. Mourchid, A.; Delville, A.; Lambard, J.; LeColier, E.; Levitz, P. Phase diagram of colloidal dispersions of anisotropic charged particles: equilibrium properties, structure, and rheology of Laponite suspensions. *Langmuir* **1995,** *11* (6), 1942-1950.

178. Mourchid, A.; Delville, A.; Levitz, P. Sol–gel transition of colloidal suspensions of anisotropic particles of Laponite. *Faraday Discussions* **1995,** *101*, 275-285.

179. Lorthioir, C.; Khalil, M.; Wintgens, V.; Amiel, C. Segmental motions of poly(ethylene glycol) chains adsorbed on Laponite platelets in clay-based hydrogels: a-NMR investigation. *Langmuir* **2012,** *28* (20), 7859-7871.

180. Zhang, J. X.; Feng, X.; Patil, H.; Tiwari, R. V.; Repka, M. A. Coupling 3D printing with hot-melt extrusion to produce controlled-release tablets. *Int. J. Pharm.* **2017,** *519* (1-2), 186-197.

181. Youssef, A.; Hollister, S. J.; Dalton, P. D. Additive manufacturing of polymer melts for implantable medical devices and scaffolds. *Biofabrication* **2017,** *9* (1).

182. Yang, C. C.; Tian, X. Y.; Liu, T. F.; Cao, Y.; Li, D. C. 3D printing for continuous fiber reinforced thermoplastic composites: mechanism and performance. *Rapid Prototyping Journal* **2017,** *23* (1), 209-215.

183. Sommer, M. R.; Alison, L.; Minas, C.; Tervoort, E.; Ruhs, P. A.; Studart, A. R. 3D printing of concentrated emulsions into multiphase biocompatible soft materials. *Soft Matter* **2017,** *13* (9), 1794-1803.

184. Nojoomi, A.; Tamjid, E.; Simchi, A.; Bonakdar, S.; Stroeve, P. Injectable polyethylene glycol-laponite composite hydrogels as articular cartilage scaffolds with superior mechanical and rheological properties. *International Journal of Polymeric Materials and Polymeric Biomaterials* **2017,** *66* (3), 105-114.

185. Davila, J. L.; d'Avila, M. A. Laponite as a rheology modifier of alginate solutions: physical gelation and aging evolution. *Carbohydr. Polym.* **2017,** *157,* 1-8.

186. Gaharwar, A. K.; Dammu, S. A.; Canter, J. M.; Wu, C. J.; Schmidt, G. Highly Extensible, Tough, and elastomeric nanocomposite hydrogels from poly(ethylene glycol) and hydroxyapatite nanoparticles. *Biomacromolecules* **2011,** *12* (5), 1641-1650.

187. Nicolai, T.; Cocard, S. Light scattering study of the dispersion of Laponite. *Langmuir* **2000,** *16* (21), 8189-8193.

188. Shahin, A.; Joshi, Y. M. Hyper-aging dynamics of nanoclay suspension. *Langmuir* **2012,** *28* (13), 5826-5833.

189. Rand, B.; Melton, I. E. Particle interactions in aqueous kaolinite suspensions. *J. Colloid Interface Sci.* **1977,** *60* (2), 308-320.

190. Gibaud, T.; Barentin, C.; Taberlet, N.; Manneville, S. Shear-induced fragmentation of laponite suspensions. *Soft Matter* **2009,** *5* (16), 3026-3037.

191. Kurokawa, A.; Vidal, V.; Kurita, K.; Divoux, T.; Manneville, S. Avalanche-like fluidization of a non-Brownian particle gel. *Soft Matter* **2015,** *11* (46), 9026-9037.

192. Martin, J. D.; Thomas Hu, Y. Transient and steady-state shear banding in aging soft glassy materials. *Soft Matter* **2012,** *8* (26), 6940-6949.

193. Truby, R. L.; Lewis, J. A. Printing soft matter in three dimensions. *Nature* **2016,** *540* (7633), 371-378.

194. Malkin, A. Y.; Isayev, A. I. Rheology - Concepts, Methods, and Applications (2nd Edition). ChemTec Publishing.

195. McFarlane, N. L.; Wagner, N. J.; Kaler, E. W.; Lynch, M. L. Poly(ethylene oxide) (PEO) and poly(vinyl pyrolidone) (PVP) induce different changes in the colloid stability of nanoparticles. *Langmuir* **2010,** *26* (17), 13823-13830.

196. Chiu, Y. L.; Chen, S. C.; Su, C. J.; Hsiao, C. W.; Chen, Y. M.; Chen, H. L.; Sung, H. W. pH-triggered injectable hydrogels prepared from aqueous N-palmitoyl chitosan: in vitro characteristics and in vivo biocompatibility. *Biomaterials* **2009,** *30* (28), 4877-4888.

197. Roux, R.; Ladaviere, C.; Montembault, A.; David, L.; Delair, T. Shear thinning three-dimensional colloidal assemblies of chitosan and poly(lactic acid) nanoparticles. *Journal of Physical Chemistry B* **2013,** *117* (24), 7455-7464.

198. Lindsey, S.; Piatt, J. H.; Worthington, P.; Sonmez, C.; Satheye, S.; Schneider, J. P.; Pochan, D. J.; Langhans, S. A. Beta Hairpin Peptide hydrogels as an injectable solid vehicle for neurotrophic growth factor delivery. *Biomacromolecules* **2015,** *16* (9), 2672-2683.

199. Dong, Y. Z.; Wang, W. H.; Veiseh, O.; Appel, E. A.; Xue, K.; Webber, M. J.; Tang, B. C.; Yang, X. W.; Weir, G. C.; Langer, R.; Anderson, D. G. Injectable and glucose-responsive hydrogels based on boronic acid-glucose complexation. *Langmuir* **2016,** *32* (34), 8743-8747.

200. Gaharwar, A. K.; Schexnailder, P.; Kaul, V.; Akkus, O.; Zakharov, D.; Seifert, S.; Schmidt, G. Highly extensible bio-nanocomposite films with direction-dependent properties. *Adv. Funct. Mater.* **2010,** *20* (3), 429-436.

201. Schexnailder, P. J.; Gaharwar, A. K.; Bartlett, R. L.; Seal, B. L.; Schmidt, G. Tuning cell adhesion by incorporation of charged silicate nanoparticles as cross-linkers to polyethylene oxide. *Macromol. Biosci.* **2010,** *10* (12), 1416-1423.

202. Gaharwar, A. K.; Rivera, C. P.; Wu, C. J.; Schmidt, G. Transparent, elastomeric and tough hydrogels from poly(ethylene glycol) and silicate nanoparticles. *Acta Biomater.* **2011,** *7* (12), 4139-4148.

203. Gaharwar, A. K.; Schexnailder, P. J.; Kline, B. P.; Schmidt, G. Assessment of using Laponite (R) cross-linked poly(ethylene oxide) for controlled cell adhesion and mineralization. *Acta Biomater.* **2011,** *7* (2), 568-577.

204. Burdick, J. A.; Anseth, K. S. Photoencapsulation of osteoblasts in injectable RGD-modified PEG hydrogels for bone tissue engineering. *Biomaterials* **2002,** *23* (22), 4315-4323.

205. Bryant, S. J.; Anseth, K. S.; Lee, D. A.; Bader, D. L. Crosslinking density influences the morphology of chondrocytes photoencapsulated in PEG hydrogels during the application of compressive strain. *J. Orthop. Res.* **2004,** *22* (5), 1143-1149.

206. Moon, J. J.; Saik, J. E.; Poché, R. A.; Leslie-Barbick, J. E.; Lee, S.-H.; Smith, A. A.; Dickinson, M. E.; West, J. L. Biomimetic hydrogels with pro-angiogenic properties. *Biomaterials* **2010,** *31* (14), 3840-3847.

207. Weber, L. M.; He, J.; Bradley, B.; Haskins, K.; Anseth, K. S. PEG-based hydrogels as an in vitro encapsulation platform for testing controlled β-cell microenvironments. *Acta Biomater.* **2006,** *2* (1), 1-8.

208. Mohanty, R. P.; Suman, K.; Joshi, Y. M. In situ ion induced gelation of colloidal dispersion of Laponite: Relating microscopic interactions to macroscopic behavior. *Applied Clay Science* **2017,** *138*, 17-24.

209. Zulian, L.; Ruzicka, B.; Ruocco, G. Influence of an adsorbing polymer on the aging dynamics of Laponite clay suspensions. *Philosophical Magazine* **2008,** *88* (33-35), 4213-4221.

210. Zulian, L.; Marques, F. A. D.; Emilitri, E.; Ruocco, G.; Ruzicka, B. Dual aging behaviour in a clay-polymer dispersion. *Soft Matter* **2014,** *10* (25), 4513-4521.

211. Hoffman, A. S. Hydrogels for biomedical applications. *Adv. Drug Deliv. Rev.* **2012,** *64*, 18-23.

212. Qiu, Y.; Park, K. Environment-sensitive hydrogels for drug delivery. *Adv. Drug Deliv. Rev.* **2012,** *64*, 49-60.

213. Hoffman, A. S. Stimuli-responsive polymers: biomedical applications and challenges for clinical translation. *Adv. Drug Deliv. Rev.* **2013,** *65* (1), 10-16.

214. Lee, K. Y.; Mooney, D. J. Hydrogels for tissue engineering. *Chemical reviews* **2001,** *101* (7), 1869-1880.

215. Peppas, N. A.; Hilt, J. Z.; Khademhosseini, A.; Langer, R. Hydrogels in biology and medicine: from molecular principles to bionanotechnology. *Advanced Materials* **2006,** *18* (11), 1345-1360.

216. Peppas, N. A.; Bures, P.; Leobandung, W.; Ichikawa, H. Hydrogels in pharmaceutical formulations. *European Journal of Pharmaceutics and Biopharmaceutics* **2000,** *50* (1), 27-46.

217. Peppas, N. A.; Keys, K. B.; Torres-Lugo, M.; Lowman, A. M. Poly(ethylene glycol)-containing hydrogels in drug delivery. *Journal of Controlled Release* **1999,** *62* (1-2), 81-87.

218. Mellott, M. B.; Searcy, K.; Pishko, M. V. Release of protein from highly cross-linked hydrogels of poly(ethylene glycol) diacrylate fabricated by UV polymerization. *Biomaterials* **2001,** *22* (9), 929-941.

219. Nguyen, K. T.; West, J. L. Photopolymerizable hydrogels for tissue engineering applications. *Biomaterials* **2002,** *23* (22), 4307-4314.

220. Nichol, J. W.; Koshy, S. T.; Bae, H.; Hwang, C. M.; Yamanlar, S.; Khademhosseini, A. Cell-laden microengineered gelatin methacrylate hydrogels. *Biomaterials* **2010,** *31* (21), 5536-5544.

221. Shingleton, W. D.; Hodges, D. J.; Brick, P.; Cawston, T. E. Collagenase: a key enzyme in collagen turnover. *Biochem Cell Biol* **1996,** *74* (6), 759-775.

222. Hutson, C. B.; Nichol, J. W.; Aubin, H.; Bae, H.; Yamanlar, S.; Al-Haque, S.; Koshy, S. T.; Khademhosseini, A. Synthesis and characterization of tunable poly (ethylene glycol): gelatin methacrylate composite hydrogels. *Tissue Engineering Part A* **2011,** *17* (13-14), 1713-1723.

223. Peak, C. W.; Nagar, S.; Watts, R. D.; Schmidt, G. Robust and degradable hydrogels from poly (ethylene glycol) and semi-interpenetrating collagen. *Macromolecules* **2014,** *47* (18), 6408–6417.

224. Karimi, A.; Navidbakhsh, M. Material properties in unconfined compression of gelatin hydrogel for skin tissue engineering applications. *Biomedical Engineering-Biomedizinische Technik* **2014,** *59* (6), 479-486.

225. Ullm, S.; Kruger, A.; Tondera, C.; Gebauer, T. P.; Neffe, A. T.; Lendlein, A.; Jung, F.; Pietzsch, J. Biocompatibility and inflammatory response in vitro and in vivo to gelatin-based biomaterials with tailorable elastic properties. *Biomaterials* **2014,** *35* (37), 9755-9766.

226. Lee, T. T.; Garcia, J. R.; Paez, J. I.; Singh, A.; Phelps, E. A.; Weis, S.; Shafiq, Z.; Shekaran, A.; Del Campo, A.; Garcia, A. J. Light-triggered in vivo activation of adhesive peptides regulates cell adhesion, inflammation and vascularization of biomaterials. *Nature materials* **2014**.

227. Cayrol, F.; Diaz Flaque, M. C.; Fernando, T.; Yang, S. N.; Sterle, H. A.; Bolontrade, M.; Amoros, M.; Isse, B.; Farias, R. N.; Ahn, H.; Tian, Y. F.; Tabbo, F.; Singh, A.; Inghirami, G.; Cerchietti, L.; Cremaschi, G. A. Integrin alphavbeta3 acting as membrane receptor for thyroid hormones mediates angiogenesis in malignant T cells. *Blood* **2015,** *125* (5), 841-51.

228. Dvir, T.; Timko, B. P.; Kohane, D. S.; Langer, R. Nanotechnological strategies for engineering complex tissues. *Nature nanotechnology* **2011,** *6* (1), 13-22.

229. Patel, R. G.; Purwada, A.; Cerchietti, L.; Inghirami, G.; Melnick, A.; Gaharwar, A. K.; Singh, A. Microscale bioadhesive hydrogel arrays for cell engineering applications. *Cel. Mol. Bioeng.* **2014,** *7* (3), 394-408.

230. Giano, M. C.; Ibrahim, Z.; Medina, S. H.; Sarhane, K. A.; Christensen, J. M.; Yamada, Y.; Brandacher, G.; Schneider, J. P. Injectable bioadhesive hydrogels with innate antibacterial properties. *Nature communications* **2014,** *5*.

231. Gaharwar, A. K.; Mihaila, S. M.; Swami, A.; Patel, A.; Sant, S.; Reis, R. L.; Marques, A. P.; Gomes, M. E.; Khademhosseini, A. Bioactive silicate nanoplatelets for osteogenic differentiation of human mesenchymal stem cells. *Adv. Mater.* **2013,** *25* (24), 3329-3336.

232. Mihaila, S. M.; Gaharwar, A. K.; Reis, R. L.; Khademhosseini, A.; Marques, A. P.; Gomes, M. E. The osteogenic differentiation of SSEA-4 sub-population of human adipose derived stem cells using silicate nanoplatelets. *Biomaterials* **2014,** *35* (33), 9087-9099.

233. Xavier, J. R.; Thakur, T.; Desai, P.; Jaiswal, M. K.; Sears, N.; Cosgriff-Hernandez, E.; Kaunas, R.; Gaharwar, A. K. Bioactive nanoengineered hydrogels for bone tissue engineering: a growth-factor-free approach. *ACS Nano* **2015,** *DOI: 10.1021/nn507488s*.

234. Gaharwar, A. K.; Schexnailder, P. J.; Dundigalla, A.; White, J. D.; Matos-Pérez, C. R.; Cloud, J. L.; Seifert, S.; Wilker, J. J.; Schmidt, G. Highly extensible bio-nanocomposite fibers. *Macromolecular rapid communications* **2011**.

235. Gaharwar, A. K.; Schexnailder, P. J.; Kline, B. P.; Schmidt, G. Assessment of using Laponite® cross-linked poly (ethylene oxide) for controlled cell adhesion and mineralization. *Acta Biomaterialia* **2011,** *7* (2), 568-577.

236. Gaharwar, A. K.; Avery, R. K.; Assmann, A.; Paul, A.; McKinley, G. H.; Khademhosseini, A.; Olsen, B. D. Shear-thinning nanocomposite hydrogels for the treatment of hemorrhage. *ACS nano* **2014,** *8* (10), 9833–9842.

237. Gaharwar, A. K.; Kishore, V.; Rivera, C.; Bullock, W.; Wu, C. J.; Akkus, O.; Schmidt, G. Physically crosslinked nanocomposites from silicate-crosslinked PEO: mechanical properties and osteogenic differentiation of human mesenchymal stem cells. *Macromolecular bioscience* **2012,** *12* (6), 779-793.

238. Gaharwar, A. K.; Rivera, C.; Wu, C.-J.; Chan, B. K.; Schmidt, G. Photocrosslinked nanocomposite hydrogels from PEG and silica nanospheres: structural, mechanical and cell adhesion characteristics. *Materials Science & Engineering C-Materials for Biological Applications* **2013,** *33* (3), 1800-1807.

239. Carrow, J. K.; Gaharwar, A. K. Bioinspired polymeric nanocomposites for regenerative medicine. *Macromolecular Chemistry and Physics* **2014**.

240. Chan, B. K.; Wippich, C. C.; Wu, C.-J.; Sivasankar, P. M.; Schmidt, G. Robust and semi-interpenetrating hydrogels from poly(ethylene glycol) and collagen for elastomeric tissue scaffolds. *Macromol. Biosci.* **2012,** *12* (11), 1490-1501.

241. Dumbauld, D. W.; Lee, T. T.; Singh, A.; Scrimgeour, J.; Gersbach, C. A.; Zamir, E. A.; Fu, J.; Chen, C. S.; Curtis, J. E.; Craig, S. W. How vinculin regulates force transmission. *Proceedings of the National Academy of Sciences* **2013,** *110* (24), 9788-9793.

242. Coyer, S. R.; Singh, A.; Dumbauld, D. W.; Calderwood, D. A.; Craig, S. W.; Delamarche, E.; García, A. J. Nanopatterning reveals an ECM area threshold for focal adhesion assembly and force transmission that is regulated by integrin activation and cytoskeleton tension. *Journal of cell science* **2012,** *125* (21), 5110-5123.

243. Liu, Y.; Meng, H.; Konst, S.; Sarmiento, R.; Rajachar, R.; Lee, B. P. Injectable dopamine-modified poly(ethylene glycol) nanocomposite hydrogel with enhanced adhesive property and bioactivity. *ACS Appl. Mater. Interfaces* **2014,** *6* (19), 16982-16992.

244. Annabi, N.; Nichol, J. W.; Zhong, X.; Ji, C.; Koshy, S.; Khademhosseini, A.; Dehghani, F. Controlling the porosity and microarchitecture of hydrogels for tissue engineering. *Tissue Engineering Part B: Reviews* **2010,** *16* (4), 371-383.

245. Mooney, D. T.; Mazzoni, C. L.; Breuer, C.; McNamara, K.; Hern, D.; Vacanti, J. P.; Langer, R. Stabilized polyglycolic acid fibre based tubes for tissue engineering. *Biomaterials* **1996,** *17* (2), 115-124.

246. Santos, M. I.; Tuzlakoglu, K.; Fuchs, S.; Gomes, M. E.; Peters, K.; Unger, R. E.; Piskin, E.; Reis, R. L.; Kirkpatrick, C. J. Endothelial cell colonization and angiogenic potential of combined nano- and micro-fibrous scaffolds for bone tissue engineering. *Biomaterials* **2008,** *29* (32), 4306-4313.

247. Zhan, W.; Seong, G. H.; Crooks, R. M. Hydrogel-based microreactors as a functional component of microfluidic systems. *Anal. Chem.* **2002,** *74* (18), 4647-4652.

248. Cuchiara, M. P.; Allen, A. C. B.; Chen, T. M.; Miller, J. S.; West, J. L. Multilayer microfluidic PEGDA hydrogels. *Biomaterials* **2010,** *31* (21), 5491-5497.

249. Zustiak, S. P.; Leach, J. B. Hydrolytically degradable poly(ethylene glycol) hydrogel scaffolds with tunable degradation and mechanical properties. *Biomacromolecules* **2010,** *11* (5), 1348-1357.

250. Michel, R.; Pasche, S.; Textor, M.; Castner, D. G. The influence of PEG architecture on protein adsorption and conformation. *Langmuir : the ACS journal of surfaces and colloids* **2005,** *21* (26), 12327-12332.

251. Schellekens, H.; Hennink, W. E.; Brinks, V. The immunogenicity of polyethylene glycol: facts and fiction. *Pharm Res-Dord* **2013,** *30* (7), 1729-1734.

252. Lee, W. K.; Ichi, T.; Ooya, T.; Yamamoto, T.; Katoh, M.; Yui, N. Novel poly(ethylene glycol) scaffolds crosslinked by hydrolyzable polyrotaxane for cartilage tissue engineering. *J. Biomed. Mater. Res. Part A* **2003,** *67A* (4), 1087-1092.

253. Hudalla, G. A.; Eng, T. S.; Murphy, W. L. An approach to modulate degradation and mesenchymal stem cell behavior in poly(ethylene glycol) networks. *Biomacromolecules* **2008,** *9* (3), 842-849.

254. Pekkanen, A. M.; Mondschein, R. J.; Williams, C. B.; Long, T. E. 3D printing polymers with supramolecular functionality for biological applications. *Biomacromolecules* **2017,** *18* (9), 2669-2687.

255. Murphy, S. V.; Atala, A. 3D bioprinting of tissues and organs. *Nature Biotechnology* **2014,** *32*, 773.

256. Suntornnond, R.; An, J.; Chua, C. K. Bioprinting of thermoresponsive hydrogels for next generation tissue engineering: a review. *Macromolecular Materials and Engineering* **2017,** *302* (1).

257. Guarino, V.; Gloria, A.; De Santis, R.; Ambrosio, L. Composite hydrogels for scaffold design, tissue engineering, and prostheses. *Biomedical Applications of Hydrogels Handbook* **2010**, 227-245.

258. Jin, R.; Dijkstra, P. J. Hydrogels for tissue engineering applications. *Biomedical Applications of Hydrogels Handbook* **2010**, 203-225.

259. Murosaki, T.; Gong, J. P. Double network hydrogels as tough, durable tissue substitutes. *Biomedical Applications of Hydrogels Handbook* **2010**, 285-301.

260. Hoare, T. R.; Kohane, D. S. Hydrogels in drug delivery: progress and challenges. *Polymer* **2008,** *49* (8), 1993-2007.

261. Browning, M. B.; Cosgriff-Hernandez, E. Development of a biostable replacement for PEGDA hydrogels. *Biomacromolecules* **2012,** *13* (3), 779-786.

262. Browning, M. B.; Cereceres, S. N.; Luong, P. T.; Cosgriff-Hernandez, E. M. Determination of the in vivo degradation mechanism of PEGDA hydrogels. *Journal of biomedical materials research. Part A* **2014,** *102* (12), 4244-4251.

263. Rashkov, I.; Manolova, N.; Li, S. M.; Espartero, J. L.; Vert, M. Synthesis, characterization, and hydrolytic degradation of PLA/PEO/PLA triblock copolymers with short poly(L-lactic acid) chains. *Macromolecules* **1996,** *29* (1), 50-56.

264. Jalili, N. A.; Jaiswal, M. K.; Peak, C. W.; Cross, L. M.; Gaharwar, A. K. Injectable nanoengineered stimuli-responsive hydrogels for on-demand and localized therapeutic delivery. *Nanoscale* **2017,** *9* (40), 15379-15389.

265. Cereceres, S.; Touchet, T.; Browning, M. B.; Smith, C.; Rivera, J.; Hook, M.; Whitfield-Cargile, C.; Russell, B.; Cosgriff-Hernandez, E. Chronic wound dressings based on collagen-mimetic proteins. *Advances in Wound Care* **2015,** *4* (8), 444-456.

266. Nair, D. P.; Podgórski, M.; Chatani, S.; Gong, T.; Xi, W.; Fenoli, C. R.; Bowman, C. N. The thiol-Michael addition click reaction: a powerful and widely used tool in materials chemistry. *Chemistry of Materials* **2014,** *26* (1), 724-744.

267. Konigsberg, W. Reduction of disulfide bonds in proteins with dithiothreitol. In *Methods in Enzymology*; Academic Press, 1972; Vol. 25, pp 185-188.

268. Parlato, M.; Johnson, A.; Hudalla, G. A.; Murphy, W. L. Adaptable poly(ethylene glycol) microspheres capable of mixed-mode degradation. *Acta Biomater.* **2013,** *9* (12), 9270-9280.

269. Parlato, M.; Reichert, S.; Barney, N.; Murphy, W. L. Poly(ethylene glycol) hydrogels with adaptable mechanical and degradation properties for use in biomedical applications. *Macromol. Biosci.* **2014,** *14* (5), 687-698.

270. Yamaoka, T.; Tabata, Y.; Ikada, Y. Distribution and tissue uptake of poly(ethylene glycol) with different molecular-weights after intravenous administration to mice. *Journal of Pharmaceutical Sciences* **1994,** *83* (4), 601-606.

271. Schexnailder, P. J.; Jin, Q.; Gaharwar, A.; Wu, C. J.; Schmidt, G. Development of bio-nanocomposite hydrogels based on silicate cross-linked PEO for tissue engineering. *Tissue Eng. Part A* **2008,** *14* (5), 836-836.

272. Takeno, H.; Kimura, Y.; Nakamura, W. Mechanical, swelling, and structural properties of mechanically tough clay-sodium polyacrylate blend hydrogels. *Gels* **2017,** *3* (1), 10.

273. Thompson, D. W.; Butterworth, J. T. The nature of Lapoonite and its aqueous dispersions. *J. Colloid Interface Sci.* **1992,** *151* (1), 236-243.

274. Mähler, J.; Persson, I. A study of the hydration of the alkali metal ions in aqueous solution. *Inorganic Chemistry* **2012,** *51* (1), 425-438.

275. de Carvalho, R.; Skipper, N. T. Atomistic computer simulation of the clay-fluid interface in colloidal laponite. *Journal of Chemical Physics* **2001,** *114* (8), 3727-3733.

276. Lockhart, N. C. Electrical-properites and the surface characteristics and structure of calys 1. Swelling clays. *J. Colloid Interface Sci.* **1980,** *74* (2), 509-519.

277. Zeynabad, F. B.; Salehi, R.; Mahkam, M. Design of pH-responsive antimicrobial nanocomposite as dual drug delivery system for tumor therapy. *Applied Clay Science* **2017,** *141*, 23-35.

278. Roozbahani, M.; Kharaziha, M.; Emadi, R. pH sensitive dexamethasone encapsulated laponite nanoplatelets: release mechanism and cytotoxicity. *Int. J. Pharm.* **2017,** *518* (1-2), 312-319.

279. Lee, S.; Tong, X.; Yang, F. The effects of varying poly(ethylene glycol) hydrogel crosslinking density and the crosslinking mechanism on protein accumulation in three-dimensional hydrogels. *Acta Biomater.* **2014,** *10* (10), 4167-4174.

280. Rodrigues, M.; Griffith, L. G.; Wells, A. Growth factor regulation of proliferation and survival of multipotential stromal cells. *Stem Cell Research & Therapy* **2010,** *1* (4), 32.

281. Schuldiner, M.; Yanuka, O.; Itskovitz-Eldor, J.; Melton, D. A.; Benvenisty, N. Effects of eight growth factors on the differentiation of cells derived from human embryonic stem cells. *Proceedings of the National Academy of Sciences* **2000,** *97* (21), 11307-11312.

282. Adams, R. H.; Alitalo, K. Molecular regulation of angiogenesis and lymphangiogenesis. *Nat Rev Mol Cell Biol* **2007,** *8* (6), 464-78.

283. Kalluri, R. Basement membranes: structure, assembly and role in tumour angiogenesis. *Nat Rev Cancer* **2003,** *3* (6), 422-33.

284. Briquez, P. S.; Clegg, L. E.; Martino, M. M.; Mac Gabhann, F.; Hubbell, J. A. Design principles for therapeutic angiogenic materials. *Nature Reviews Materials* **2016,** *1*, 15006.

285. Chimene, D.; Alge, D. L.; Gaharwar, A. K. Two-dimensional nanomaterials for biomedical applications: emerging trends and future prospects. *Adv Mater* **2015,** *27* (45), 7261-84.

286. Dawson, J. I.; Kanczler, J. M.; Yang, X. B.; Attard, G. S.; Oreffo, R. O. Clay gels for the delivery of regenerative microenvironments. *Adv Mater* **2011,** *23* (29), 3304-8.

287. Bayless, K. J.; Davis, G. E. Sphingosine-1-phosphate markedly induces matrix metalloproteinase and integrin-dependent human endothelial cell invasion and lumen formation in three-dimensional collagen and fibrin matrices. *Biochem Biophys Res Commun* **2003,** *312* (4), 903-13.

288. Cao, R.; Brakenhielm, E.; Pawliuk, R.; Wariaro, D.; Post, M. J.; Wahlberg, E.; Leboulch, P.; Cao, Y. Angiogenic synergism, vascular stability and improvement of hind-limb ischemia by a combination of PDGF-BB and FGF-2. *Nat Med* **2003,** *9* (5), 604-13.

289. Rouwkema, J.; Rivron, N. C.; van Blitterswijk, C. A. Vascularization in tissue engineering. *Trends Biotechnol* **2008,** *26* (8), 434-41.

290. Phelps, E. A.; Garcia, A. J. Update on therapeutic vascularization strategies. *Regen Med* **2009,** *4* (1), 65-80.

291. Novosel, E. C.; Kleinhans, C.; Kluger, P. J. Vascularization is the key challenge in tissue engineering. *Adv. Drug Deliv. Rev.* **2011,** *63* (4), 300-311.

292. Hersel, U.; Dahmen, C.; Kessler, H. RGD modified polymers: biomaterials for stimulated cell adhesion and beyond. *Biomaterials* **2003,** *24* (24), 4385-4415.

293. Woolfson, D. N.; Mahmoud, Z. N. More than just bare scaffolds: towards multi-component and decorated fibrous biomaterials. *Chemical Society Reviews* **2010,** *39* (9), 3464-3479.

294. Rieger, K. A.; Birch, N. P.; Schiffman, J. D. Designing electrospun nanofiber mats to promote wound healing – a review. *Journal of Materials Chemistry B* **2013,** *1* (36), 4531.

295. Balkawade, R. S.; Mills, D. K. Bioactive nanomaterials for enhanced wound healing. *The FASEB Journal* **2012,** *26* (1 Supplement), 198.4.

296. Kalashnikova, I.; Das, S.; Seal, S. Nanomaterials for wound healing: scope and advancement. *Nanomedicine (Lond)* **2015,** *10* (16), 2593-612.

297. Cleland, J. L.; Duenas, E. T.; Park, A.; Daugherty, A.; Kahn, J.; Kowalski, J.; Cuthbertson, A. Development of poly-(D,L-lactide--coglycolide) microsphere formulations containing recombinant human vascular endothelial growth factor to promote local angiogenesis. *J Control Release* **2001,** *72* (1-3), 13-24.

298. Freed, L. E.; Vunjak-Novakovic, G.; Biron, R. J.; Eagles, D. B.; Lesnoy, D. C.; Barlow, S. K.; Langer, R. Biodegradable polymer scaffolds for tissue engineering. *Biotechnology (N Y)* **1994,** *12* (7), 689-93.

299. Silva, E. A.; Mooney, D. J. Effects of VEGF temporal and spatial presentation on angiogenesis. *Biomaterials* **2010,** *31* (6), 1235-41.

300. Ozawa, C. R.; Banfi, A.; Glazer, N. L.; Thurston, G.; Springer, M. L.; Kraft, P. E.; McDonald, D. M.; Blau, H. M. Microenvironmental VEGF concentration, not total dose,

determines a threshold between normal and aberrant angiogenesis. *Journal of Clinical Investigation* **2004,** *113* (4), 516-527.

301. Ellis, L. M.; Hicklin, D. J. VEGF-targeted therapy: mechanisms of anti-tumour activity. *Nat Rev Cancer* **2008,** *8* (8), 579-91.

302. Olsson, A. K.; Dimberg, A.; Kreuger, J.; Claesson-Welsh, L. VEGF receptor signalling - in control of vascular function. *Nat Rev Mol Cell Biol* **2006,** *7* (5), 359-71.

303. Thompson, D. W.; Butterworth, J. T. The nature of Laponite and its aqueous dispersions. *Journal of Colloid and Interface Science* **1992,** *151* (1), 236-243.

304. Jung, H.; Kim, H.-M.; Choy, Y. B.; Hwang, S.-J.; Choy, J.-H. Itraconazole–Laponite: kinetics and mechanism of drug release. *Applied Clay Science* **2008,** *40* (1), 99-107.

305. Wang, S.; Wu, Y.; Guo, R.; Huang, Y.; Wen, S.; Shen, M.; Wang, J.; Shi, X. Laponite nanodisks as an efficient platform for doxorubicin delivery to cancer cells. *Langmuir* **2013,** *29* (16), 5030-6.

306. Sainson, R. C.; Aoto, J.; Nakatsu, M. N.; Holderfield, M.; Conn, E.; Koller, E.; Hughes, C. C. Cell-autonomous notch signaling regulates endothelial cell branching and proliferation during vascular tubulogenesis. *FASEB J* **2005,** *19* (8), 1027-9.

307. Kedrin, D.; van Rheenen, J.; Hernandez, L.; Condeelis, J.; Segall, J. E. Cell motility and cytoskeletal regulation in invasion and metastasis. *J Mammary Gland Biol Neoplasia* **2007,** *12* (2-3), 143-52.

308. Koh, W.; Mahan, R. D.; Davis, G. E. Cdc42- and Rac1-mediated endothelial lumen formation requires Pak2, Pak4 and Par3, and PKC-dependent signaling. *J Cell Sci* **2008,** *121* (Pt 7), 989-1001.

309. Saunders, W. B.; Bohnsack, B. L.; Faske, J. B.; Anthis, N. J.; Bayless, K. J.; Hirschi, K. K.; Davis, G. E. Coregulation of vascular tube stabilization by endothelial cell TIMP-2 and pericyte TIMP-3. *J Cell Biol* **2006,** *175* (1), 179-91.

310. Stratman, A. N.; Saunders, W. B.; Sacharidou, A.; Koh, W.; Fisher, K. E.; Zawieja, D. C.; Davis, M. J.; Davis, G. E. Endothelial cell lumen and vascular guidance tunnel formation requires MT1-MMP-dependent proteolysis in 3-dimensional collagen matrices. *Blood* **2009,** *114* (2), 237-47.

311. Su, S. C.; Mendoza, E. A.; Kwak, H. I.; Bayless, K. J. Molecular profile of endothelial invasion of three-dimensional collagen matrices: insights into angiogenic sprout induction in wound healing. *Am J Physiol Cell Physiol* **2008,** *295* (5), C1215-29.

312. Bayless, K. J.; Kwak, H.-I.; Su, S.-C. Investigating endothelial invasion and sprouting behavior in three-dimensional collagen matrices. *Nat. Protocols* **2009,** *4* (12), 1888-1898.

313. Bayless, K. J.; Kwak, H. I.; Su, S. C. Investigating endothelial invasion and sprouting behavior in three-dimensional collagen matrices. *Nat Protoc* **2009,** *4* (12), 1888-98.

314. Ruzicka, B.; Zaccarelli, E.; Zulian, L.; Angelini, R.; Sztucki, M.; Moussaid, A.; Narayanan, T.; Sciortino, F. Observation of empty liquids and equilibrium gels in a colloidal clay. *Nat Mater* **2011,** *10* (1), 56-60.

315. Xiao, S.; Castro, R.; Maciel, D.; Goncalves, M.; Shi, X.; Rodrigues, J.; Tomas, H. Fine tuning of the pH-sensitivity of laponite-doxorubicin nanohybrids by polyelectrolyte multilayer coating. *Mater Sci Eng C Mater Biol Appl* **2016,** *60*, 348-356.

316. Roozbahani, M.; Kharaziha, M.; Emadi, R. pH sensitive dexamethasone encapsulated laponite nanoplatelets: release mechanism and cytotoxicity. *Int J Pharm* **2017,** *518* (1-2), 312-319.

317. Gibbs, D. M.; Black, C. R.; Hulsart-Billstrom, G.; Shi, P.; Scarpa, E.; Oreffo, R. O.; Dawson, J. I. Bone induction at physiological doses of BMP through localization by clay nanoparticle gels. *Biomaterials* **2016,** *99*, 16-23.

318. Duran, C. L.; Kaunas, R.; Bayless, K. J. S1P Synergizes with wall shear stress and other angiogenic factors to induce endothelial cell sprouting responses. Humana Press: Totowa, NJ, pp 1-17.

319. Langlois, S.; Gingras, D.; Beliveau, R. Membrane type 1-matrix metalloproteinase (MT1-MMP) cooperates with sphingosine 1-phosphate to induce endothelial cell migration and morphogenic differentiation. *Blood* **2004,** *103* (8), 3020-8.

320. Spiegel, S.; Milstien, S. Sphingosine-1-phosphate: an enigmatic signalling lipid. *Nat Rev Mol Cell Biol* **2003,** *4* (5), 397-407.

321. Jakeman, L. B.; Armanini, M.; Phillips, H. S.; Ferrara, N. Developmental expression of binding sites and messenger ribonucleic acid for vascular endothelial growth factor suggests a role for this protein in vasculogenesis and angiogenesis. *Endocrinology* **1993,** *133* (2), 848-59.

322. Shweiki, D.; Itin, A.; Neufeld, G.; Gitay-Goren, H.; Keshet, E. Patterns of expression of vascular endothelial growth factor (VEGF) and VEGF receptors in mice suggest a role in hormonally regulated angiogenesis. *J Clin Invest* **1993,** *91* (5), 2235-43.

323. Gaharwar, A. K.; Mihaila, S. M.; Swami, A.; Patel, A.; Sant, S.; Reis, R. L.; Marques, A. P.; Gomes, M. E.; Khademhosseini, A. Bioactive silicate nanoplatelets for osteogenic differentiation of human mesenchymal stem cells. *Adv Mater* **2013,** *25* (24), 3329-36.

324. Chowdhury, F.; Na, S.; Li, D.; Poh, Y. C.; Tanaka, T. S.; Wang, F.; Wang, N. Material properties of the cell dictate stress-induced spreading and differentiation in embryonic stem cells. *Nat Mater* **2010,** *9* (1), 82-8.

325. Peppas, N. A.; Hilt, J. Z.; Thomas, J. B. *Nanotechnology in Therapeutics: Current Technology and Applications*; Horizon Bioscience2007.

326. Lowman, A. M.; Dziubla, T. D.; Bures, P.; Peppas, N. A. Structural and dynamic response of neutral and intelligent networks in biomedical environments. *Advances in Chemical Engineering* **2004,** *29*, 75-130.

327. Carrow, J. K.; Gaharwar, A. K. Bioinspired polymeric nanocomposites for regenerative medicine. *Macromolecular Chemistry and Physics* **2015,** *216* (3), 248-264.

328. Gaharwar, A. K.; Peppas, N. A.; Khademhosseini, A. Nanocomposite hydrogels for biomedical applications. *Biotechnol Bioeng* **2014,** *111* (3), 441-53.

329. Bayless, K. J.; Davis, G. E. Microtubule depolymerization rapidly collapses capillary tube networks in vitro and angiogenic vessels in vivo through the small GTPase Rho. *J Biol Chem* **2004,** *279* (12), 11686-95.

330. Stratman, A. N.; Schwindt, A. E.; Malotte, K. M.; Davis, G. E. Endothelial-derived PDGF-BB and HB-EGF coordinately regulate pericyte recruitment during vasculogenic tube assembly and stabilization. *Blood* **2010,** *116* (22), 4720-30.

331. Singh, M.; Berkland, C.; Detamore, M. S. Strategies and applications for incorporating physical and chemical signal gradients in tissue engineering. *Tissue Eng Part B Rev* **2008,** *14* (4), 341-66.

332. Lin, X.; Chen, J.; Qiu, P.; Zhang, Q.; Wang, S.; Su, M.; Chen, Y.; Jin, K.; Qin, A.; Fan, S.; Chen, P.; Zhao, X. Biphasic hierarchical extracellular matrix scaffold for osteochondral defect regeneration. *Osteoarthritis and cartilage* **2018,** *26* (3), 433-444.

333. Cross, L. M.; Thakur, A.; Jalili, N. A.; Detamore, M.; Gaharwar, A. K. Nanoengineered biomaterials for repair and regeneration of orthopedic tissue interfaces. *Acta Biomater* **2016,** *42*, 2-17.

334. Lu, H. H.; Thomopoulos, S. Functional attachment of soft tissues to bone: development, healing, and tissue engineering. *Annu Rev Biomed Eng* **2013,** *15*, 201-26.

335. Atala, A.; Kasper, F. K.; Mikos, A. G. Engineering Complex Tissues. *Science Translational Medicine* **2012,** *4* (160).

336. Agarwal, R.; Garcia, A. J. Biomaterial strategies for engineering implants for enhanced osseointegration and bone repair. *Adv. Drug Deliv. Rev.* **2015,** *94*, 53-62.

337. Badylak, S. F.; Weiss, D. J.; Caplan, A.; Macchiarini, P. Engineered whole organs and complex tissues. *Lancet* **2012,** *379* (9819), 943-952.

338. Lee, T. T.; Garcia, J. R.; Paez, J. I.; Singh, A.; Phelps, E. A.; Weis, S.; Shafiq, Z.; Shekaran, A.; del Campo, A.; Garcia, A. J. Light-triggered in vivo activation of adhesive peptides regulates cell adhesion, inflammation and vascularization of biomaterials. *Nat. Mater.* **2015,** *14* (3), 352-360.

339. Zorlutuna, P.; Annabi, N.; Camci-Unal, G.; Nikkhah, M.; Cha, J. M.; Nichol, J. W.; Manbachi, A.; Bae, H. J.; Chen, S. C.; Khademhosseini, A. Microfabricated biomaterials for engineering 3D tissues. *Adv. Mater.* **2012,** *24* (14), 1782-1804.

340. Langer, R. Perspectives and challenges in tissue engineering and regenerative medicine. *Adv. Mater.* **2009,** *21* (32-33), 3235-3236.

341. Griffith, L. G.; Naughton, G. Tissue engineering--current challenges and expanding opportunities. *Science* **2002,** *295* (5557), 1009-1014.

342. M. Jonker, A.; A. Bode, S.; H. Kusters, A.; van Hest, J. C. M.; Löwik, D. W. P. M. Soft PEG-hydrogels with independently tunable stiffness and RGDS-content for cell adhesion studies. *Macromol. Biosci.* **2015,** *15* (10), 1338-1347.

343. Missirlis, D.; Spatz, J. P. Combined effects of PEG hydrogel elasticity and cell-adhesive coating on fibroblast adhesion and persistent migration. *Biomacromolecules* **2014,** *15* (1), 195-205.

344. Rehmann, M. S.; Skeens, K. M.; Kharkar, P. M.; Ford, E. M.; Maverakis, E.; Lee, K. H.; Kloxin, A. M. Tuning and predicting mesh size and protein release from step growth hydrogels. *Biomacromolecules* **2017,** *18* (10), 3131-3142.

345. Thuresson, A.; Segad, M.; Plivelic, T. S.; Skepö, M. Flocculated Laponite-PEG/PEO dispersions with multivalent salt: a SAXS, cryo-TEM, and computer simulation study. *The Journal of Physical Chemistry C* **2017,** *121* (13), 7387-7396.

346. Sridhar, B. V.; Brock, J. L.; Silver, J. S.; Leight, J. L.; Randolph, M. A.; Anseth, K. S. Development of a cellularly degradable PEG hydrogel to promote articular cartilage extracellular matrix deposition. *Advanced Healthcare Materials* **2015,** *4* (5), 702-713.

347. Nicodemus, G. D.; Skaalure, S. C.; Bryant, S. J. Gel structure has an impact on pericellular and extracellular matrix deposition, which subsequently alters metabolic activities in chondrocyte-laden PEG hydrogels. *Acta Biomater.* **2011,** *7* (2), 492-504.

APPENDIX A

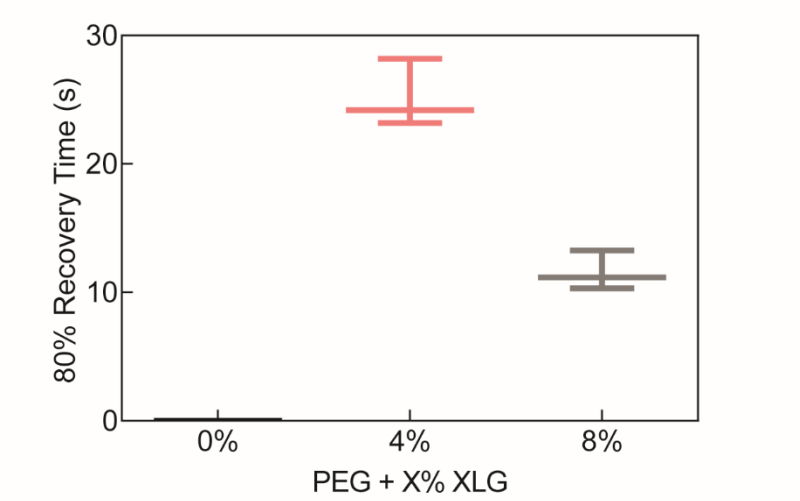

Figure A-1. Recovery time of materials from a peak-hold rheometry test. After the solution was shear-thinned the time for 80% recovery was examined.

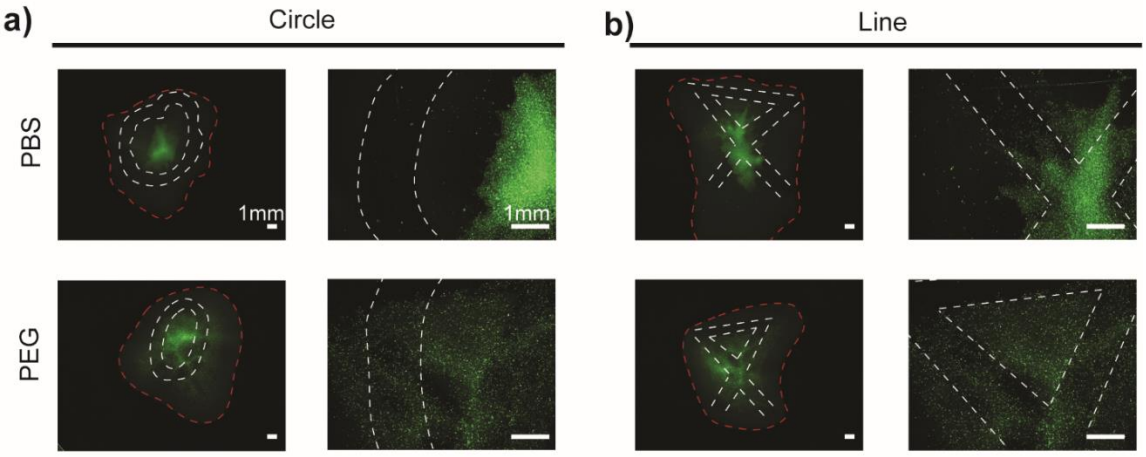

Figure A-2. (a) Extrusion of PBS, PEG, and PEG/Laponite solutions with cells stained with Cell Tracker Green in circlular pattern. (b) Extrusion of PBS, PEG, and PEG/Laponite solutions with cells stained with Cell Tracker Green in linear pattern. Note: For both (a) and (b) white dashed lines represent the programed print path and red dashed lines represent the 3D printed contruct

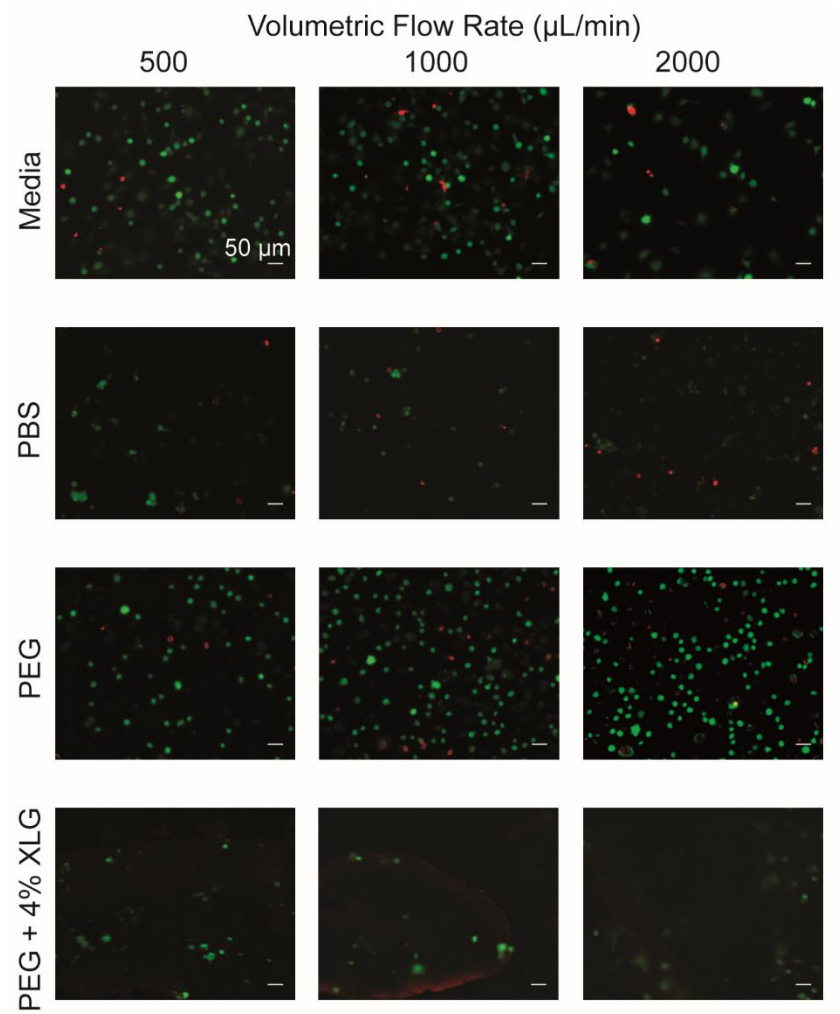

Figure A-3. Live/Dead analysis of extruded solutions at various volumetric flow rates. Analysis indicates that viability is above 90% with all samples. Green are live cells. Red are dead cells.

APPENDIX B

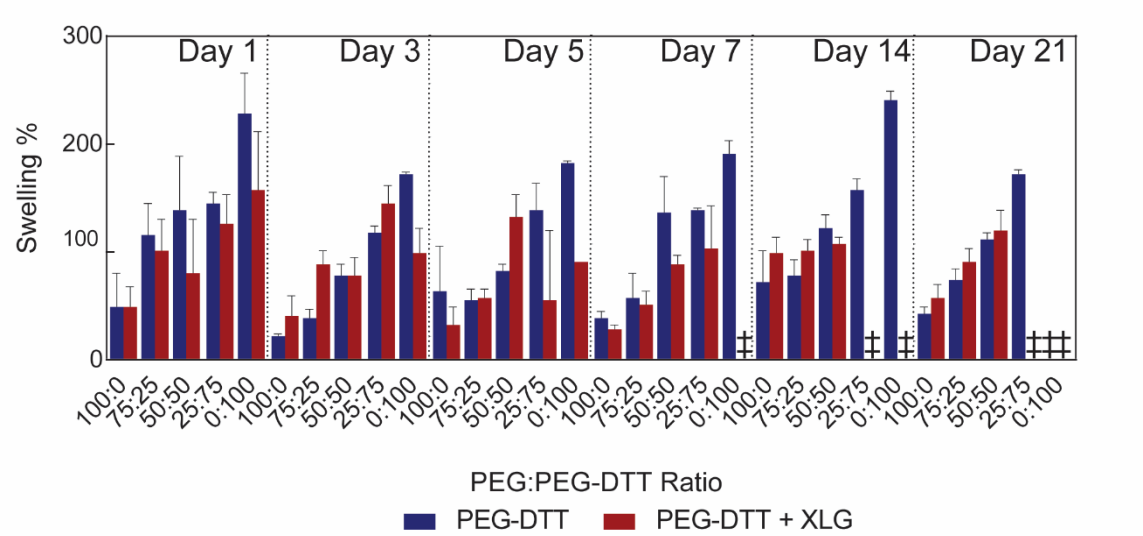

Figure B-1. Swelling of PEG:PEG-DTT ± XLG across multiple days. ‡ indicates completed degraded (swollen until rupture) of sample.

APPENDIX C

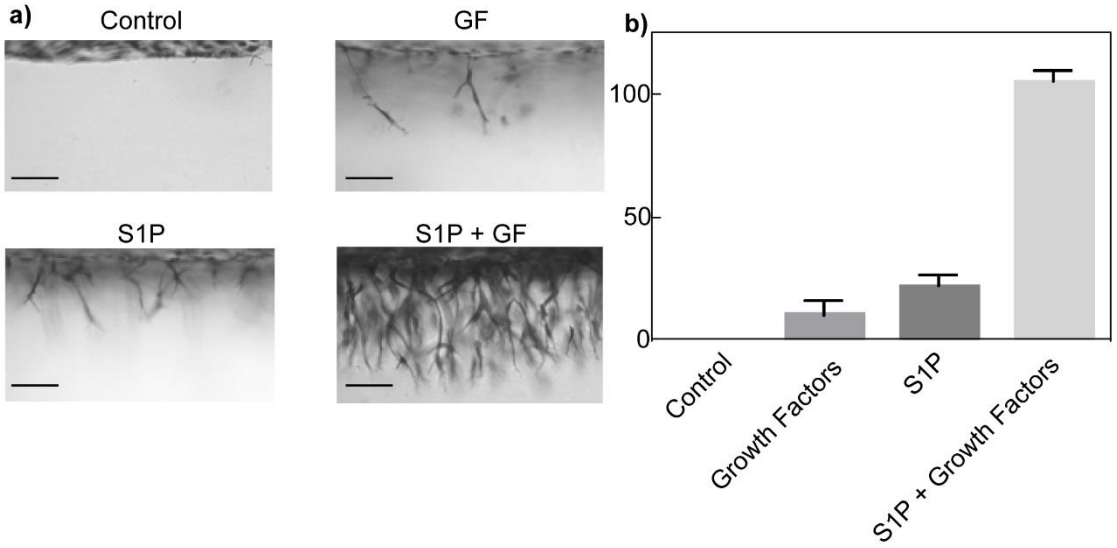

Figure C-1. Invasion assay using S1P. (a) images of control (collagen) gel, gel loaded with growth factors, gel loaded with S1P, and gel loaded with S1P and growth factors; scale bar = 50µm (b) quantification of number of sprouts per each treatment group